NATIONAL ADVISORY COMMITTEE FOR AERONAUTICS

WARTIME REPORT

ORIGINALLY ISSUED

May 1945 as
Memorandum Report L5D27a

WIND-TUNNEL TESTS OF THE 0.15-SCALE POWERED MODEL OF THE FLEETWINGS XBTK-1 AIRPLANE LONGITUDINAL STABILITY AND CONTROL

By Joseph Weil and Rebecca I. Boykin

Langley Memorial Aeronautical Laboratory
Langley Field, Va.

NACA

WASHINGTON

MR No. L5D27a

NATIONAL ADVISORY COMMITTEE FOR AERONAUTICS

MEMORANDUM REPORT

for the

Bureau of Aeronautics, Navy Department

WIND-TUNNEL TESTS OF THE 0.15-SCALE POWERED MODEL OF THE FLEETWINGS XBTK-1 AIRPLANE LONGITUDINAL STABILITY AND CONTROL

By Joseph Weil and Rebecca I. Boykin

SUMMARY

An investigation was undertaken to determine the probable static stability and control characteristics of the XBTK-1 airplane. Data from which these characteristics can be determined were obtained from tests of a 0.15-scale powered model in the Langley 7- by 10-foot tunnel.

The results of that part of the investigation which deals specifically with static longitudinal stability and control and stall characteristics are presented in this paper.

The longitudinal stability will probably be satisfactory for all contemplated flight conditions at the rearmost center-of-gravity location with the elevator fixed and free. Power effects were small.

Sufficient elevator control will be available to trim in any flight condition away from the ground. The stick forces may be light if the spring stiffness presently contemplated is used.

Increasing the slotted flap deflection above 30° increased $C_{L_{max}}$ only slightly.

Stalling characteristics will probably be satisfactory. In general, stall started at the wing fold line

and spread inboard faster than toward the tip. Power delayed the stall over portions of the wing immersed in the slipstream. The presence of the fuel tank, radar, and wing guns did not appreciably affect the stall trends.

INTRODUCTION

At the request of the Bureau of Aeronautics, Navy Department, a series of wind-tunnel tests was made in the Langley 7- by 10-foot tunnel of the Fleetwings XBTK-1 model (0.15 scale) with power. In addition, tests were made in the Langley 4- by 6-foot tunnel in order to determine isolated horizontal-tail characteristics.

The objective of these tests was to determine the complete stability and control characteristics of the model and provide data from which the flying qualities of the airplane could be estimated. The information thus obtained can be used to ascertain the amount and extent of modifications necessary to insure satisfactory handling qualities of the contemplated airplane.

The present report includes the results of the investigation of the longitudinal stability and control characteristics of the model. Photographs of tuft surveys made to determine the stall progression for various model conditions are also presented.

COEFFICIENTS AND SYMBOLS

The results of the tests are presented as standard NACA coefficients of forces and moments. Pitching-moment coefficients are given about the center-of-gravity location shown in figure 1 (25.6 percent of the mean aerodynamic chord). The data are referred to a system of axes originating at the center of gravity in which the Z axis is in the plane of symmetry and perpendicular to the relative wind, the X axis is in the plane of symmetry, and perpendicular to the Z axis, and the Y axis is perpendicular to the plane of symmetry.

The coefficients and symbols are defined as follows:

C_L	lift coefficient (Z/qS)
C_{L_t}	tail-lift coefficient $(\text{Tail lift}/qS_t)$
C_{D_R}	resultant-drag coefficient (X/qS)
C_m	pitching-moment coefficient (M/qSc)
C_{h_e}	elevator hinge-moment coefficient $(H/qb_e\bar{c}_e^2)$
T_c'	effective thrust coefficient (T_e/qS)
nD/V	propeller diameter-advance ratio
Q_c	torque coefficient $(Q/\rho V^2D^3)$
η	propulsive efficiency $(T_eV/2\pi nQ)$

where the quantities are defined below

Z	force along Z axis, positive when directed upward, pounds
X	force along X axis, positive when directed backward, pounds
M	moment about Y axis, pound-feet
H_e	elevator hinge moment, pound-feet
T_e	effective thrust, pounds
Q	torque, pound-feet
q	dynamic pressure $(\rho V^2/2)$, pounds per square foot
S	wing area (8.55 square feet on model)
S_t	horizontal-tail area (1.80 square feet on model)
c	wing mean aerodynamic chord (1.22 feet on model)
$\bar{c}_e$	root mean square chord of elevator behind hinge line (0.191 foot on model)

b_w wing span (7.30 feet on model)

b_e span of elevator (2.64 feet on model)

V air velocity, feet per second

D propeller diameter (2.04 feet on model)

n revolutions per second

and

ρ mass density of air, slugsper cubic foot

α angle of attack of thrust line, degrees

i_t angle of stabilizer with respect to thrust line, degrees; positive when trailing edge is down

δ control-surface deflection, degrees

ϵ average downwash angle, degrees

β propeller blade angle at 0.75 radius (18° on model)

Side-force factor $\frac{10^5}{32}\int_{0.2}^{1.0}\frac{b}{D}\sin\beta\, d\left(\frac{r}{R}\right)$

c_w wing chord at any station

r propeller radius to given section, feet

b propeller blade width, feet

R D/2, feet

l_t tail length

n_o tail-off aerodynamic center location, percent mean aerodynamic chord

n_p neutral-point location, percent mean aerodynamic chord

c_t tail chord at any station

$\frac{dC_m}{di_t}$ rate of change of pitching-moment coefficient with stabilizer setting

$\frac{dC_m}{dC_L}$ rate of change of pitching-moment coefficient with model lift coefficient

$\frac{d\epsilon}{d\alpha}$ rate of change of average downwash angle with angle of attack of thrust line

$\left(\frac{dC_L}{d\alpha}\right)_1$ rate of change of trim lift coefficient with angle of attack of thrust line

C_{m_t} pitching-moment coefficient required of tail for trim at elevator-fixed neutral-point location

$\frac{q_t}{q}$ ratio of effective dynamic pressure over the horizontal tail to free-stream dynamic pressure

$\frac{d(q_t/q)}{dC_L}$ rate of change of q_t/q with model lift coefficient

Subscripts:

o tail off

e elevator

r rudder

f flap

t_i isolated horizontal tail

t horizontal tail; tab (when used with δ)

MODEL AND APPARATUS

The XBTK-1 airplane is a single-engine, single-place, carrier-based dive and torpedo bomber with a

full cantilever low wing. It has partial-span extensible slotted flaps, "picket-fence" dive brakes, adjustable stabilizer, and a fully retractable conventional landing gear. The elevator is aerodynamically balanced by a shielded horn type of balance (medium nose shape) in combination with a spring tab. Trim changes are accomplished with the adjustable stabilizer. At design gross weight the airplane carries a radar unit under the right wing panel and an auxiliary droppable fuel tank under the left wing panel in addition to one 1000-pound bomb under the fuselage. The physical characteristics of the airplane which were supplied by the manufacturer are presented in tables I, II, and III.

The model was supplied by the Fleetwings Division of the Kaiser Cargo Corporation. It was not checked for accuracy. A three-view drawing of the model, as received, is shown in figure 1 and photographs of the original model are presented in figures 2(a) and 2(b).

The center wing panel has an NACA 2416 airfoil section with no taper or twist and is set at 2° with respect to the thrust line. The outer panels have a 0.50 taper ratio and -2.2° geometric twist. The theoretical tip section is an NACA 4412. All of the tests reported herein were made with a wing dihedral of $8\frac{1}{4}^{\circ}$ in the outboard panel. The flaps are of the extensible slotted type constructed in three sections, namely, a center section below the fuselage of about 5.4 inches span on the model and two outboard sections which extend from the center section to the wing outer panels. For normal operation (all tests reported in this paper) these three sections operate as a single unit but when a torpedo is carried, the center-section flap is locked in the retracted position. Details of the flap positions for various deflections tested are presented in figure 3.

The model was normally tested with a radar dome under the right wing and a fuel tank under the left wing. Two 1/4-inch diameter dowels 1 inch long were placed in the leading edge of the wing 18.09 inches from the center line of the model to represent cannon.

The horizontal tail had a modified NACA 66,2-015 root section tapering to a modified NACA 66,2-009 theoretical tip section. The airfoils were modified

in that the cusped trailing edge was replaced by a straight-line fairing which was tangent to the true contour at the $0.70c_t$ station and extended to the trailing edge. The elevator, which was statically mass-balanced, had an area of about 28.2 percent of the horizontal-tail area, was of constant percent chord $\left(\frac{c_e}{c_t} = 0.30\right)$ up to the horn and was unsealed for most of the tests. Details of the horizontal tail surface and elevator are shown in figure 4.

The model configurations referred to in the text and on the figures are as follows:

1. Cruising configuration:
   Flaps neutral
   Landing gear retracted

2. Landing configuration:
   Flaps extended (45°)
   Landing gear extended
   (a) Main wheels down
   (b) Wheel-well cut-out in wing open
   (c) Tail wheel down
   (d) Tail-wheel door open
   (e) Arresting hook extended

The precision of setting the angular deflections of the movable surfaces on the model is estimated to be as follows: i_t ±0°5', δ_e ±0°30', δ_f and δ_t ±1°0'.

Power was obtained from a 56-horsepower, three-phase induction motor. The speed of this motor was determined by observation of a cathode-ray oscillograph which indicates the output of a small alternator connected to the shaft of the motor. The time base for the oscillograph pattern is controlled by an audio-oscillator of the electrically driven tuning-fork type, the frequency of which is known within 0.1 percent.

TESTS

Test conditions.- Tests of the complete model were made at dynamic pressures of 9.21 and 16.37 pounds per square foot, which correspond to airspeeds of about 60 and 80 miles per hour. The test Reynolds numbers

were about 685,000 and 910,000 based on the wing mean aerodynamic chord of 1.22 feet. Because of the turbulence factor of 1.6 for the Langley 7- by 10-foot tunnel, effective Reynolds numbers (for maximum lift coefficients) were about 1,000,000 and 1,460,000, respectively.

The tests of the isolated horizontal tail were made at a dynamic pressure of 13 pounds per square foot, corresponding to an airspeed of 71 miles per hour under standard sea-level atmospheric conditions. The test Reynolds number was about 323,000 based on the average chord of 5.81 inches. The turbulence factor is 1.93 for the Langley 4- by 6-foot tunnel, and hence, the the effective Reynolds number (for maximum lift coefficient) was about 624,000 for these tests.

Test procedure.- The thrust calibration of the model propeller was obtained by measuring the resultant drag of the model (cruising configuration) for a range of propeller speeds near zero lift. The thrust coefficients were then computed from the equation

$$T_c' = C_D - C_{D_R}$$

where C_D is the drag of the model with the propeller removed. The torque coefficients were obtained from a motor calibration (torque as a function of minimum current) using the values of minimum current at each propeller speed. The results of the propeller calibration are presented in figure 5.

Using the data of figure 5, it is only necessary to vary the propeller speed for a particular tunnel speed to obtain a range of thrust coefficients assuming that in the normal angle-of-attack range the propeller thrust is independent of the angle of inclination of the propeller at constant nD/V.

The effective thrust coefficients at which the power-on tests were made are shown in figure 6 as a function of lift coefficient for constant power with a constant-speed propeller. These curves were supplied by the manufacturer.

All tests were made at a dynamic pressure of 16.37 pounds per square foot except tests simulating

the take-off power condition in the landing configuration which were made at a dynamic pressure of 9.21 pounds per square foot. This difference was necessitated because of power limitations of the model motor.

The thrust coefficient at which windmilling tests were made was about -0.010.

CORRECTIONS

Langley 7- by 10-foot tunnel.- All data have been corrected for tares caused by the model support strut. Jet-boundary corrections have been applied to the angles of attack, the drag coefficients, and the tail-on pitching-moment coefficients. The corrections were computed as follows:

$$\Delta\alpha = 57.3\ \delta_w \frac{S}{C} C_L \text{ (degrees)}$$

$$\Delta C_D = \delta_w \frac{S}{C} C_L^2$$

$$\Delta C_m = -57.3\left(\frac{\delta_T}{\sqrt{q_t/q}} - \delta_w\right) \frac{S}{C} \frac{dC_m}{di_t} C_L$$

where

δ_w jet-boundary correction factor at the wing (0.116)

δ_T total jet-boundary correction factor at the tail (0.196)

S model wing area (8.55 square feet)

C tunnel cross-sectional area (69.59 square feet)

$\frac{dC_m}{di_t}$ rate of change of pitching-moment coefficient with stabilizer setting as determined in tests

$\frac{q_t}{q}$ ratio of effective dynamic pressure over the horizontal tail to free-stream dynamic pressure

All jet-boundary corrections were added to the test data.

Langley 4- by 6-foot tunnel.- The angles of attack of the tail have been corrected for the effect of the jet boundaries. The correction was added to the measured values and was as follows:

$$\Delta\alpha_t = 1.097C_{L_t} \text{ (degrees)}$$

The lift coefficients were corrected for support-strut tares. No tares or jet-boundary corrections were applied to the hinge-moment coefficients inasmuch as these corrections were estimated to be negligible.

PRESENTATION OF DATA

Tests were made at various stabilizer settings for several power and model conditions. These tests were made with the elevator both fixed at 0° and free to float. Elevator and elevator-tab tests were also made on the complete model for similar power and model conditions. In addition, isolated horizontal-tail characteristics were determined. Several slotted flap deflections were tested. Photographs of tufts placed on the wing were made to determine the stall progression for several power and model conditions.

A short outline of the figures showing the results of the longitudinal stability and control investigation is presented in the following table:

DISCUSSION

Elevator-fixed stability.- The elevator of the XBTK-1 airplane is equipped with a spring tab. With the stick fixed, the elevator, therefore, is not necessarily fixed as is true for a conventional control system without cable stretch. However, neutral points obtained from flight data are generally determined from the variation of elevator angle with velocity rather than the variation of stick position with velocity. Thus, the presence of the spring may be treated as an additional source of flexibility in the control system and neutral points can then be obtained by usual methods. (See reference 1.)

The static margin is positive for all conditions tested at all contemplated airplane center-of-gravity locations. (See fig. 8.) The effect of power on the longitudinal stability was unusually small.

The propeller used on the model was of the same diameter as the scaled-down airplane propeller diameter but the side-force factor was 65.8 as compared to an

airplane value of 91.3. However, a similar difference of model and airplane propeller side-force factors in another investigation was found to give a forward neutral-point shift of less than 0.01 mean aerodynamic chord. Inasmuch as this value is well within the accuracy of the neutral-point calculation, it can be neglected.

An attempt has been made to analyze the effects of power on the longitudinal stability. In order to do this various factors which affect the stability of the airplane have been calculated and are shown on figure 9. It may be shown that for neutral stability and assuming a constant tail lift-curve slope

$$\frac{dC_m}{dC_L} = 0 = \left(\frac{dC_m}{dC_L}\right)_o - \frac{\frac{S_t l_t}{Sc}\left(\frac{\partial C_L}{\partial \alpha}\right)_{t_i} \frac{q_t}{q}\left(1 - \frac{d\epsilon}{d\alpha}\right)}{\left(\frac{dC_L}{d\alpha}\right)_1} + \frac{C_{m_t}}{\frac{q_t}{q}} \frac{d\left(\frac{q_t}{q}\right)}{dC_L} \qquad (1)$$

which reduces to

$$n_p = n_o + \frac{\left|\frac{dC_m}{di_t}\right|}{\left(\frac{dC_L}{d\alpha}\right)_1}\left(1 - \frac{d\epsilon}{d\alpha}\right) - \frac{C_{m_t}}{\frac{q_t}{q}} \frac{d\left(\frac{q_t}{q}\right)}{dC_L} \qquad (2)$$

inasmuch as

$$\left|\frac{dC_m}{di_t}\right| = \frac{S_t l_t}{Sc}\left(\frac{\partial C_L}{\partial \alpha}\right)_{t_i} \frac{q_t}{q}$$

and

$$n_p - n_o = \left(\frac{dC_m}{dC_L}\right)_o \text{ (at the neutral point)}$$

where the notations are as previously defined in the text.

Thus, the relative weight of the various factors which contribute both favorably and unfavorably to the longitudinal stability can be estimated for any condition from the preceding equations. In addition, the effects of power can be separated to some degree.

In the cruising configuration and at moderate lift coefficients the model has more stability with take-off power than it does with the propeller windmilling. Using figures 7 and 9 to obtain the values of the various stability determinants at $C_L = 0.8$, it is found from equation (2) that the stabilizing effects of a rearward movement of n_o (0.055 mean aerodynamic chord) and of increased $\frac{d(q_t/q)}{dC_L}$ at the tail (0.030 mean aerodynamic chord) more than compensate for the 0.060 mean aerodynamic chord loss in stability caused mainly by a higher value of $\partial\epsilon/\partial\alpha$ with power. Thus, the total change in stability due to power at $C_L = 0.8$ as determined from the summation of individual effects is found to be a 0.025 mean aerodynamic chord rearward shift of the neutral point. This value compares with the measured value of 0.022 mean aerodynamic chord (fig. 8). The discrepancy is quite small in this instance and, in general, it is believed to be within the accuracy of the neutral-point determination (approximately 0.02 mean aerodynamic chord).

At very low-lift coefficients the stability in the cruising configuration becomes less power on than power off. This is seen to be chiefly caused by the rate of change of dynamic pressure at the tail. For while at a higher coefficient $\frac{d(q_t/q)}{dC_L}$ is responsible for a favorable effect, $\Delta n_p = 0.03$ mean aerodynamic chord, at $C_L = 0.2$ an adverse shift of $\Delta n_p = 0.015$ is realized. The main reason for this change is that the tail load for trim is negative and hence favorable at higher lift coefficients but becomes positive at low values of C_L.

In the landing configuration the change in neutral-point location with the application of power is fairly constant, small, and always stabilizing. (See fig. 8.) This may be explained by the extremely

large rearward shift in tail-off aerodynamic center location with power. The difference in n_o increases at high lifts and thus counteracts the loss in the stability contributed by the empennage, inasmuch as progressively larger values of $d\epsilon/d\alpha$ and $\frac{d(q_t/q)}{dC_L}$ are both destabilizing.

Some of the design features, which may in part account for the small change in stability with power through the lift range as well as the over-all satisfactory stability characteristics, are the high location of the horizontal tail and rectangular inboard wing panels with constant chord flaps. Data showing favorable effects of the two aforementioned model features can be found in reference 2. In addition, the design center-of-gravity location is considerably below the thrust line so that the direct thrust moment is favorable.

Elevator-free stability.- The static margin will be positive for all conditions tested at all contemplated airplane center-of-gravity locations with the elevator free (fig. 11).

In general, the elevator-free neutral points are from 0 to 6 percent mean aerodynamic chord farther aft than the corresponding elevator-fixed neutral points for similar conditions. Compare figures 11 and 8. An exception to this trend is found in the take-off power condition, in the landing configuration, and at high lift coefficients where the stability is considerably less with the elevator free.

It can be seen from the isolated-tail data of figure 12 that the ratio of the hinge-moment parameters $-\frac{\left(\partial C_{h_e}/\partial\alpha\right)_{t_i}}{\left(\partial C_{h_e}/\partial\delta\right)_{t_i}}$ which determines the floating characteristics of the elevator is of such sign as to cause the elevator to float against the relative wind and thus increase the tail effectiveness and hence the stability (inasmuch as $d\epsilon/d\alpha$ is less than unity). Apparently, however, in the landing configuration with take-off power $\left(dC_{h_e}/d\alpha\right)_t$ becomes negative at high-lift coefficients (fig. 14(e)) thus reducing the tail effectiveness. It might be noted

that this change in $\left(dC_{h_e}/d\alpha\right)_t$ is probably a result of the nonlinear hinge-moment characteristics (fig. 12) combined with a large reduction in tail angle of attack over the right inboard portion of the tail and a similar increase in angle of attack over the left inboard portion which is caused by right-hand propeller operation (reference 3). The greatest part of the decrease in stability is not thought to be caused by a reduction in tail effectiveness due to negative $\left(dC_{h_e}/d\alpha\right)_t$ but rather by the rate of change of tail effectiveness with lift coefficient. Thus, in order to determine the power effects with the elevator free, the following term must be added to equation (2):

$$\frac{-C_{m_t}}{\left(\frac{dC_L}{d\alpha}\right)_t} \frac{d\left(\frac{dC_L}{d\alpha}\right)_t}{dC_L}$$

where the notation used has been previously defined.

The elevator-free curves shown as dashed lines on figures 10(a) and 10(b) were obtained by cross-plotting the hinge-moment data of figures 14(a) and 14(b). This was necessary inasmuch as severe oscillations of the elevator occurred with the stabilizer incidence set at a value lower than 3° or 4° in the cruising configuration. This might be attributed to a positive value of $\left(dC_{h_e}/d\alpha\right)_t$.

The presence and type of oscillations on the airplane will depend on such factors as control surface and airplane inertia, control system friction, stability, and certain other factors. (See reference 4.)

Isolated horizontal tail.- A series of tests was made for various elevator and elevator-tab settings on the isolated horizontal tail. (See figs. 12 and 13.) The elevator-free curve, shown on figure 12, was obtained using the hinge-moment data. The difference between the hinge-moment curves at zero tab and elevator deflections (figs. 12 and 13) may be attributed to the fact that these tests were run at different times and the differences in the two curves are an indication of the experimental accuracy.

The following table summarizes the elevator parameters:

	Original	Gap sealed	Elevator free
$\left(\frac{\partial C_L}{\partial \alpha}\right)_{t_i}$	0.0565	0.0575	0.069
$\left(\frac{\partial C_L}{\partial \delta}\right)_{t_i}$	.034	------	-----
$\left(\frac{\partial C_{h_e}}{\partial \alpha}\right)_{t_i}$	= 0.000 (average for two tests)	------	-----
$\left(\frac{\partial C_{h_e}}{\partial \delta}\right)_{t_i}$	-0.0057	------	-----

As is shown by the preceding table, sealing the gap increased the lift-curve slope by about 2 percent, which is of the expected magnitude inasmuch as the gap was only from about 0.001 to $0.002c_t$.

The slope of the elevator-free lift curve showed about a 22-percent average increase over the elevator-fixed slope. Although this appears contradictory in view of the tabulated value of $\left(\partial C_{h_e}/\partial \alpha\right)_{t_i}$, it must be remembered that the hinge-moment characteristics are nonlinear and the tabulated value is an average value of slopes measured over a small angle-of-attack range at the origin.

The tab effectiveness $\left(\partial C_{h_e}/\partial \delta_t\right)_{t_i}$ averaged about -0.0053 at moderate deflections in the angle-of-attack range likely to be encountered under normal operating conditions of the airplane.

Effect of elevator and elevator-tab deflection.- The elevator effectiveness as determined from figure 14(a) is about 0.9 as high as that obtained from isolated-tail data using the relationship

$$\frac{\partial C_m}{\partial \delta_e} = -\left(\frac{\partial C_L}{\partial \delta_e}\right)_{t_i} \times \frac{S_t l_t}{Sc} \qquad (3)$$

where the symbols have been previously denoted in the text. This effectiveness ratio of 0.9 indicates that the average dynamic pressure over the elevator on the complete model is about 0.9 of the free stream q.

The data (fig. 14) indicate that the elevator should be sufficiently powerful to trim the airplane at any speed away from the ground for all conditions.

As has been stated earlier in the text, a large degree of the aerodynamic balance of the elevator is supplied by a spring tab. Although it is beyond the scope of this paper to present detailed control-force characteristics, estimates using the hinge-moment data of figures 14 and 15 indicate that the control forces for conditions of steady flight will be very light if the spring stiffness contemplated for the prototype airplane is used. However, since it is believed to be a relatively simple task to change the spring constant on the airplane, no major difficulty is likely to be encountered in obtaining a spring constant which will give satisfactory stick-force characteristics.

The power-off tab effectiveness $dC_{h_e}/d\delta_t$ (figs. 15 (a) and 15(c)) agrees well with that obtained from isolated-tail tests. It might be noted that the ratio of $\frac{dC_{h_e}}{d\delta_t} / \frac{dC_{h_e}}{d\delta_e}$ increases with C_L for the power-on conditions, indicating that the average dynamic pressure over the tab is greater than that over the elevator. This increases the spring-tab effectiveness but has no bearing on elevator-free stability inasmuch as the tab is not used for trimming purposes.

It may also be noted from the data of figure 15 that tab deflection appears to have a considerable effect on the pitching-moment curve. It is believed, however, that the neutral-point location will be negligibly affected by tab deflection because of the small spring-tab deflections which will be required with trim elevator deflections at the center of gravity for neutral stability.

Effect of slotted-flap deflection.- Tail-off data were obtained at various slotted-flap deflections. (See fig. 16.) The maximum lift coefficients obtained from this figure are tabulated in the following table and have been corrected for tail load required for trim at the design center-of-gravity location.

Configuration	δ_f (deg)	$C_{L_{max}}$
Cruising	0	1.34
Landing	30	1.79
↓	35	1.78
	40	1.84
	45	1.84

The change in maximum lift coefficient when the flap deflection is increased from 30° to 45° is seen to be quite small. It may also be seen that at angles of attack slightly below the stall an appreciable increment in lift is obtained when the flap deflection is increased in the higher range.

Stalling characteristics.- Photographs of the tufts showing the stall progression are shown for the different model configurations. (See figs. 17 through 22.)

In the windmilling, cruising configuration, the stall appears to start at the trailing edge slightly inboard of the fold line. As the angle of attack is increased the stall progresses forward over the inboard wing panel while not progressing markedly toward the tip. The final photograph (fig. 17) at $\alpha = 17.3°$ shows the inboard wing panels almost completely stalled while over a large portion of the outboard panel the flow is merely unsteady. Removal of the radar, wing tank, and guns seems to have a very slight effect on the stall progression in the cruising configuration. (Compare figs. 17 and 18.) When take-off power is applied in the cruising condition, the portion of the wing immersed in the slipstream remains unstalled after most of the remainder of the wing is stalled. The stall appears to be earlier and more pronounced over the left inboard wing panel than it is over the right panel which might be expected for right-hand propeller operation (fig. 19).

In the landing condition, with the propeller windmilling, the flaps appear to be generally stalled or in a region of unsteady flow at low angles of attack. As the angle of attack increases, the flow through the slot improves and the flaps become unstalled. The wing remains unstalled up to about 15° or 16° angle of attack. The stall then begins at the left inboard fold line spreading inboard much more rapidly than it progresses toward the tip. The last photograph on figure 20 shows that while a good portion of the left panel is stalled, the right panel is either unstalled or only in a region of unsteady flow at $\alpha = 18.1°$, except at the extreme right wing tip where stall has begun. The pictures on figure 21, guns, radar, and fuel tank off would seem to indicate that the absence of the latter auxiliary equipment causes stall over the left inboard panel much earlier than is shown in figure 20 (auxiliary equipment on). The reason for this effect is not known. Otherwise, except for a lesser tendency for tip stall on the right wing tip, the progression of the stall with and without the auxiliary equipment is similar. The chief effect of power on the stall is again a stall delay in regions close to the wing-fuselage juncture (fig. 22).

Because of differences in scale, the amount of stall indicated at each angle may differ from that on the full-scale airplane but the stall progression should be correct.

CONCLUSIONS

The results of the longitudinal stability and control investigation of a 0.15-scale model of the XBTK-1 airplane indicate that:

1. The longitudinal stability will probably be satisfactory for all probable flight conditions at the rearmost center-of-gravity location with the elevator both fixed and free. Power effects were quite small.

2. Sufficient elevator control will be available to trim in any flight condition away from the ground. Indications are that the stick forces may be light if the spring stiffness now contemplated is used.

3. Increasing the slotted flap deflection above 30° increased $C_{L_{max}}$ only slightly.

4. Stalling characteristics will probably be satisfactory. In general, stall started at the wing fold line and spread inboard faster than toward the tip. Power delayed stall over portions of the wing immersed in the slipstream. The presence of the fuel tank, radar, and wing guns do not appreciably affect the stall trends.

Langley Memorial Aeronautical Laboratory
National Advisory Committee for Aeronautics
Langley Field, Va.

REFERENCES

1. Schuldenfrei, Marvin: Some Notes on the Determination of the Stick-Fixed Neutral Point from Wind-Tunnel Data. NACA RB No. 3I20, 1943.

2. Weil, Joseph, and Wells, Evalyn G.: Wind-Tunnel Tests of the 1/8-Scale Powered Model of the Curtiss XBTC-2 Airplane. I - Preliminary Investigation of Longitudinal Stability. NACA MR, June 1, 1944.

3. Pass, H. R.: Wind-Tunnel Study of the Effects of Propeller Operation and Flap Deflection on the Pitching Moments and Elevator Hinge Moments of a Single-Engine Pursuit-Type Airplane. NACA ARR, July 1942.

4. Greenberg, Harry, and Sternfield, Leonard: A Theoretical Investigation of Longitudinal Stability of Airplanes with Free Controls Including Effect of Friction in Control System. NACA Rep. No. 791, 1944.

TABLE I

DESCRIPTION OF FLEETWINGS XBTK-1 AIRPLANE

Name and type	XBTK-1 (Navy dive-torpedo bomber)
Engine	Pratt & Whitney R-2800-22W
Ratings:	
Normal power	1700 bhp at 2600 rpm at sea level 1700 bhp at 2600 rpm at 7000 ft 1450 bhp at 2600 rpm at 18,500 ft
Take-off power	2100 bhp at 2800 rpm at sea level
Military power	2100 bhp at 2800 rpm at 1000 ft 1600 bhp at 2800 rpm at 16,000 ft
Propeller	Hamilton Standard
Diameter, ft	13.58
Blades (number and designation)	four, 2C15B1
Gear ratio	0.45
Activity factor	95.6
Blade thickness $(h/b)_{0.75R}$	0.060
Normal gross weight, lb	14,850
Over-all length, ft	39.0
Over-all height, ft	11.86
Wing span, ft	48.67

NATIONAL ADVISORY
COMMITTEE FOR AERONAUTICS

TABLE II

AIRPLANE WING-AND TAIL-SURFACE DATA

	Wing	Horizontal tail	Vertical tail
Area, sq ft	380	80	[a]51.25
Span, ft	48.67	18.5	8.38
Aspect ratio	6.23	4.26	1.42
Taper ratio	.50	.59	----------
Dihedral, deg	8.25	0	----------
Incidence, deg	2	2 to -7	0
Geometric twist, deg	-2.2	0	0
Root section	NACA 2416	NACA 66.2-015 modified	NACA 66.2-015 modified
Tip section	NACA 4412	NACA 66.2-009 modified	NACA 66.2-009 modified
Mean aerodynamic chord, ft	8.17	----------	----------
Root chord, ft	9.17	5.45	6.89
Theoretical tip chord, ft	4.585	3.20	2.67

[a]Includes dorsal fin.

NATIONAL ADVISORY
COMMITTEE FOR AERONAUTICS

TABLE III

AIRPLANE CONTROL-SURFACE DATA

	Ailerons	Elevators	Rudder	Flaps	Dive brakes
Percent span	54.0	95.0	100	43.1	Upper 31.4 Lower 35.1
Area, aft of hinge line, sq ft	36.86	22.50	15.66	42.0	----------
Balance area, sq ft	15.11	2.96	[a]5.02	-----	----------
Trim-tab area, sq ft	[b].52	None	1.00	-----	----------
Percent span	2.8	----------	23.0	-----	----------
Tab travel, deg	±15	----------	±5	-----	----------
Balance tab area, sq ft	2.76	3.36	1.00	-----	----------
Percent span	13.3	35.7	23.0	-----	----------
Tab travel, deg	±15(±30 lb)	±15(±55 lb)	±15(δ_t=-0.51δ_r)	-----	----------
Control travel, deg	±15	15, -25	±30	45	[c]Upper 73 Lower 80
Root mean square chord, ft	1.37	1.27	1.90	2.06	Upper 1.45 Lower 1.55
Distance to hinge line from normal c.g. (25.6), ft	----------	22.00	23.67	-----	----------

[a]1.20-square-foot horn.
[b]Left aileron only.
[c]Measured from airfoil contour.

Flap deflections (corresponding powers)

Landing, deg . . . . . 45 (power off)
Take-off, deg . . . . . 32.5 (2100 hp)
All other conditions . flaps retracted

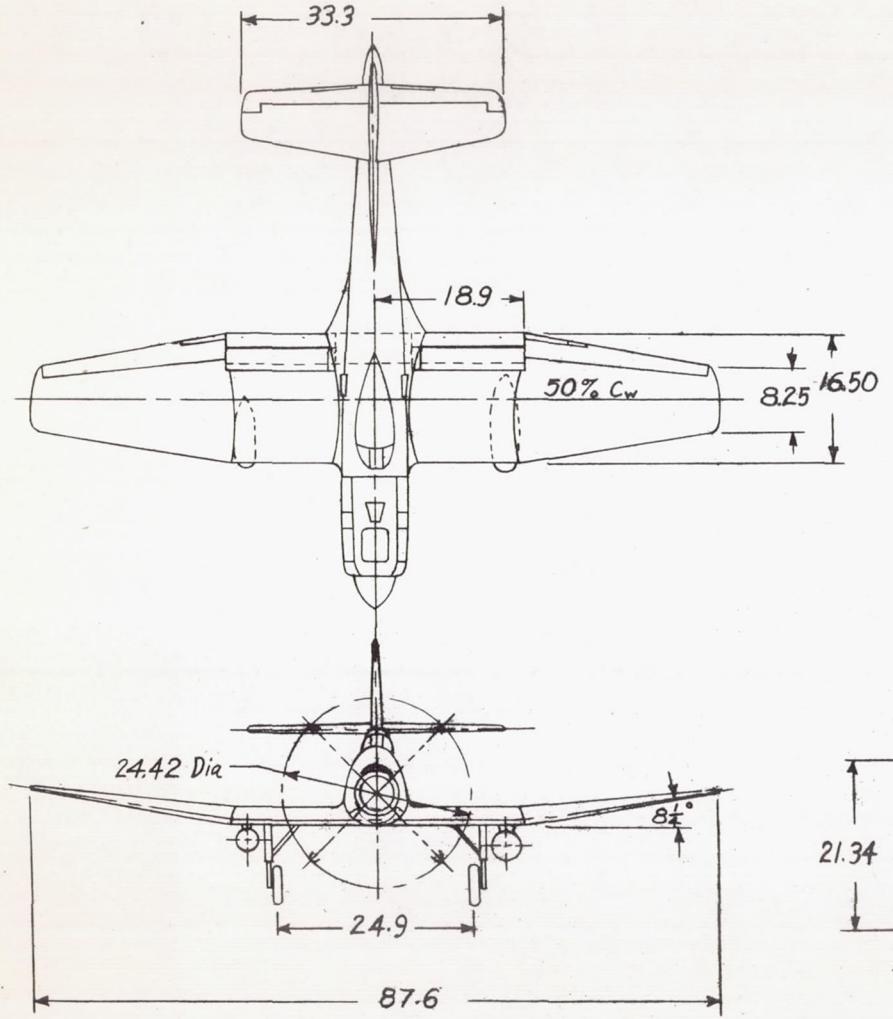

Root section - NACA 2416
Tip section - NACA 4412
Wing area - 8.55 ft.²
M.A.C. = 14.64 in.
Design CG (Wheels up) 25.6 % MAC
Taper ratio, outboard panel - .50
Geometric twist of outboard panel - -2.2°
Incidence of inboard panel - 2°0'

All dimensions in inches

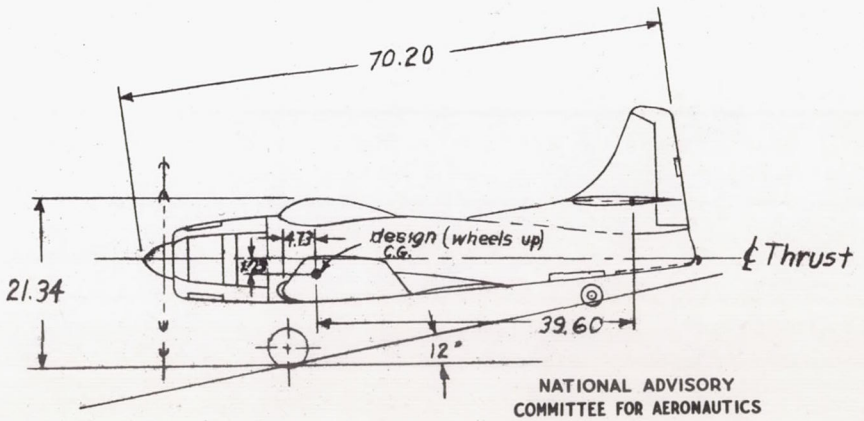

Figure 1 .- Three view drawing of 0.15-scale model of Fleetwings XBTK-1 airplane.

MR No. L5D27a

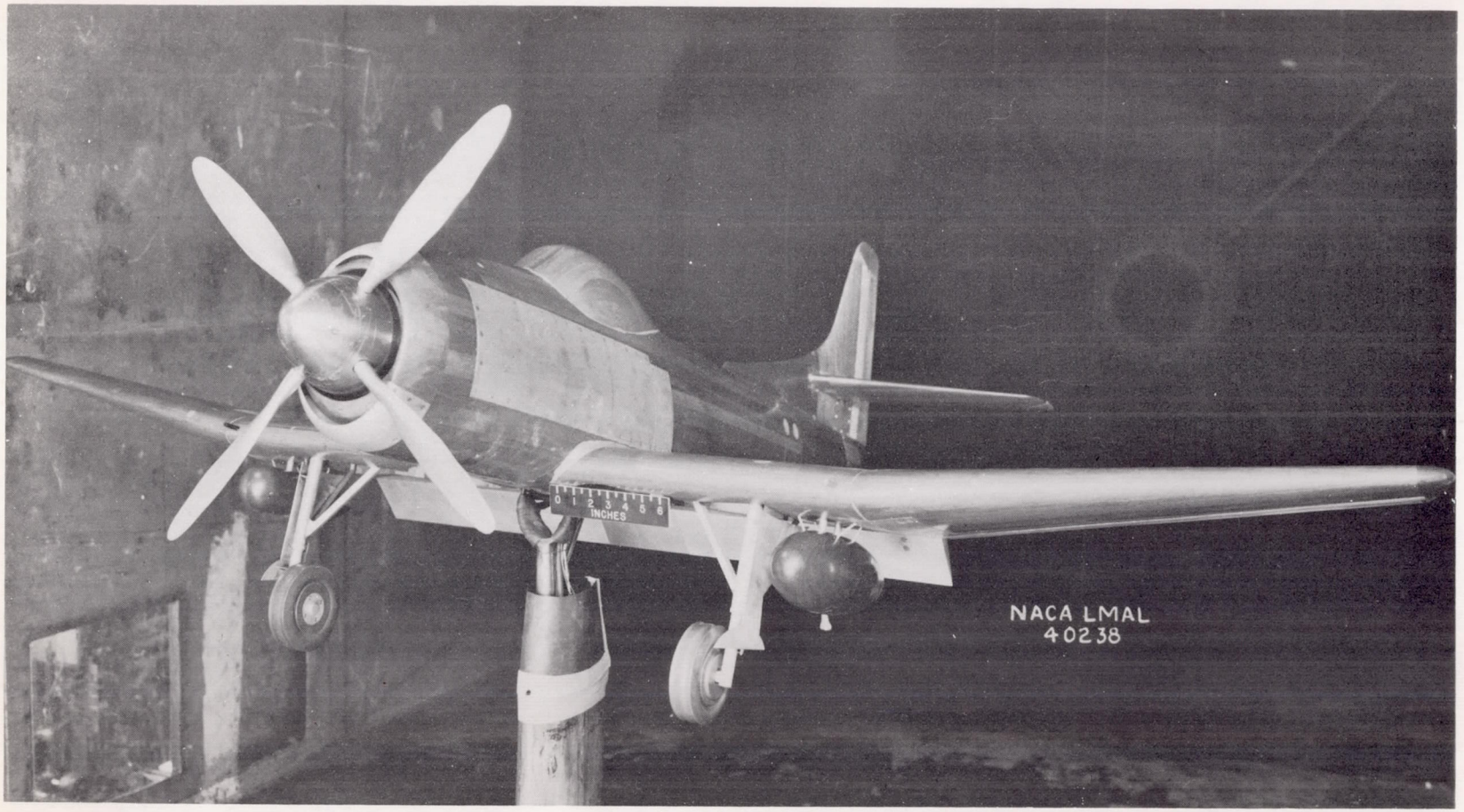

Figure 2(a).- Three-quarter front view of the 0.15-scale model of the XBTK-1 airplane.

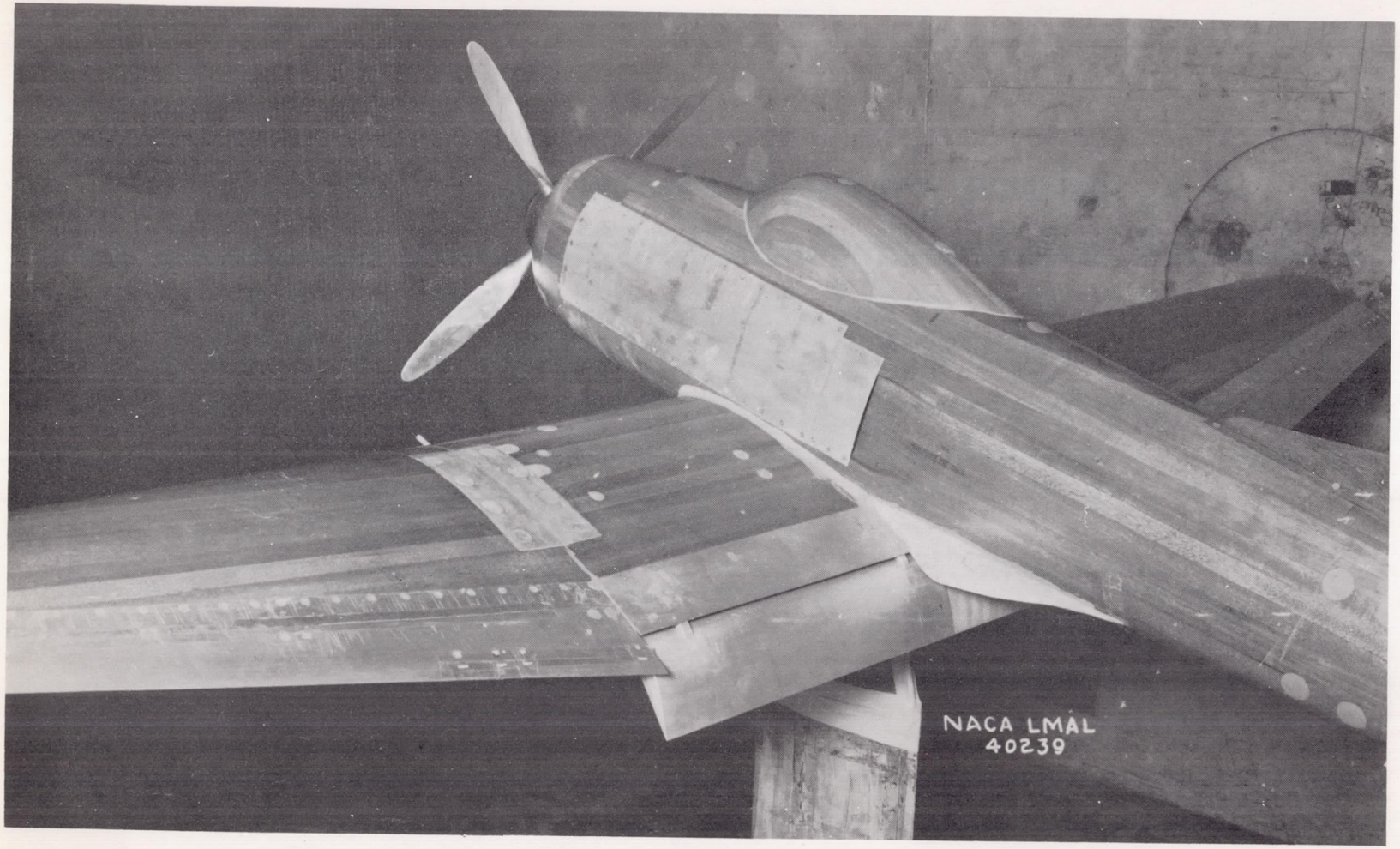

Figure 2(b).- Three-quarter rear view of the 0.15-scale model of the XBTK-1 airplane.

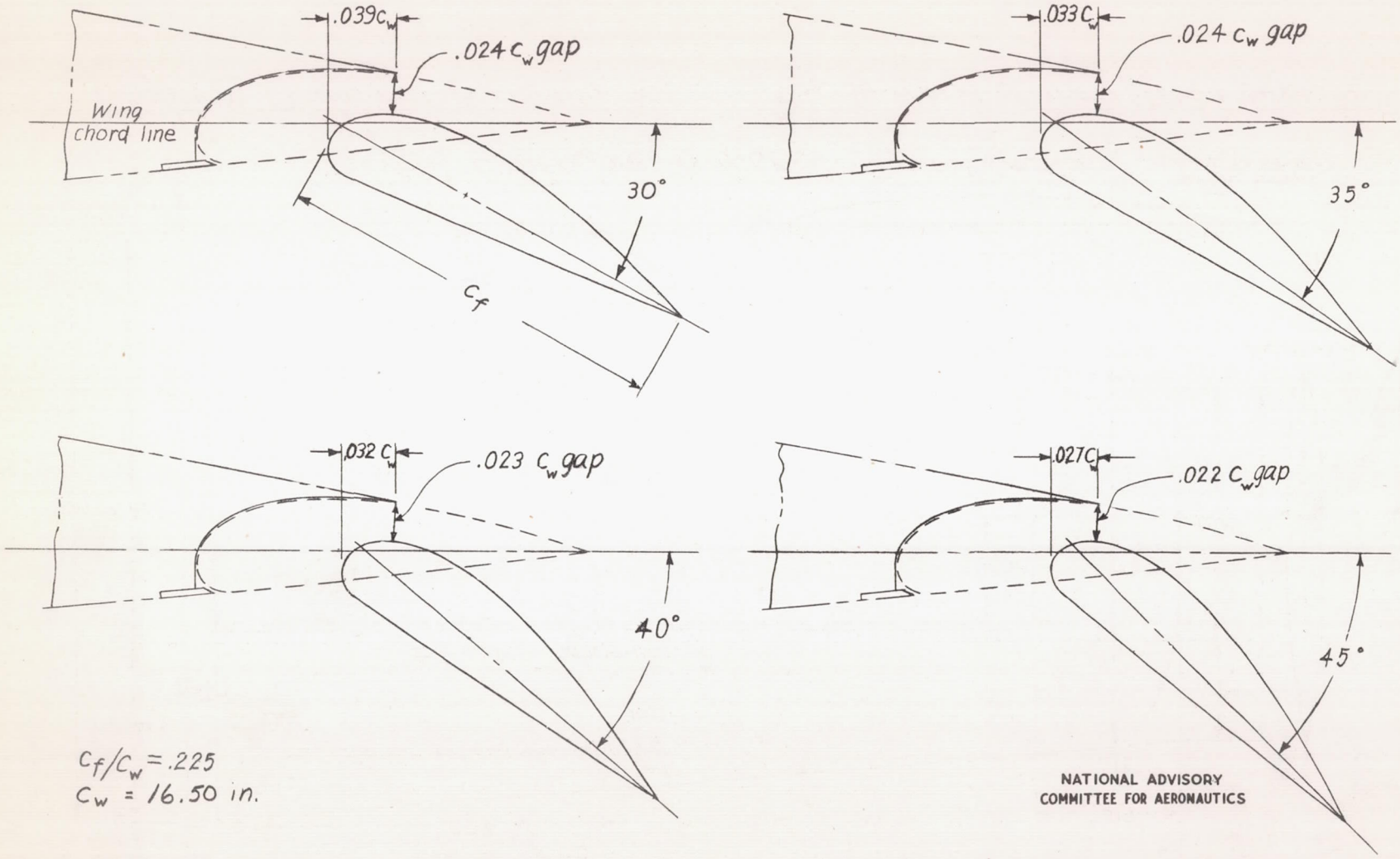

Figure 3 -- Details of slotted flap positions for various deflections tested on the 0.15 scale model of the XBTK-1 airplane.

MR No. L5D27a

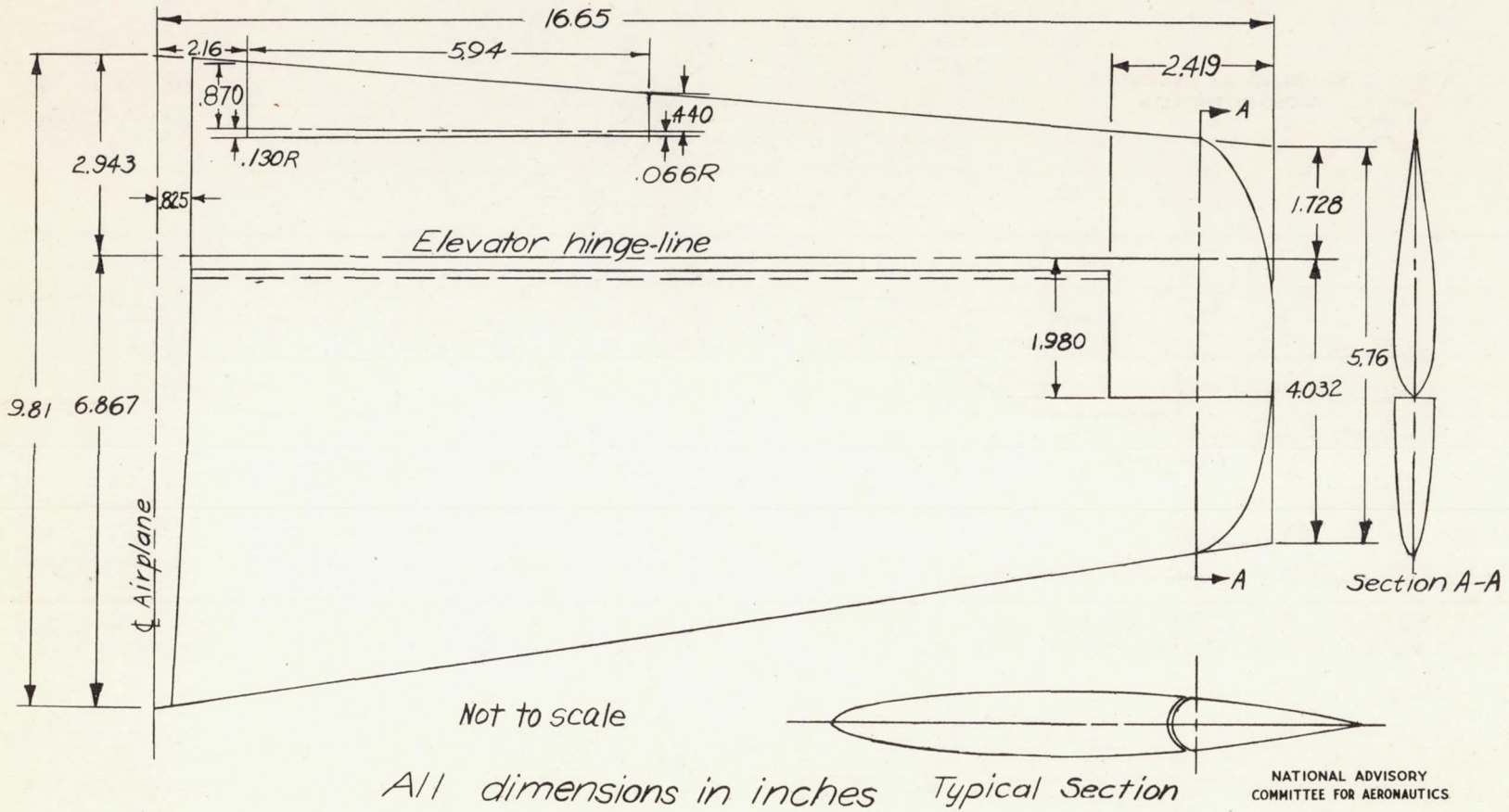

Figure 4.- Drawing of horizontal tail of 0.15-scale model of the XBTK-1 airplane

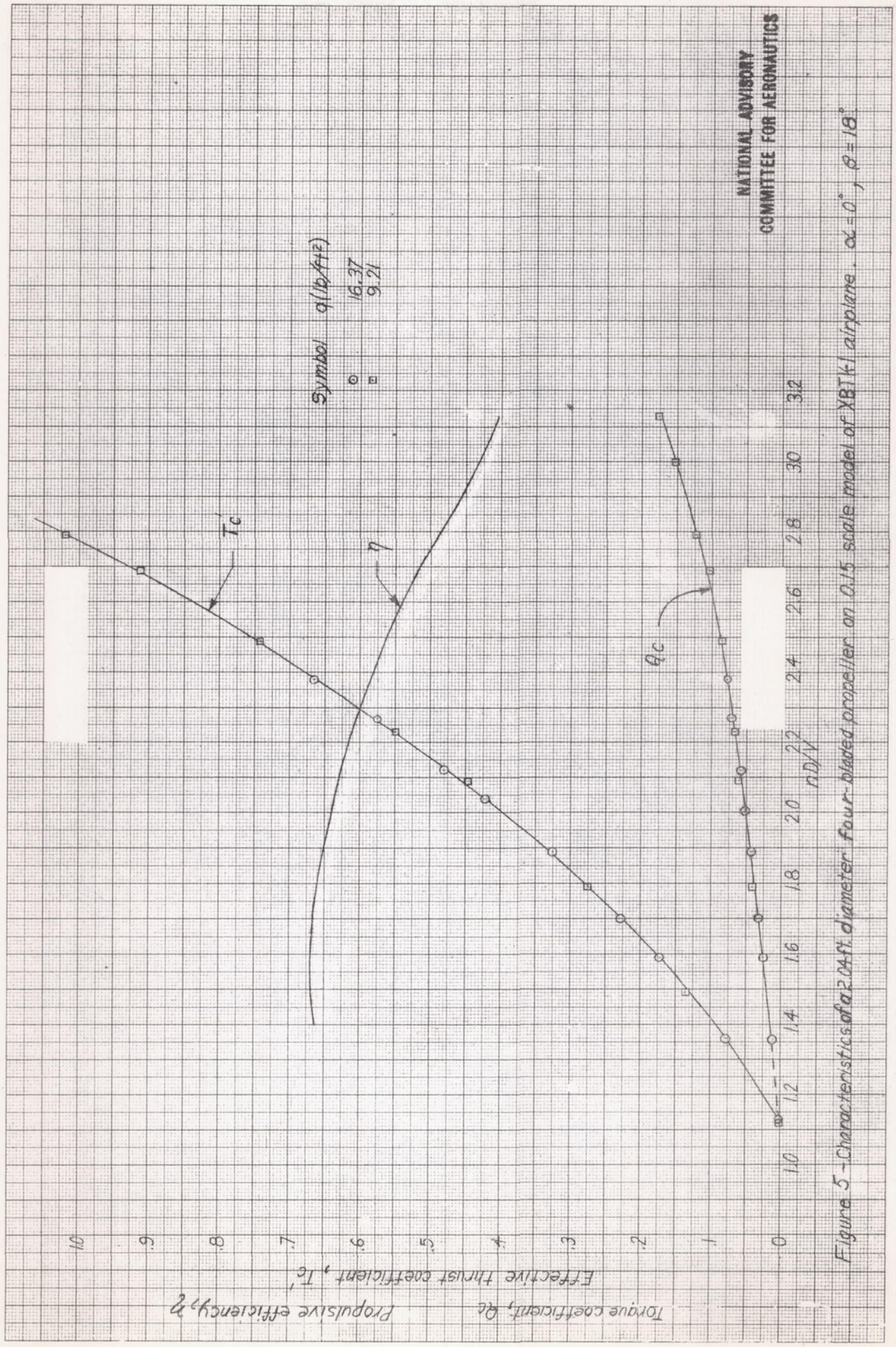

Figure 5.- Characteristics of a 2.04-ft. diameter four-bladed propeller on 0.15 scale model of XBT-1 airplane. $\alpha = 0°$, $\beta = 18°$.

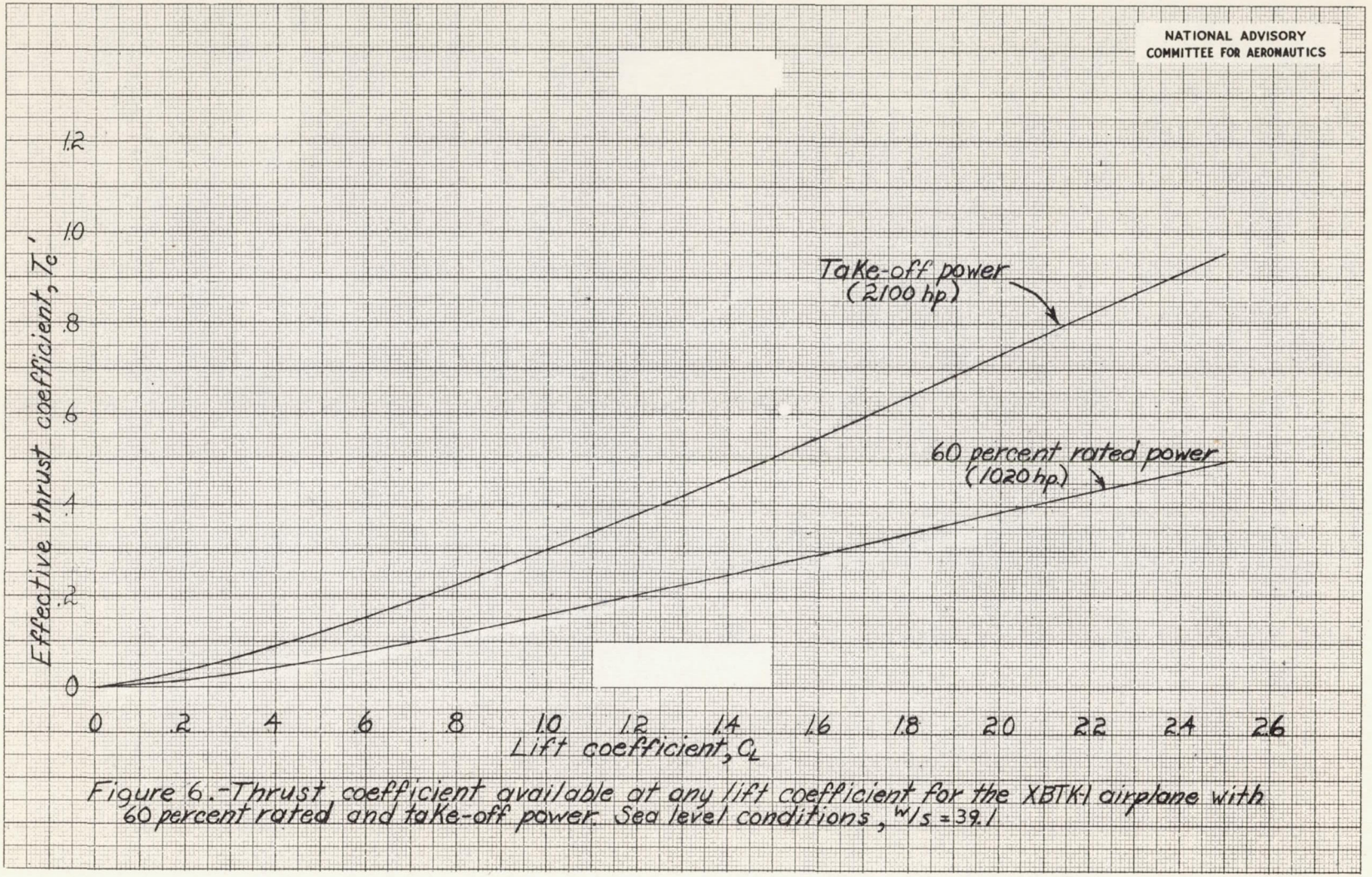

Figure 6.-Thrust coefficient available at any lift coefficient for the XBTK-1 airplane with 60 percent rated and take-off power. Sea level conditions, $W/S = 39.1$

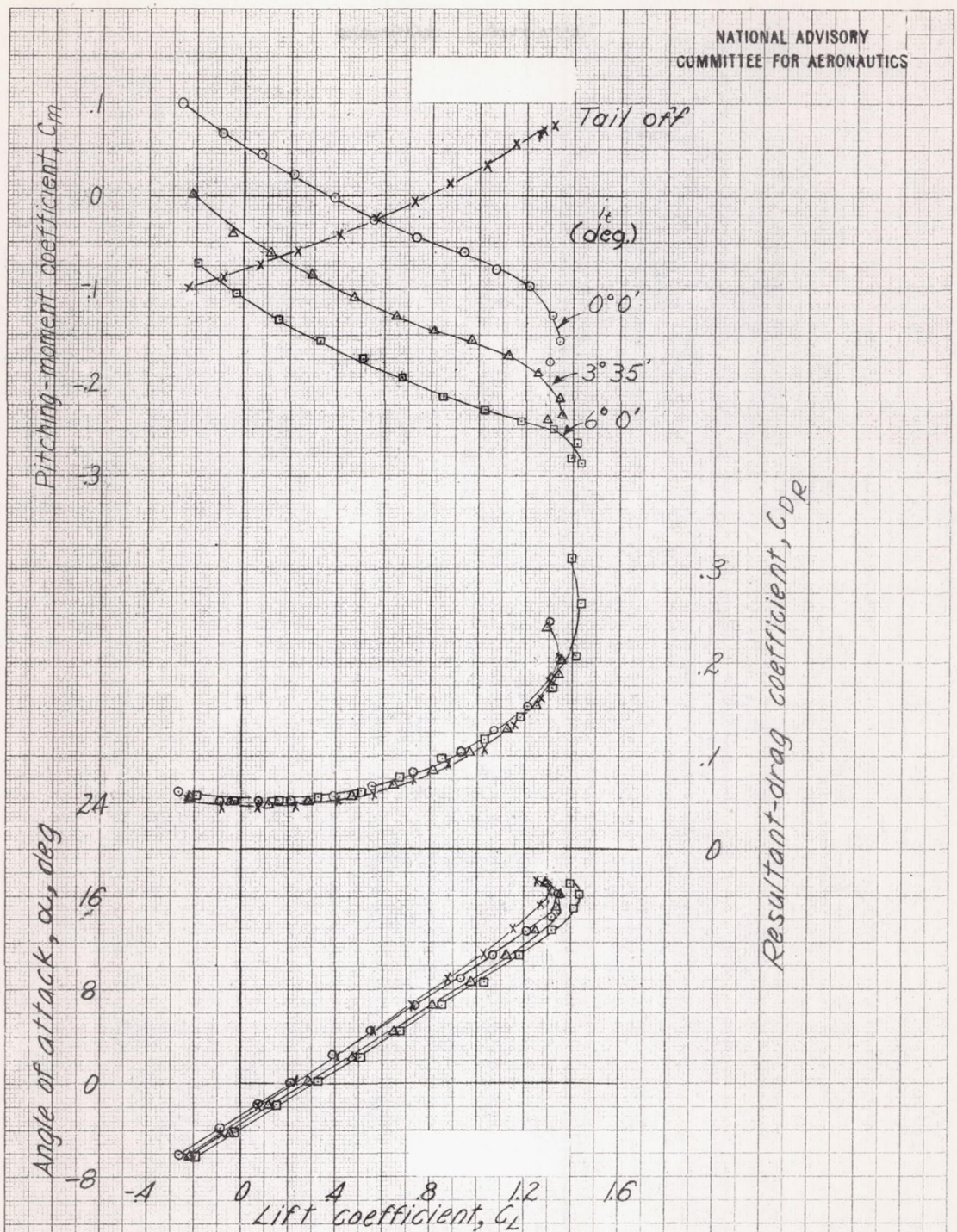

(a) Windmilling, cruising configuration

Figure 7.- Effect of stabilizer on the aerodynamic characteristics in pitch of the 0.15-scale model of the XBTK-1 airplane.

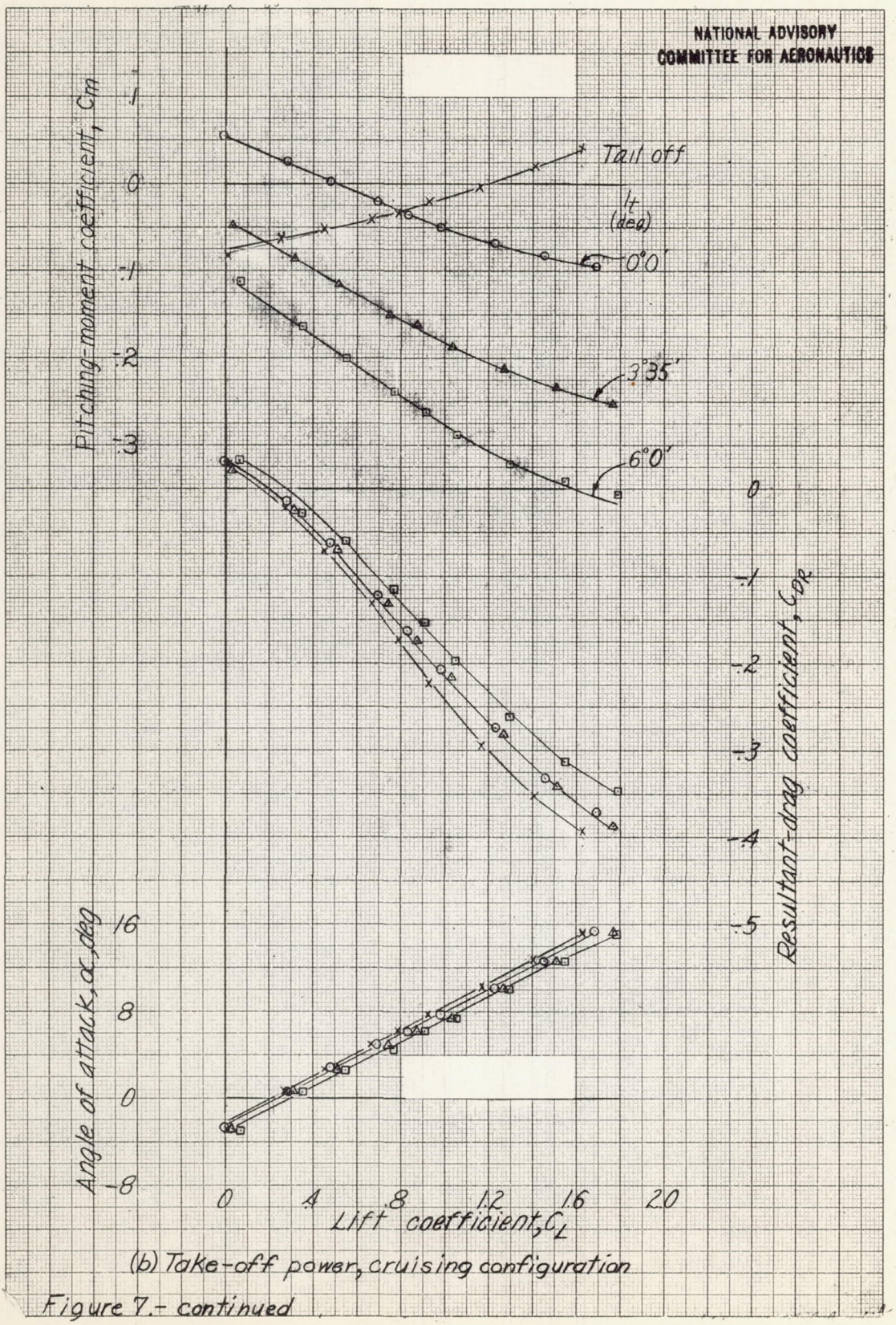

(b) Take-off power, cruising configuration

Figure 7.- continued

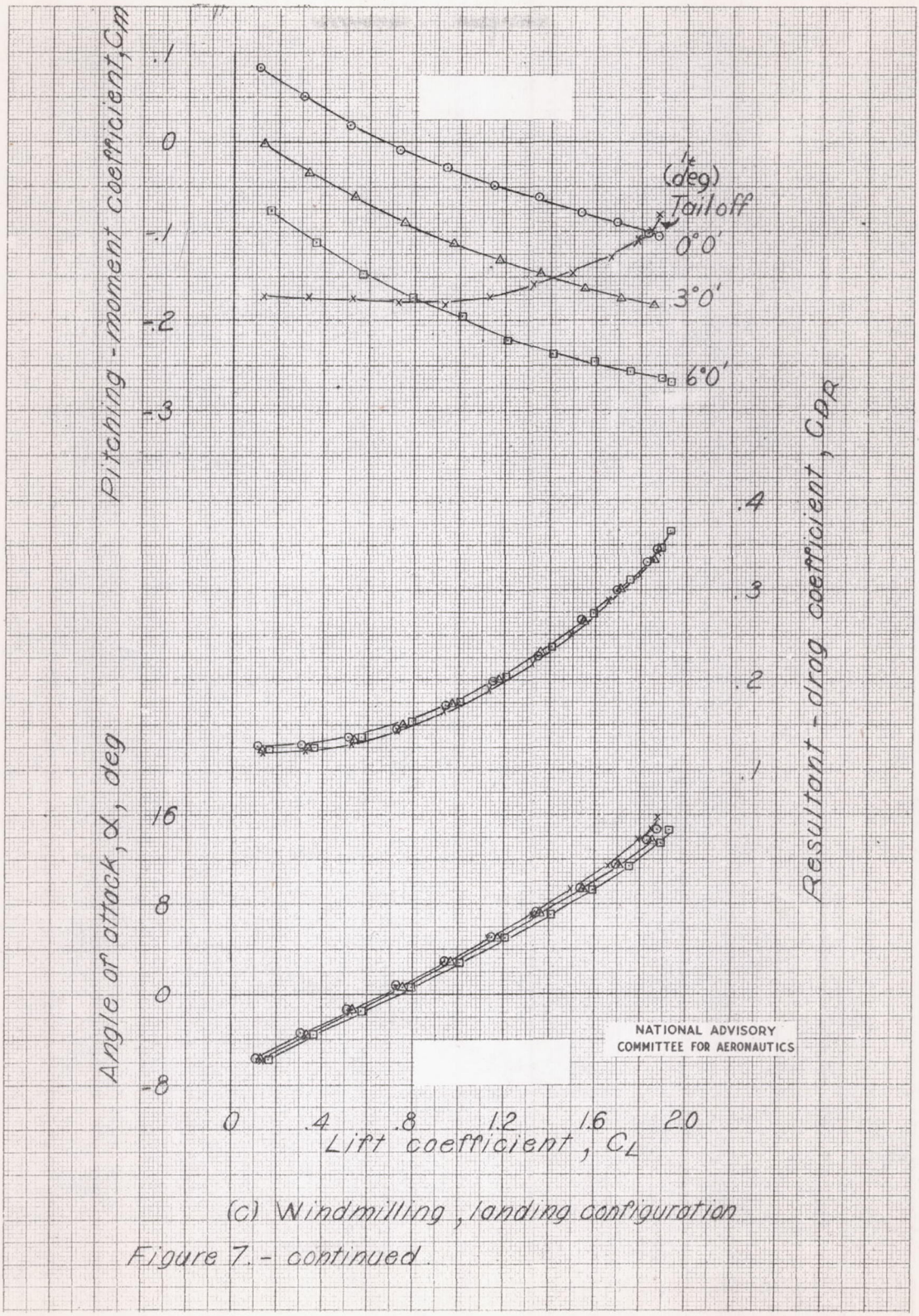

(c) Windmilling, landing configuration

Figure 7. - continued.

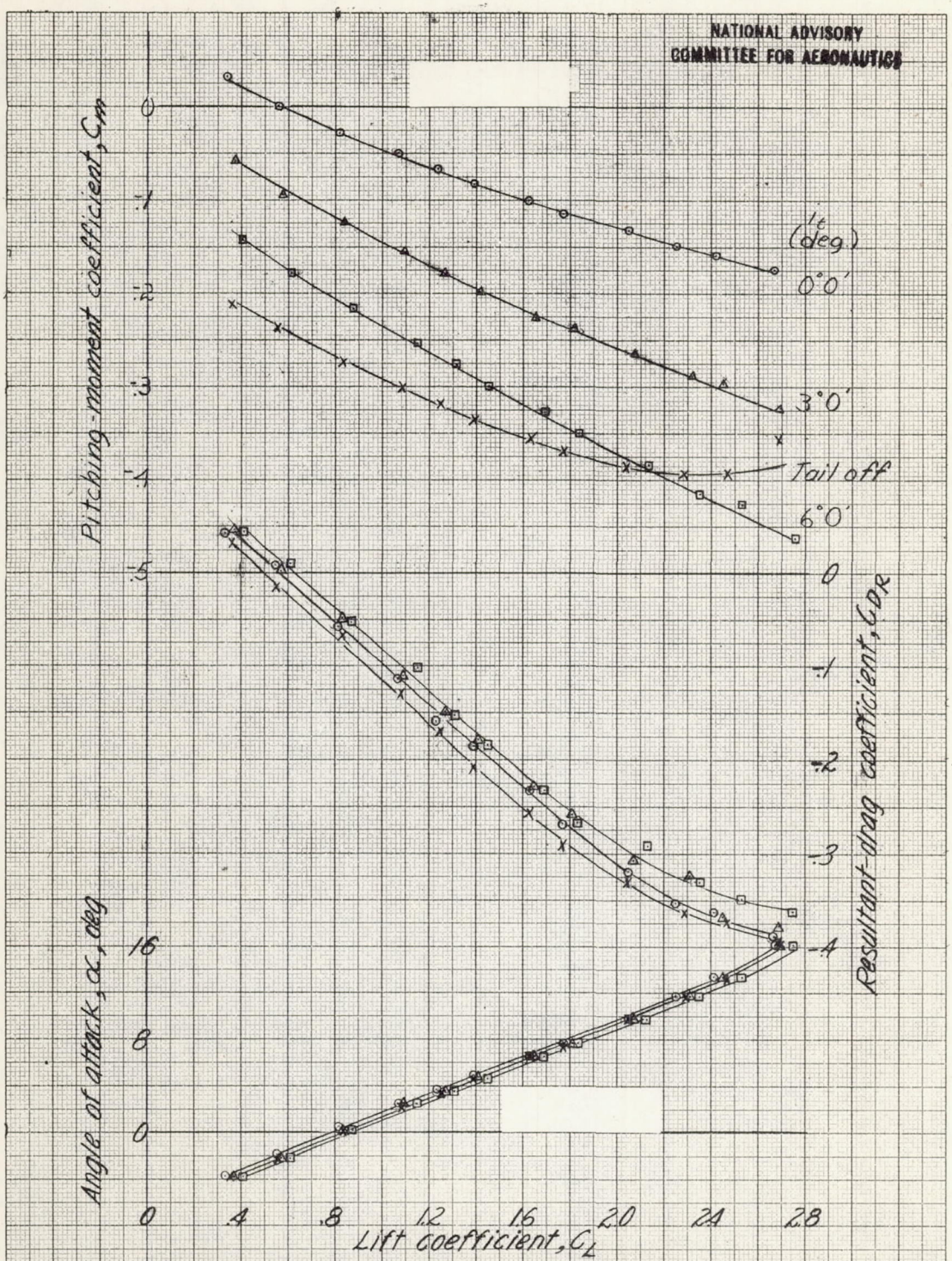

(d) Take-off power, landing configuration

Figure 7.- concluded

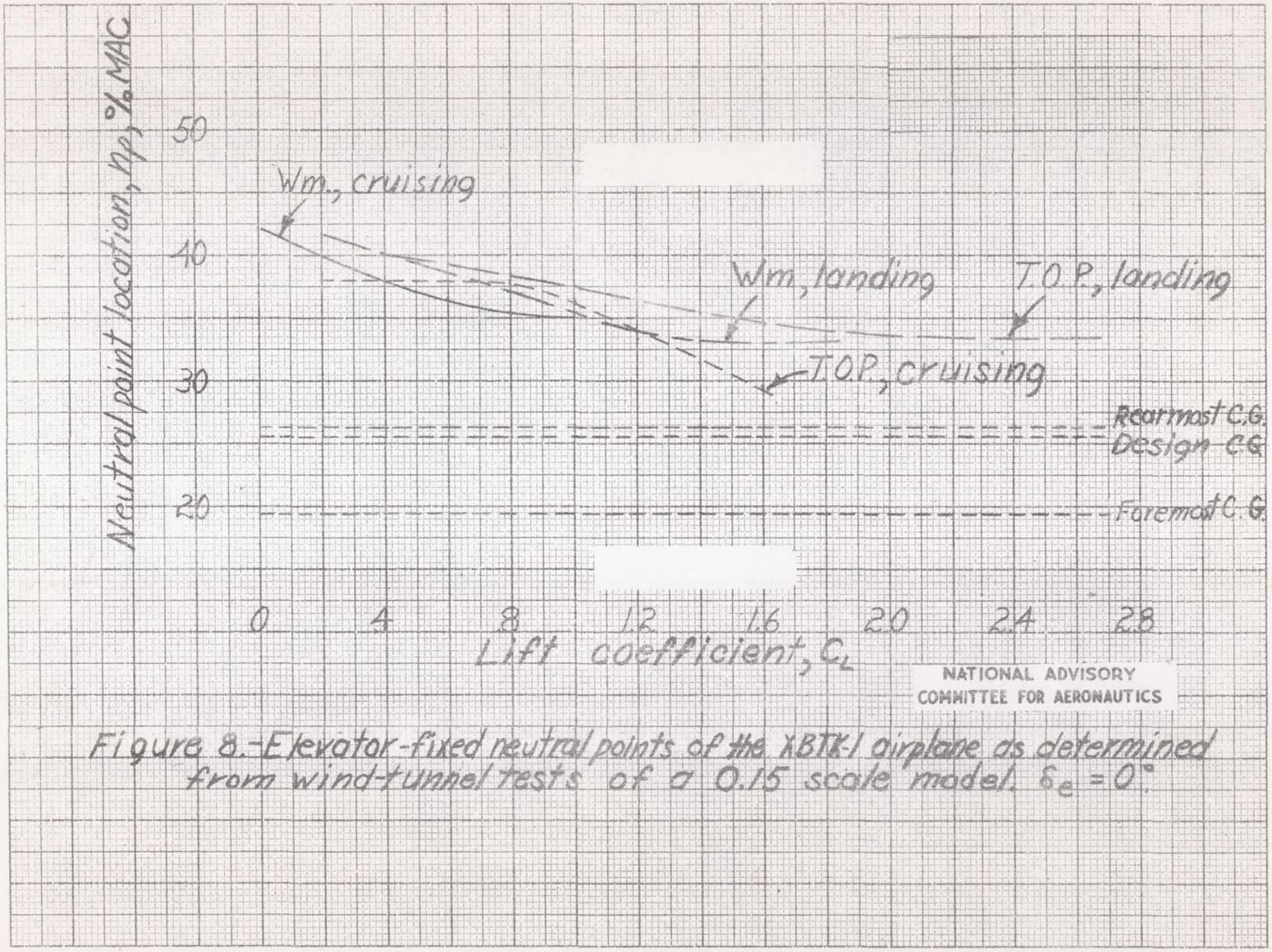

Figure 8.-Elevator-fixed neutral points of the XBTK-1 airplane as determined from wind-tunnel tests of a 0.15 scale model. $\delta_e = 0°$.

MR No. L5D27a

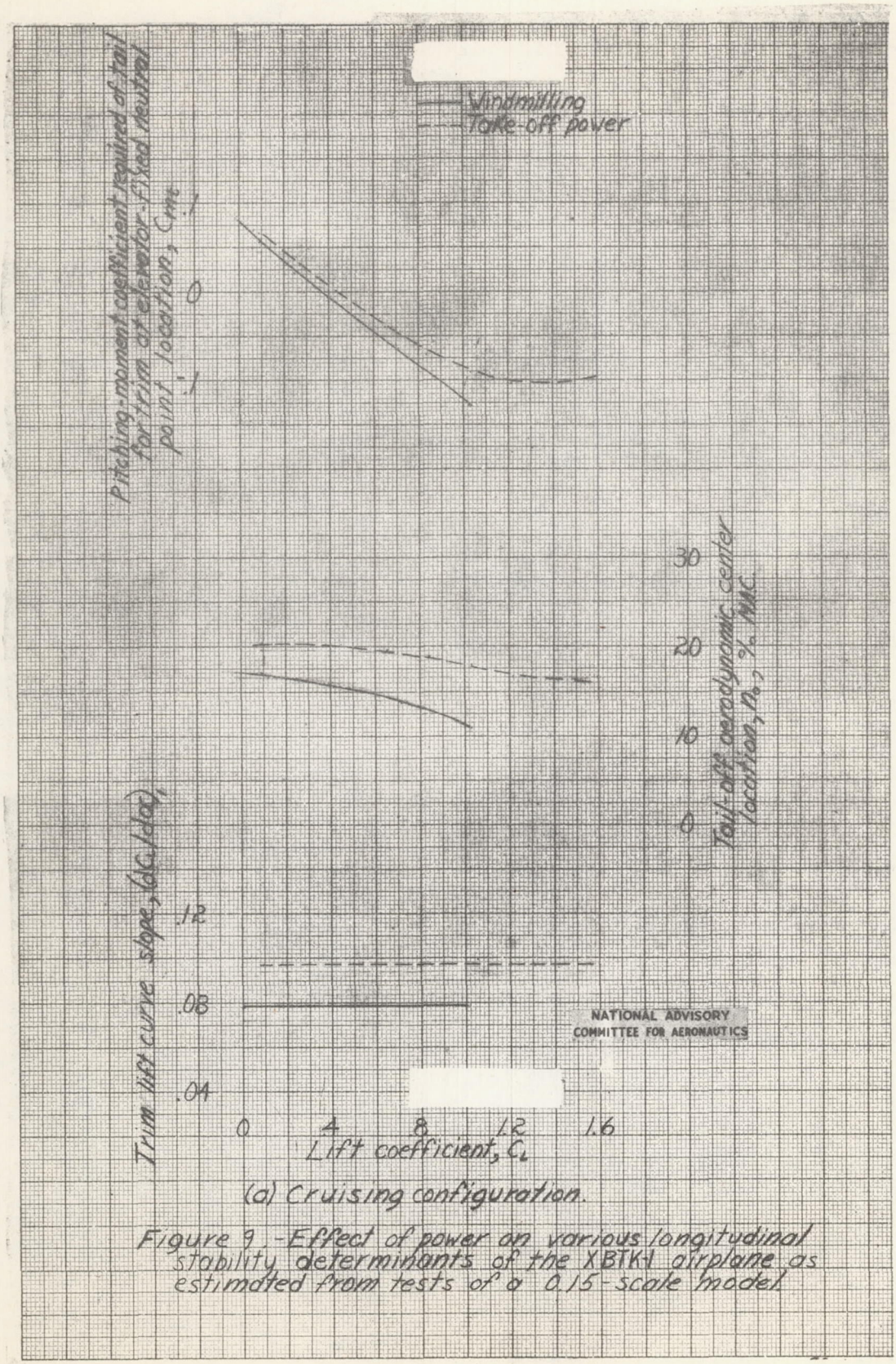

(a) Cruising configuration.

Figure 9.- Effect of power on various longitudinal stability determinants of the XBTK-1 airplane as estimated from tests of a 0.15-scale model.

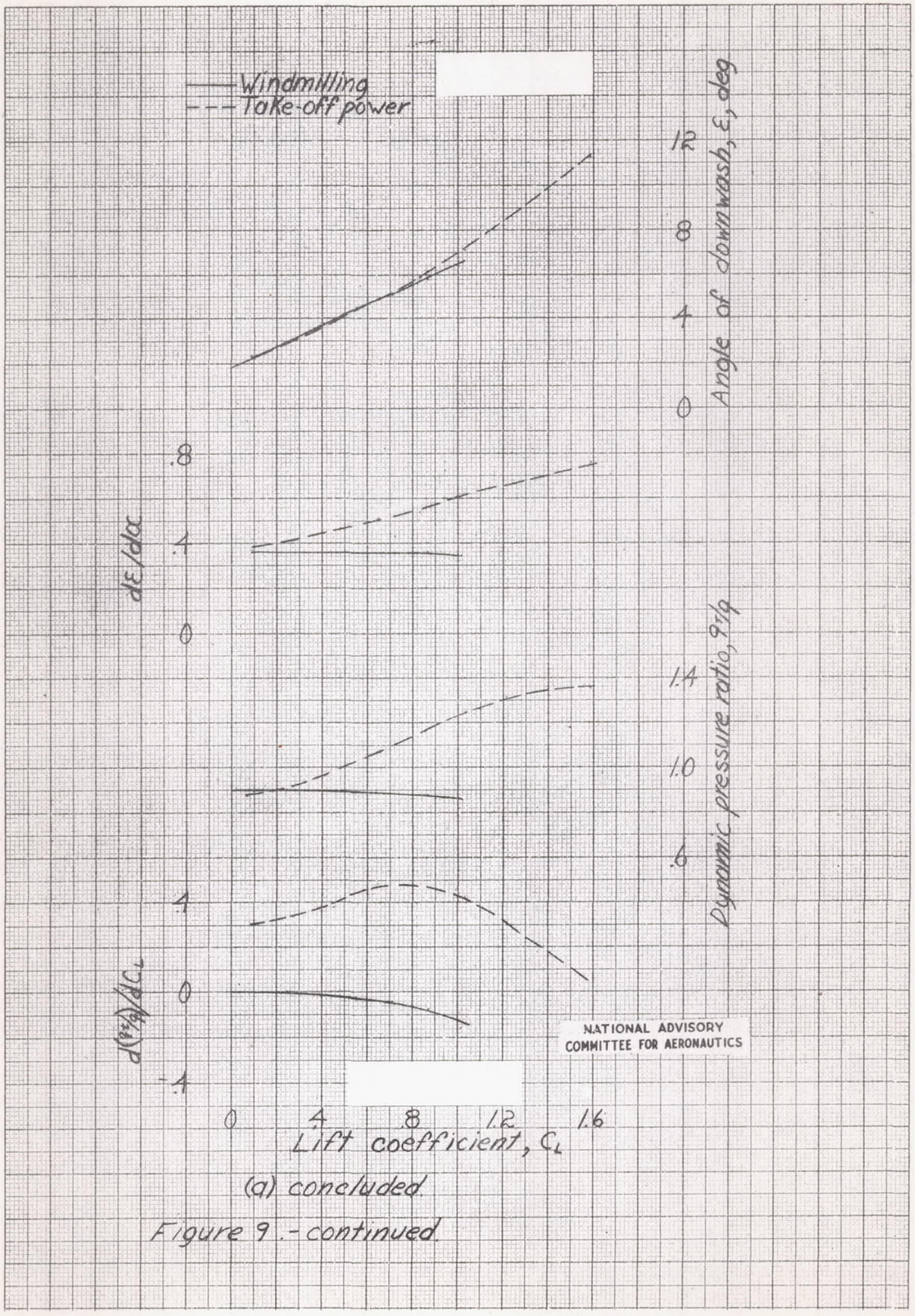

(a) concluded.

Figure 9.- continued.

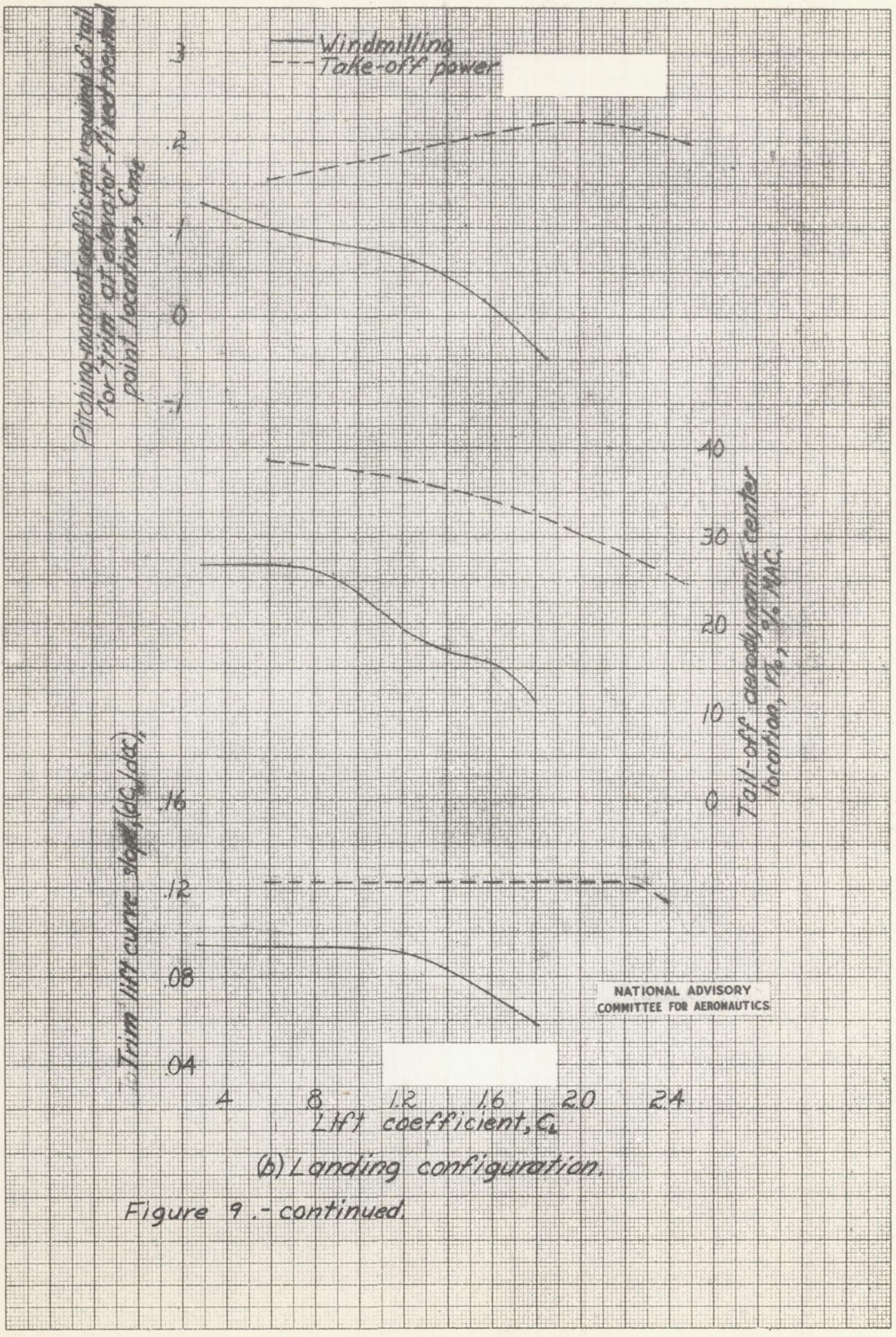

(b) Landing configuration.

Figure 9.- continued.

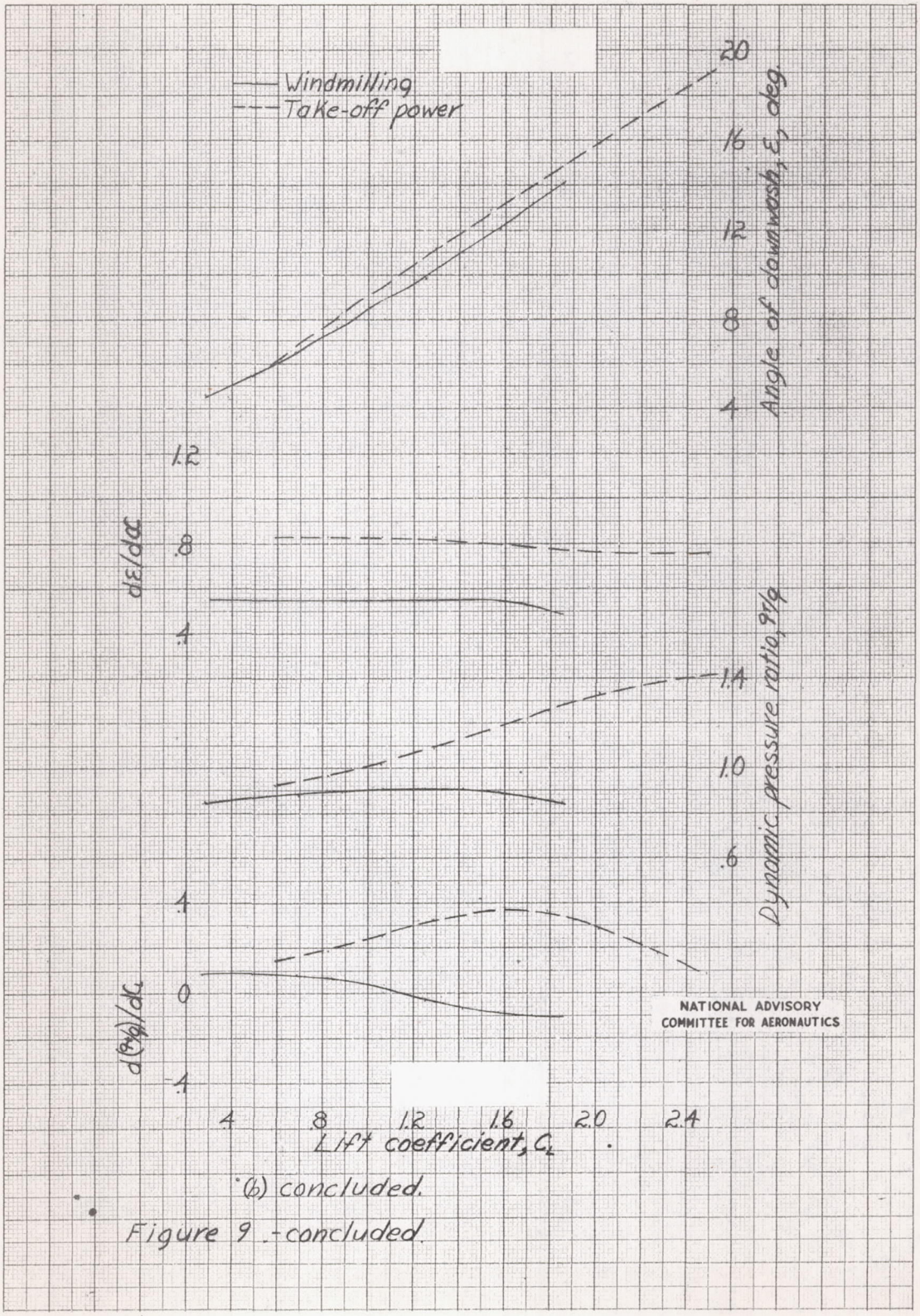

(b) concluded.

Figure 9.- concluded.

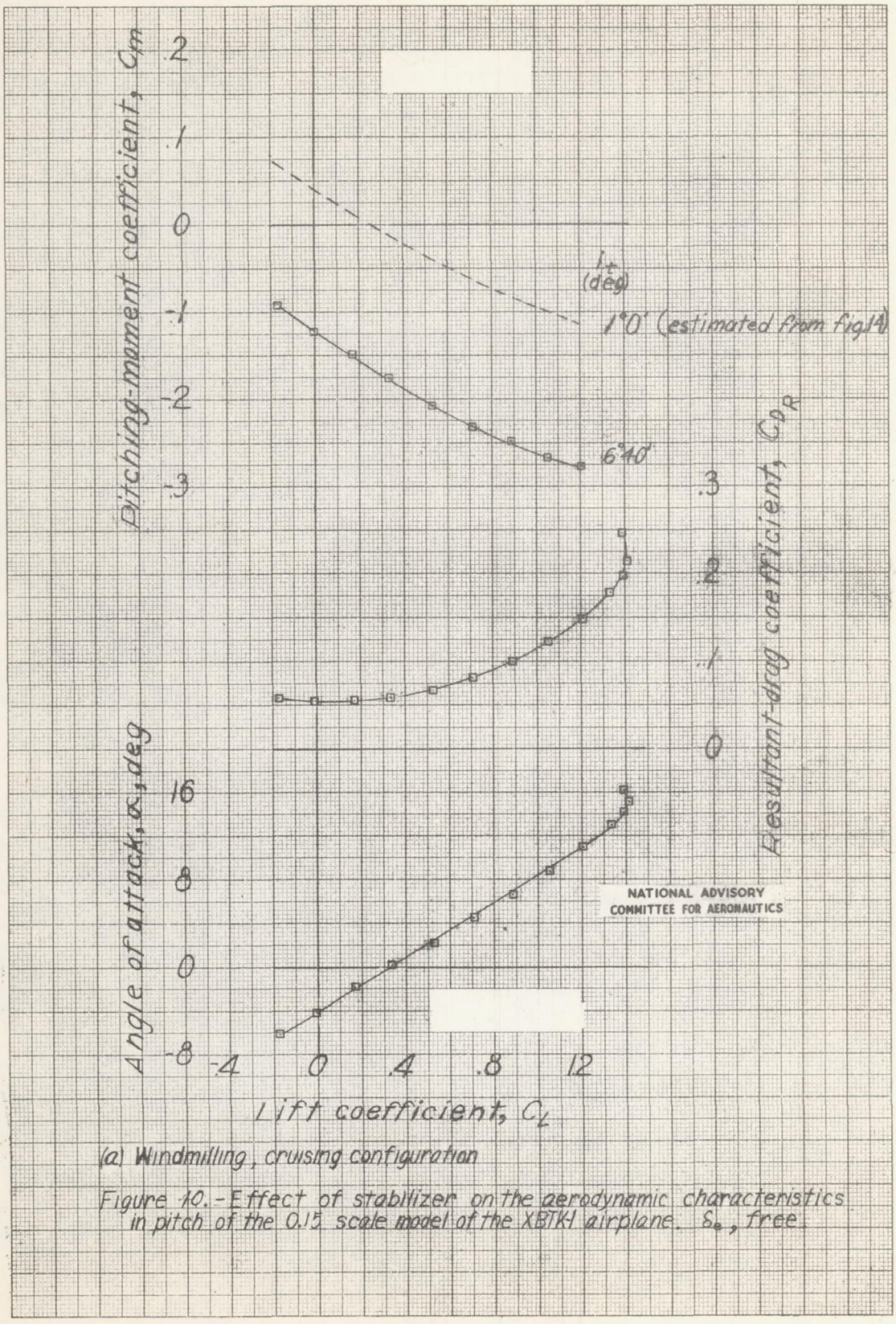

(a) Windmilling, cruising configuration

Figure 10.- Effect of stabilizer on the aerodynamic characteristics in pitch of the 0.15 scale model of the XBTK-1 airplane. δ_e, free.

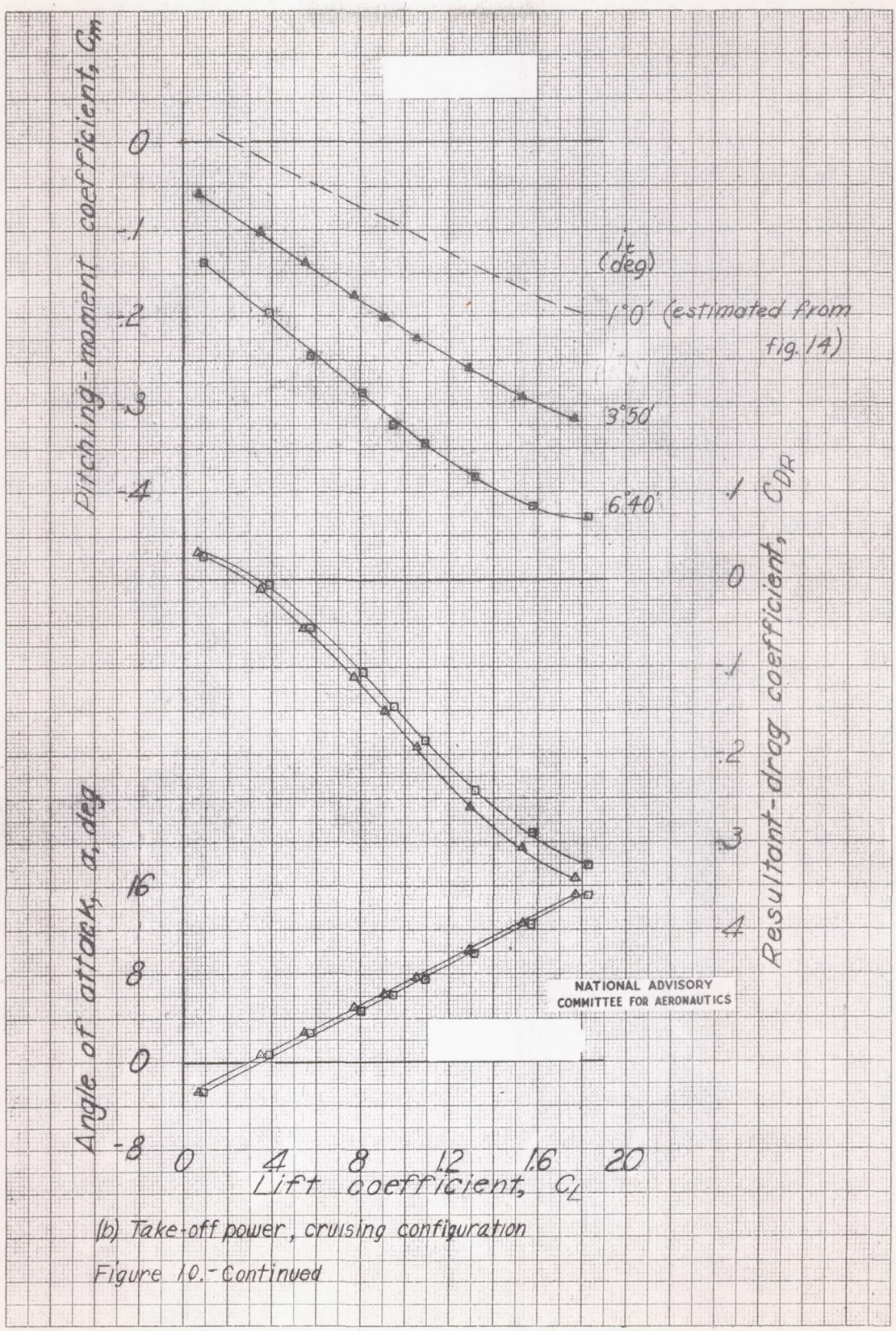

(b) Take-off power, cruising configuration

Figure 10.- Continued

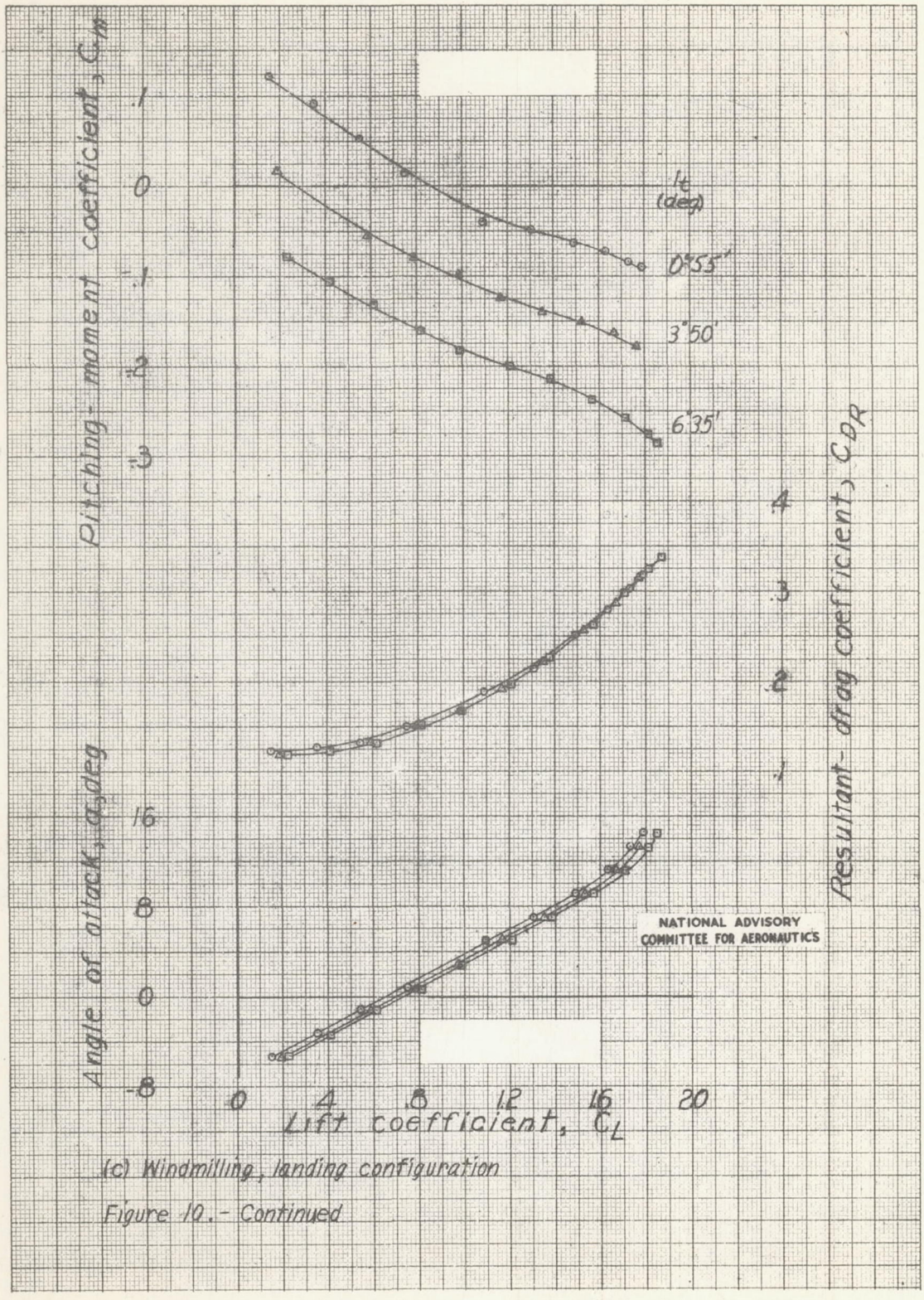

(c) Windmilling, landing configuration

Figure 10.- Continued

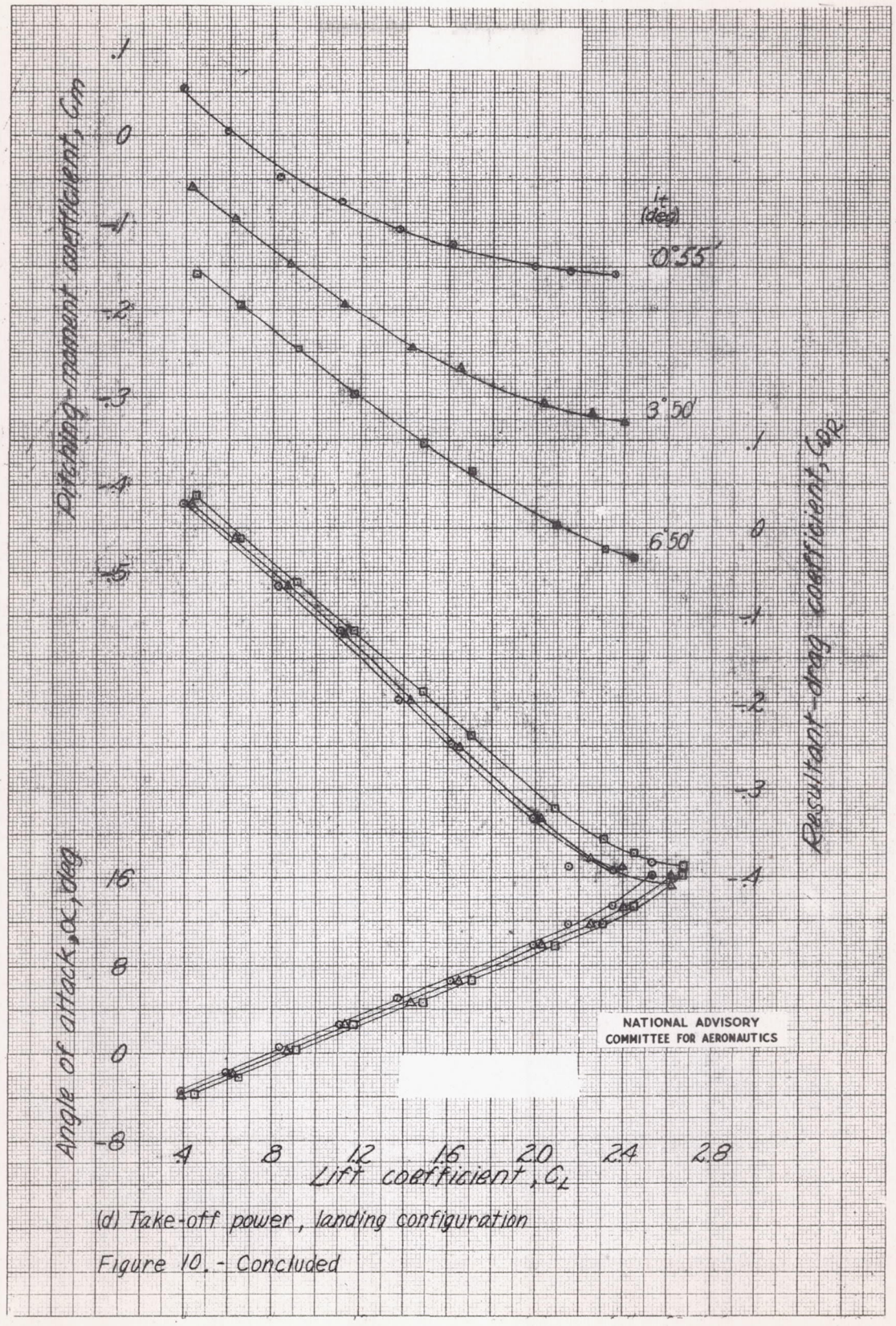

(d) Take-off power, landing configuration

Figure 10.- Concluded

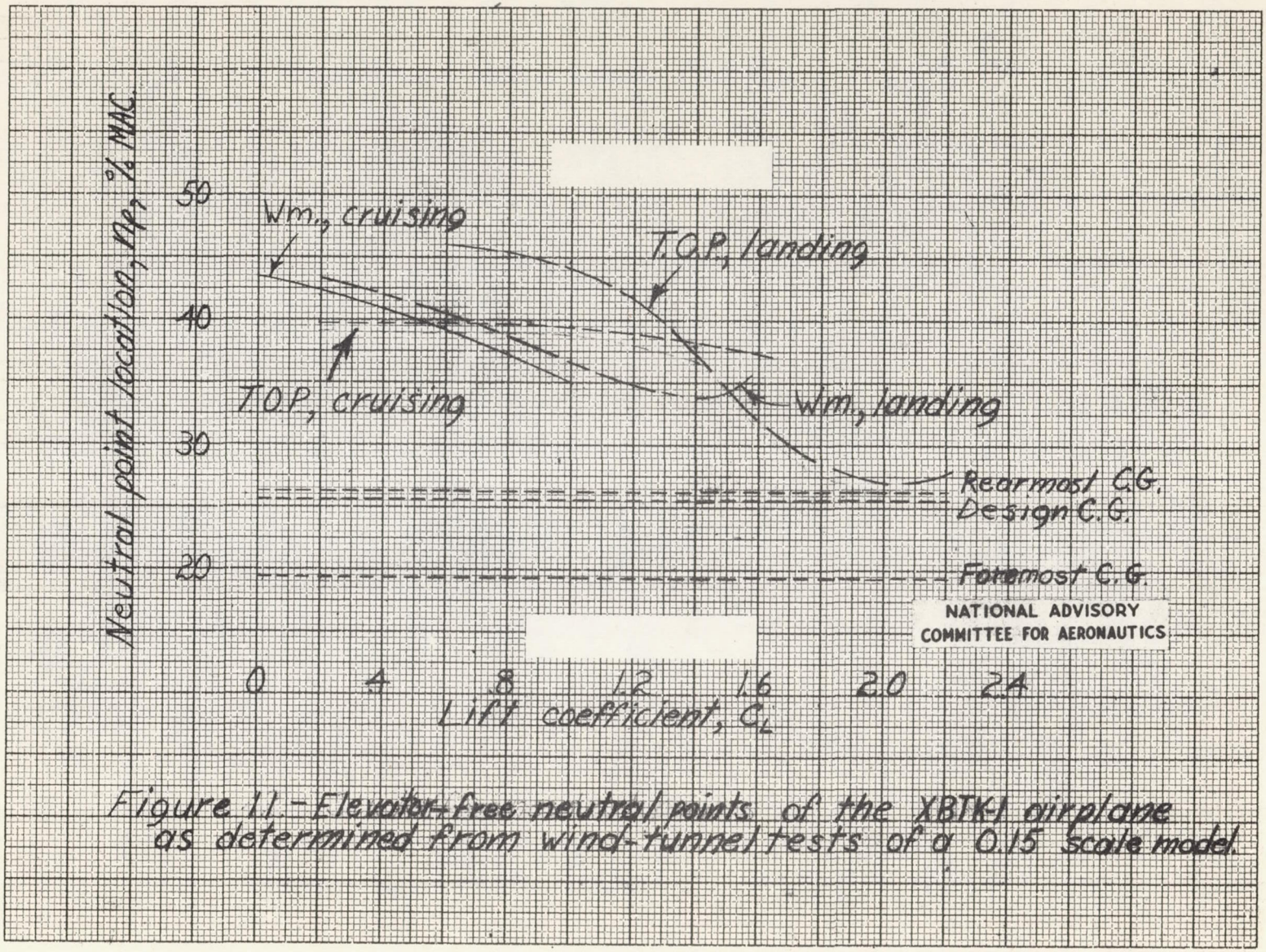

Figure 11.- Elevator-free neutral points of the XBTK-1 airplane as determined from wind-tunnel tests of a 0.15 scale model.

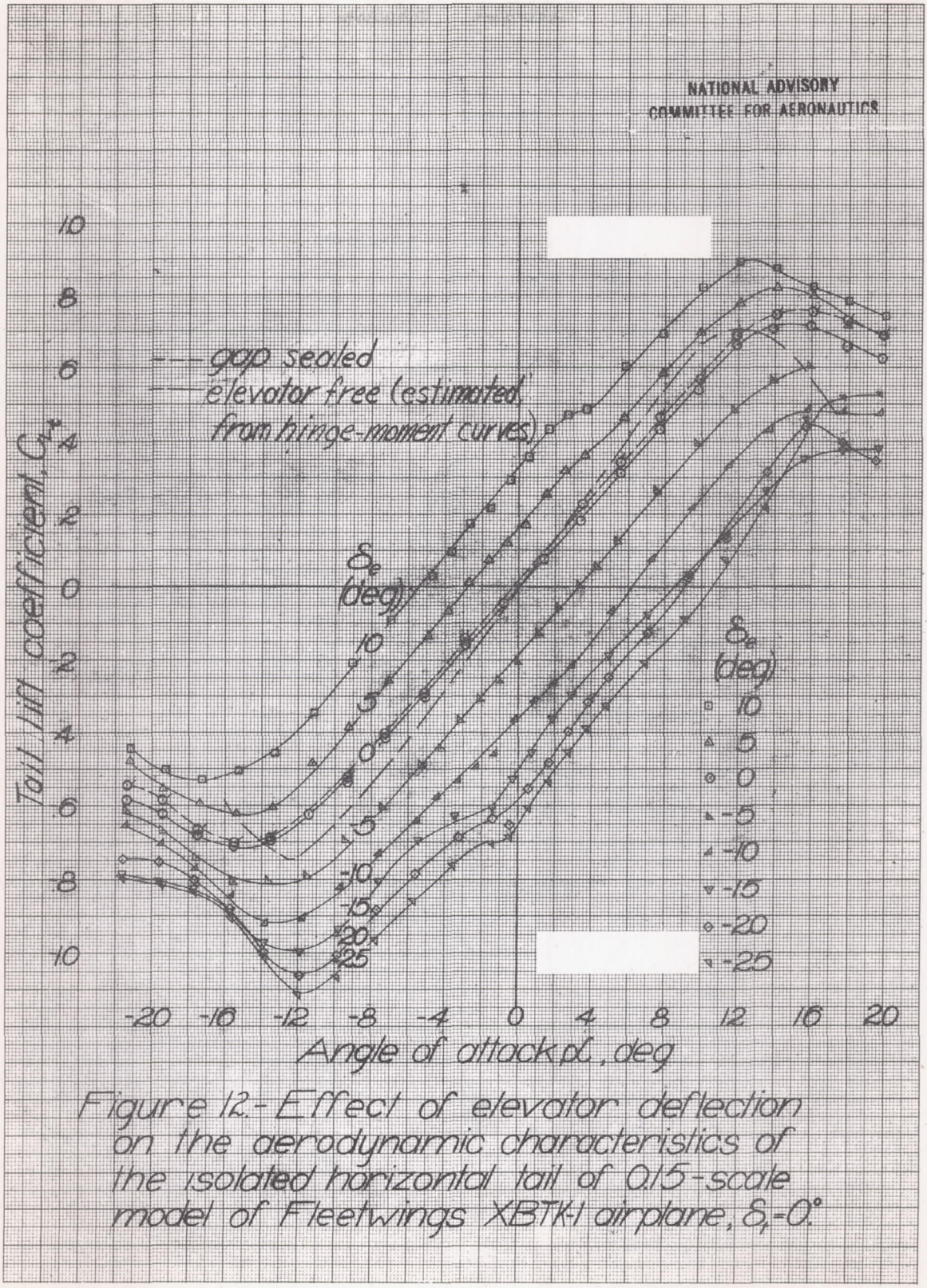

Figure 12.- Effect of elevator deflection on the aerodynamic characteristics of the isolated horizontal tail of 0.15-scale model of Fleetwings XBTK-1 airplane, δ_t=0°.

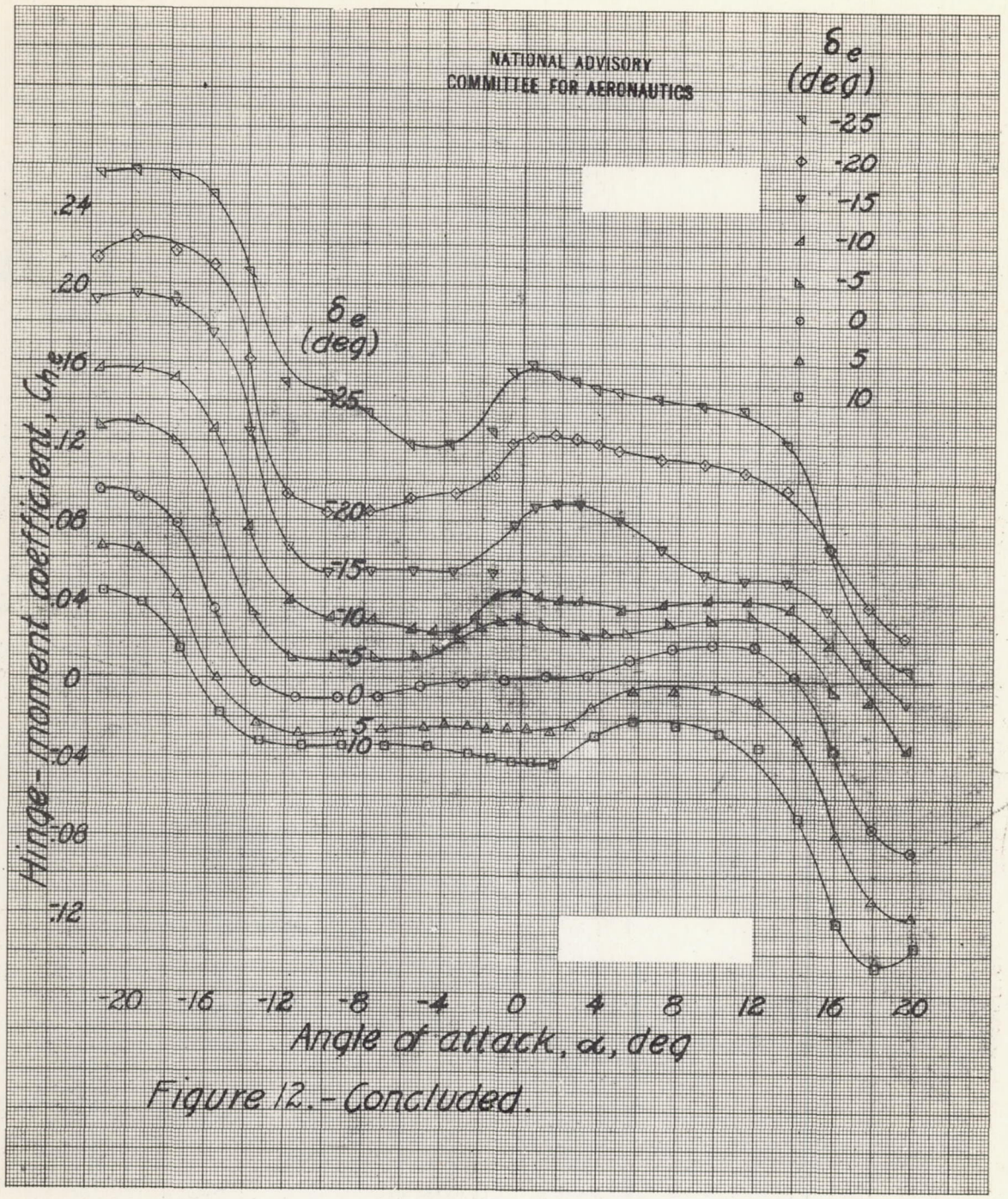

Figure 12.- Concluded.

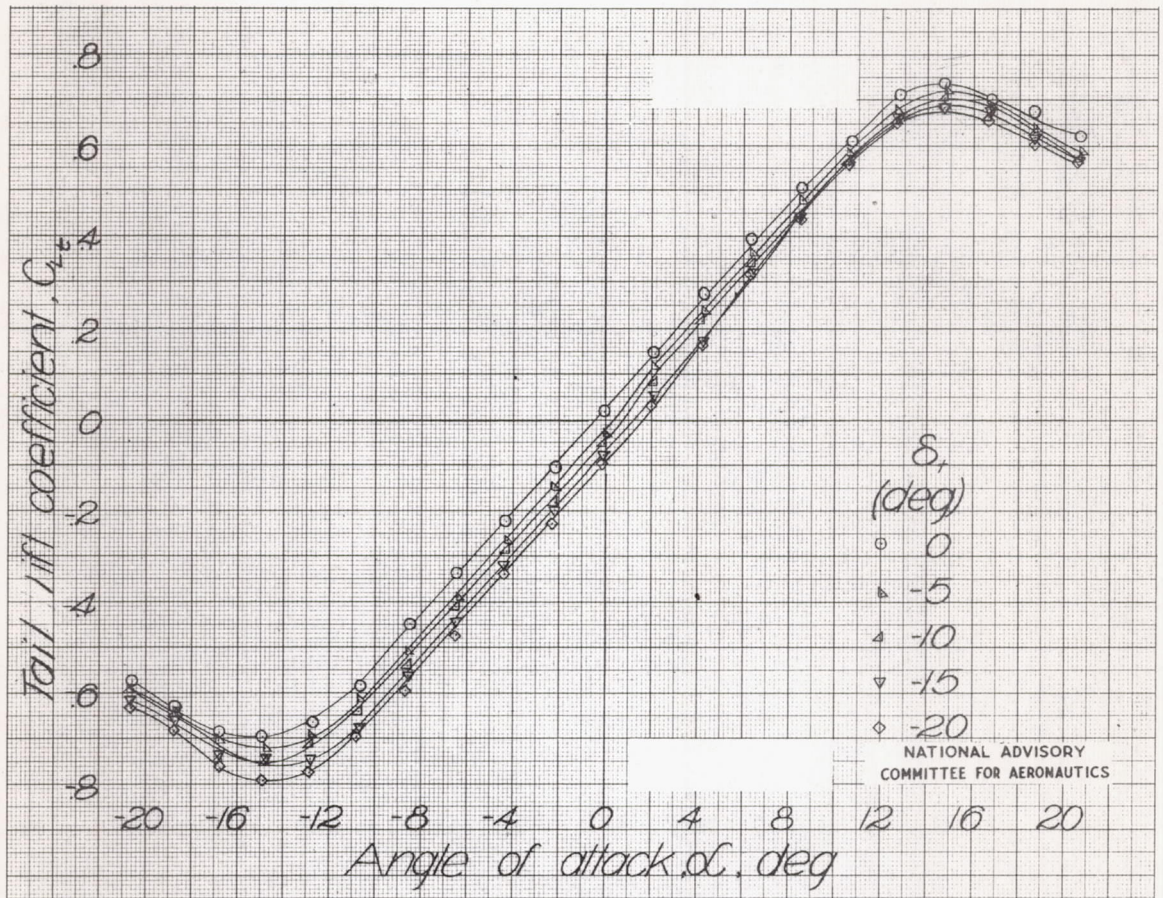

Figure 13 - Effect of tab deflection on the aerodynamic characteristics of the isolated horizontal tail of 0.15-scale model of Fleetwings XBTK-1 airplane, $\delta_e = 0°$.

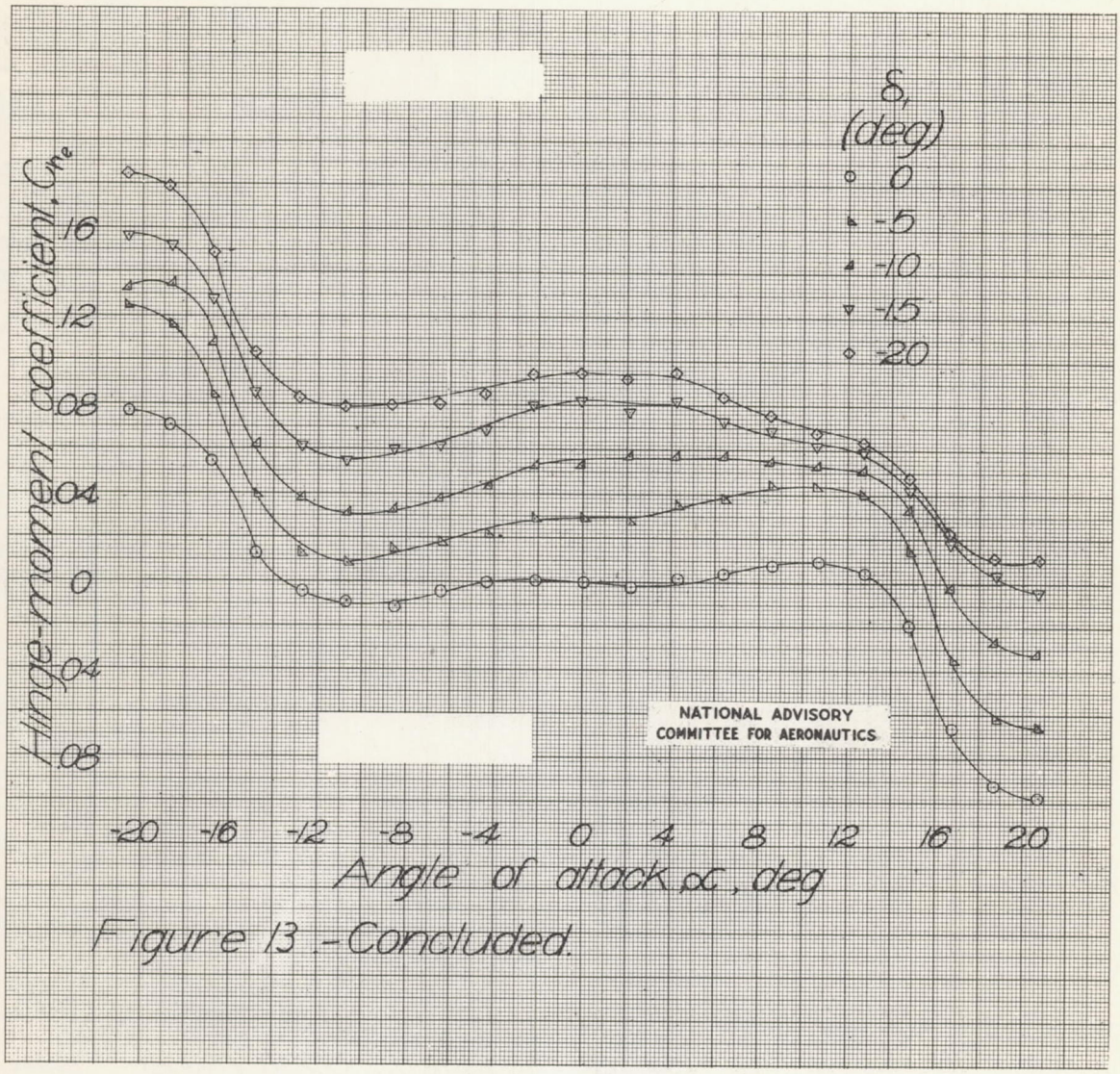

Figure 13.-Concluded.

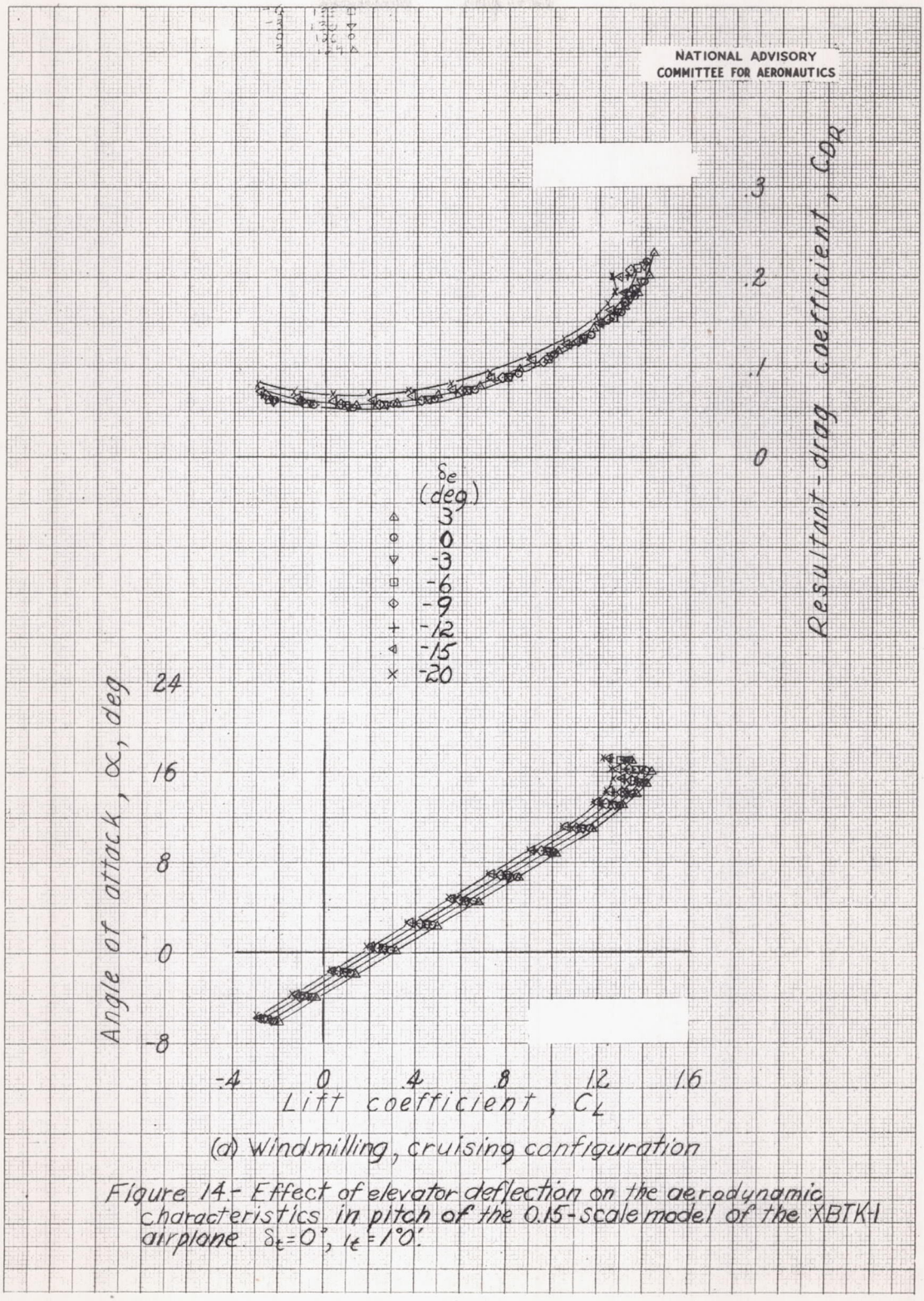

(a) Windmilling, cruising configuration

Figure 14.- Effect of elevator deflection on the aerodynamic characteristics in pitch of the 0.15-scale model of the XBTK-1 airplane. $\delta_t = 0°$, $i_t = 1°0'$.

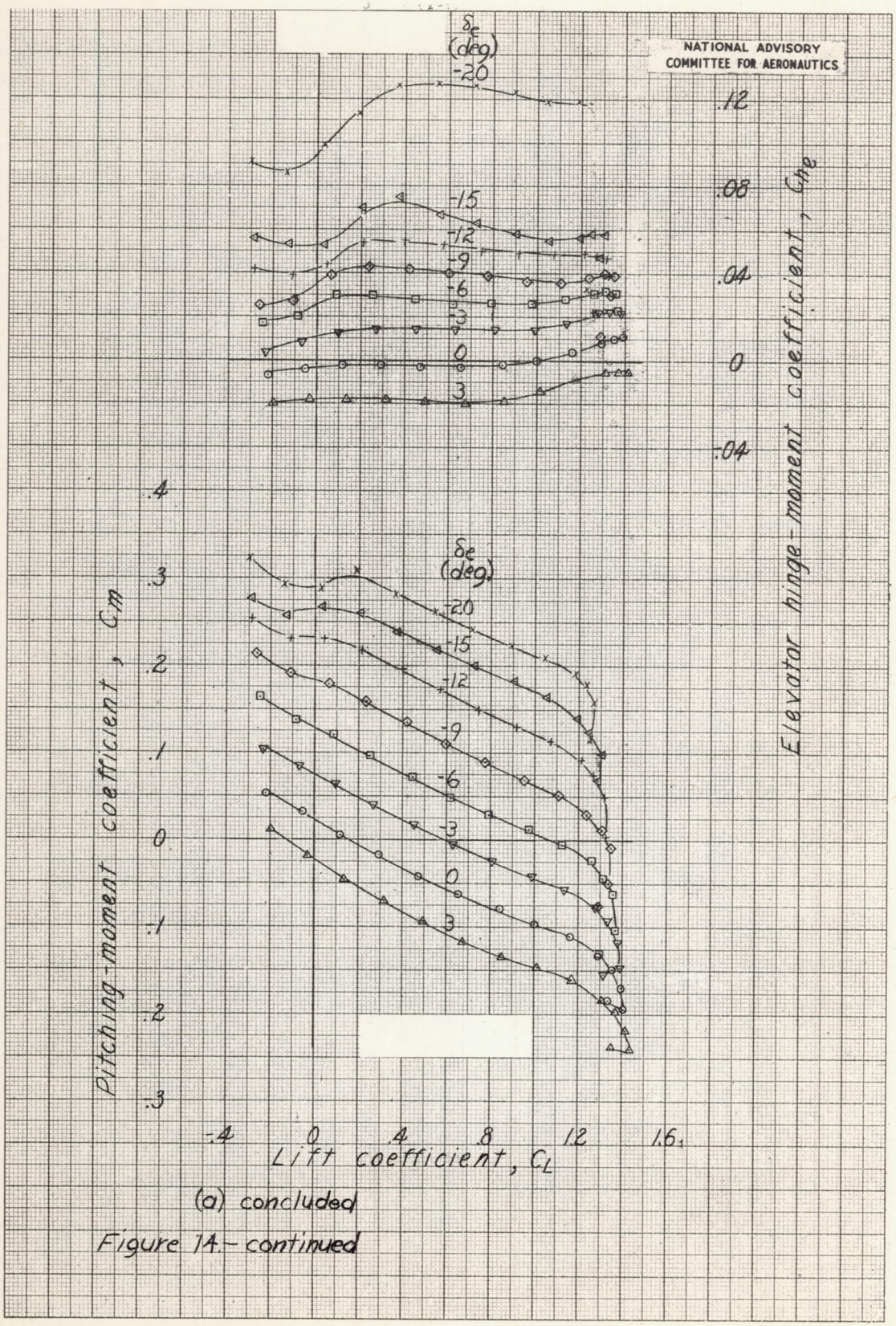

(a) concluded

Figure 14.- continued

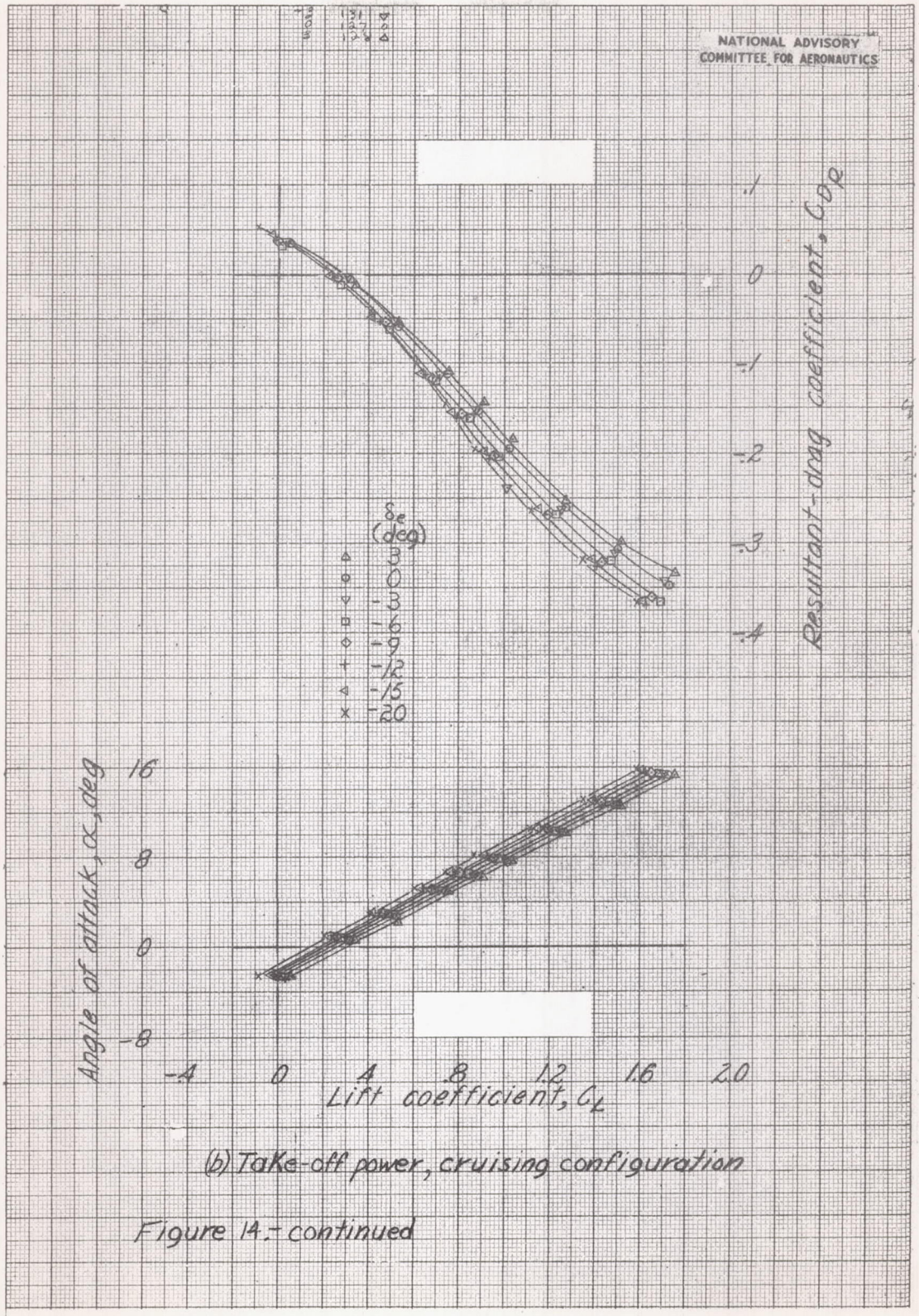

(b) Take-off power, cruising configuration

Figure 14.- continued

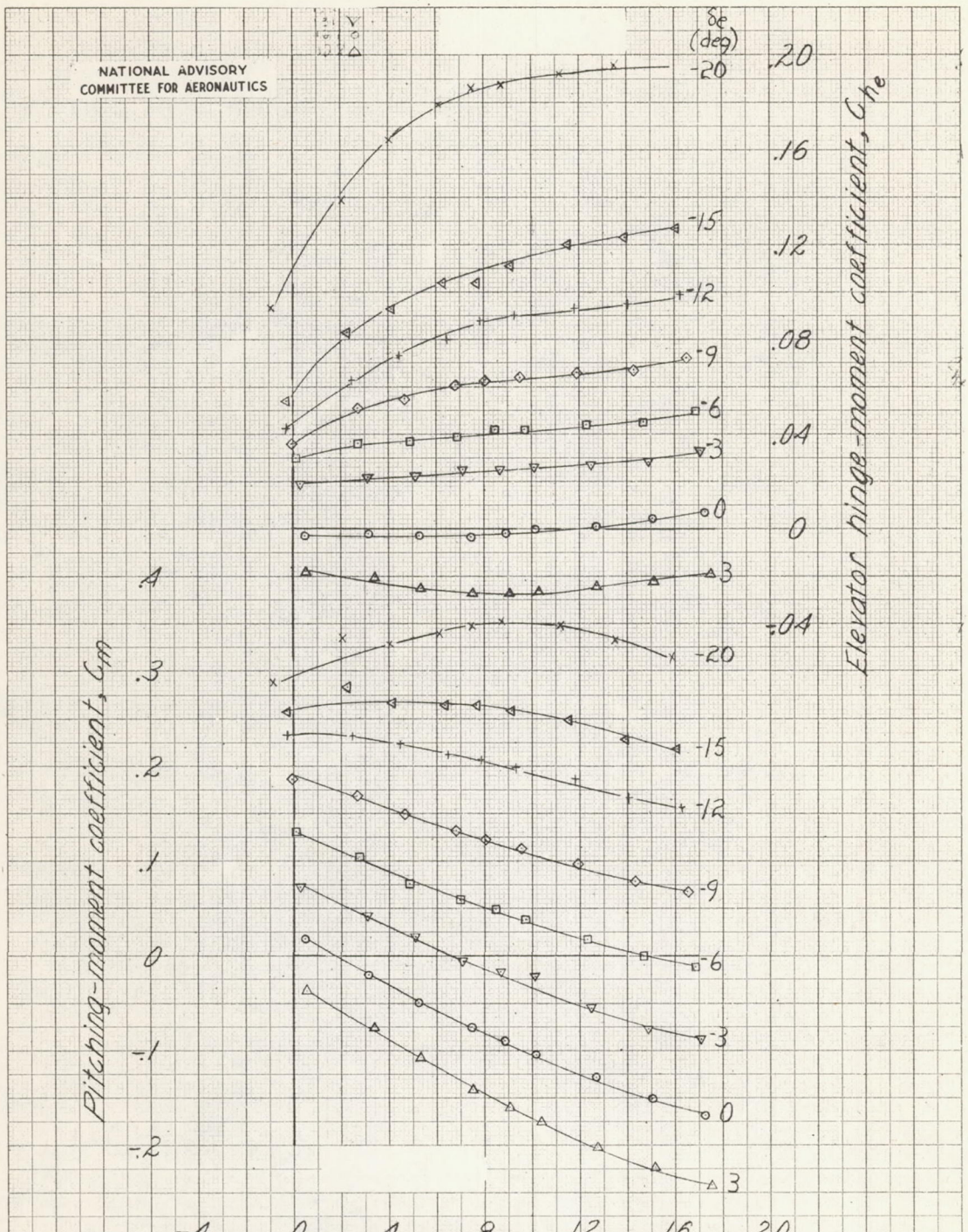

(b) concluded

Figure 14 - continued

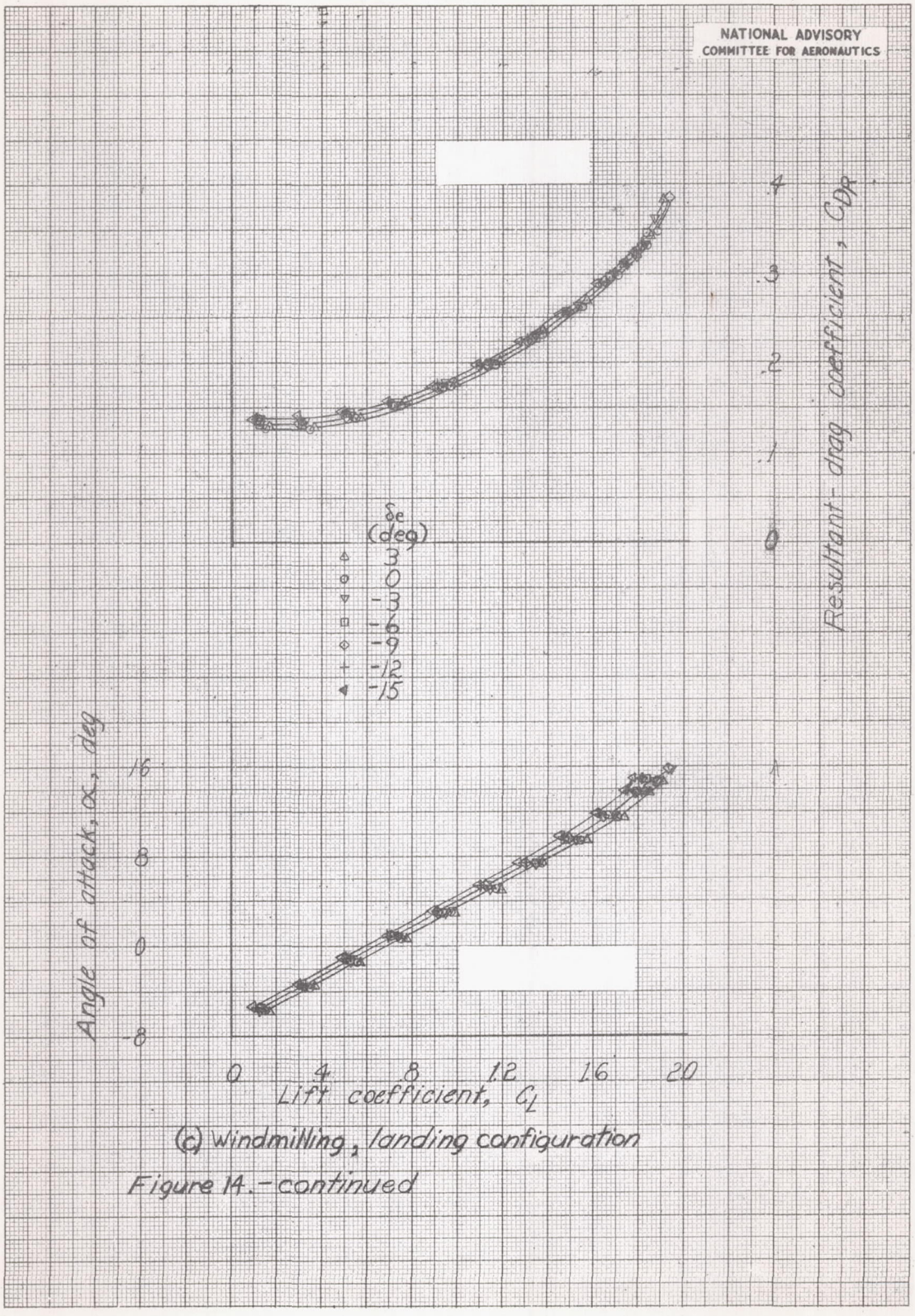

(c) Windmilling, landing configuration

Figure 14.- continued

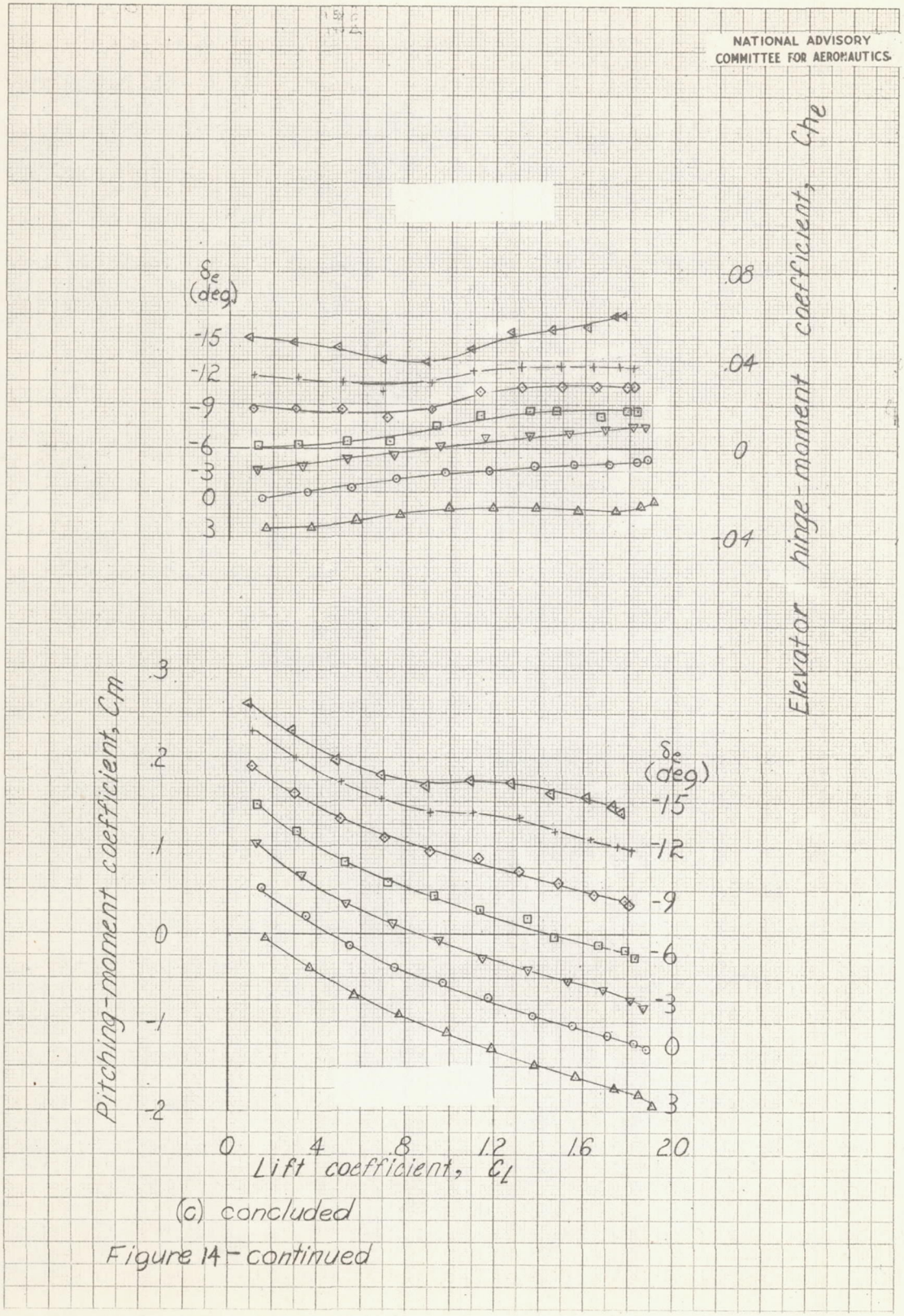

(c) concluded

Figure 14 - continued

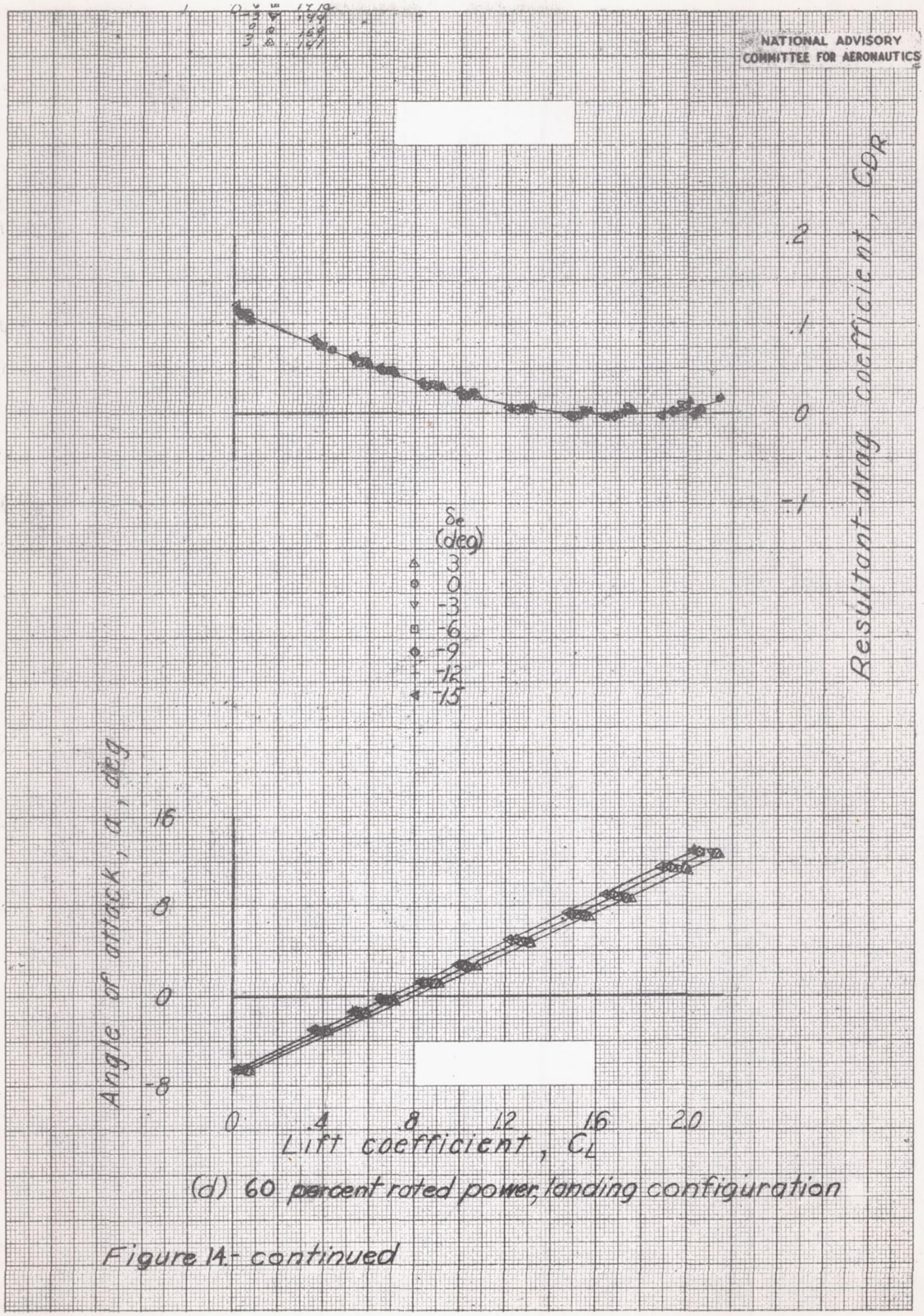

(d) 60 percent rated power, landing configuration

Figure 14.- continued

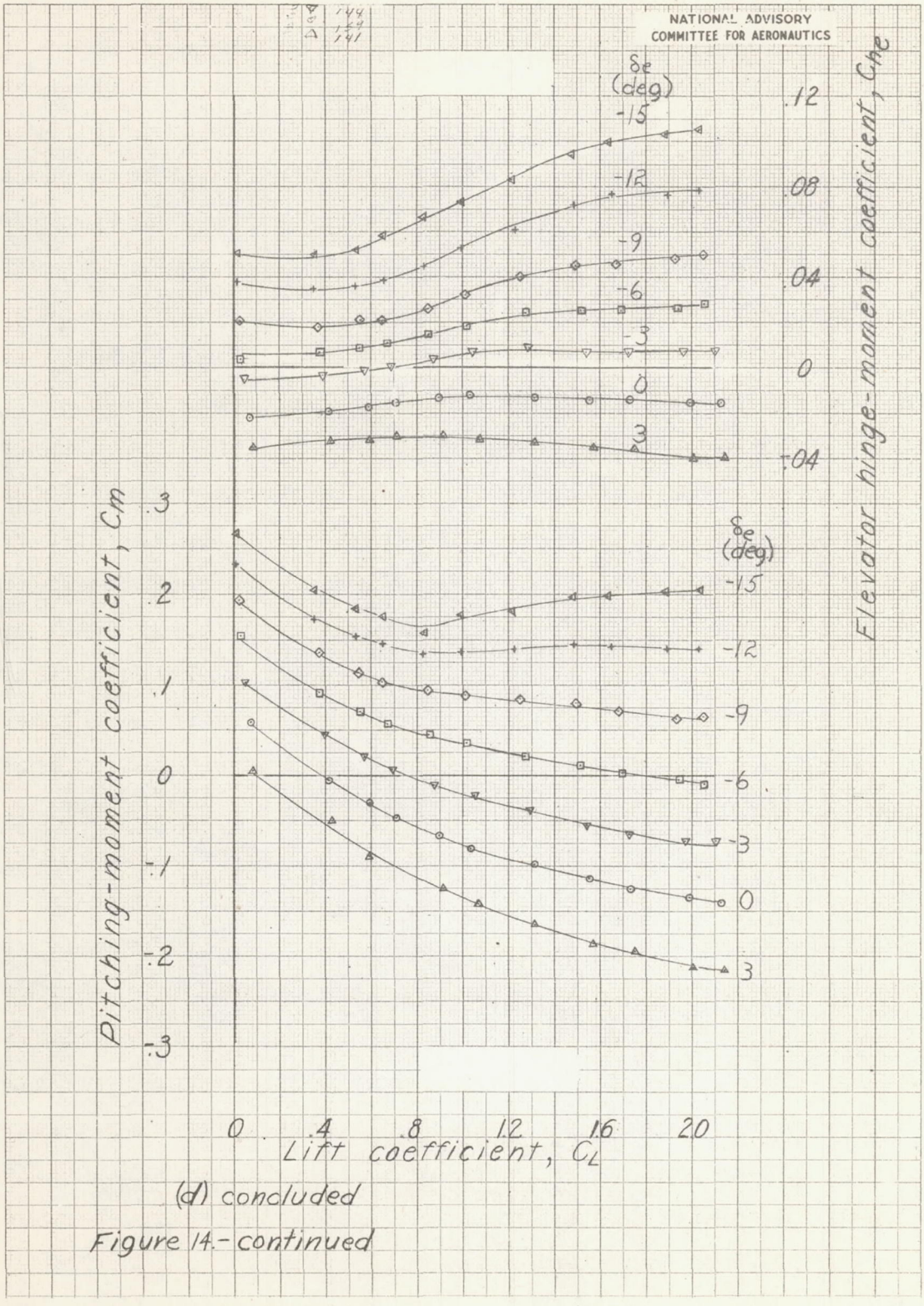

(d) concluded

Figure 14.- continued

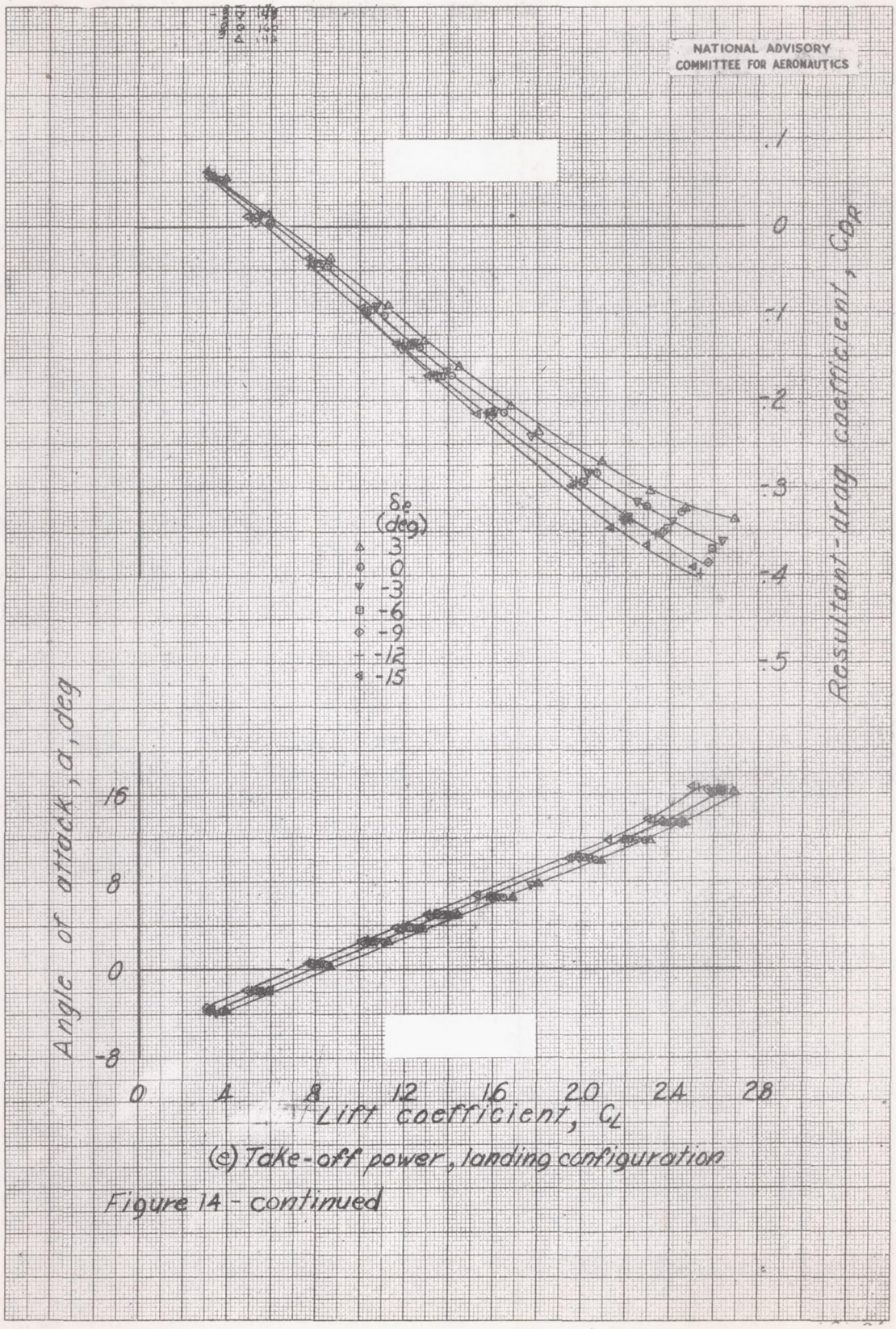

(c) Take-off power, landing configuration

Figure 14 - continued

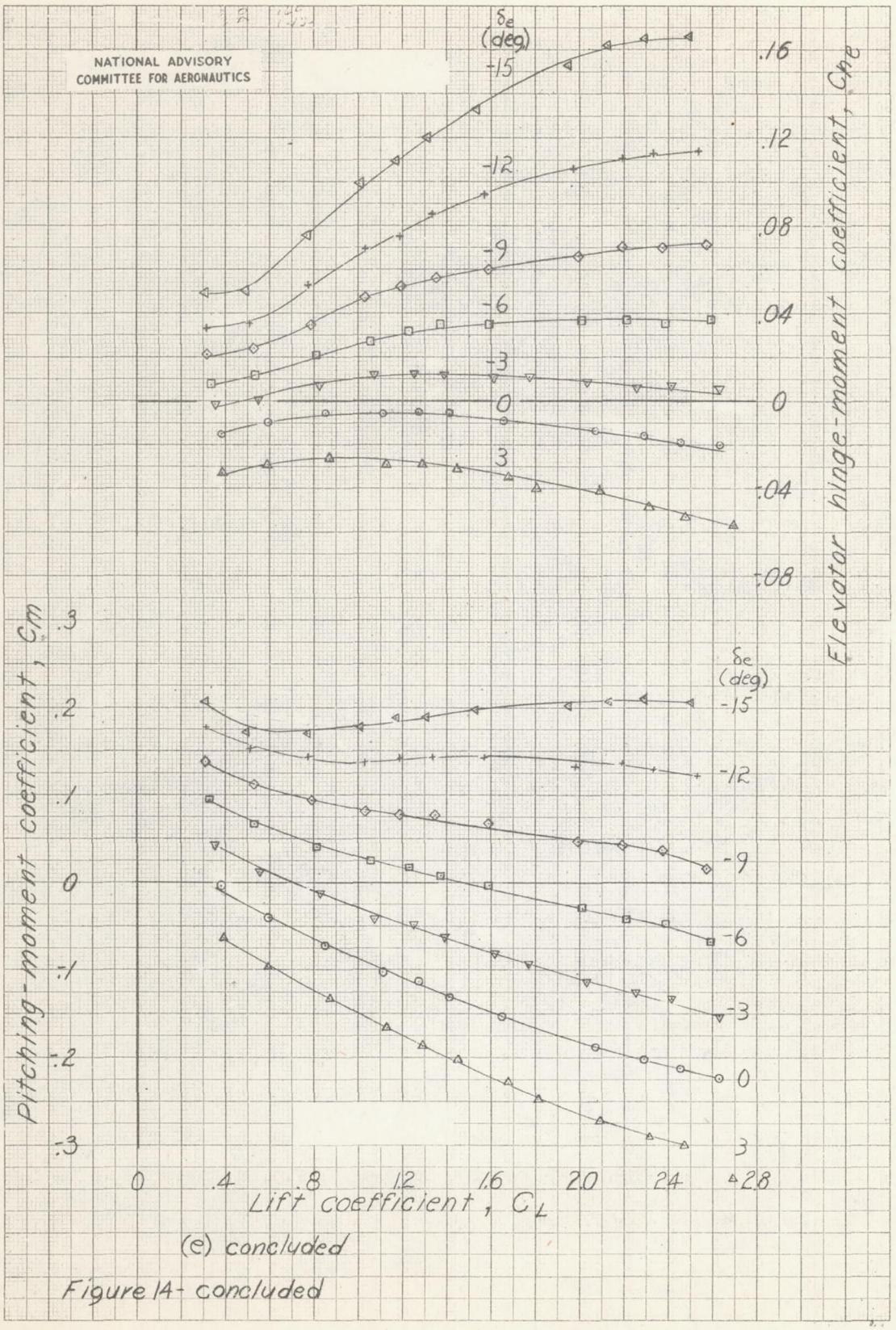

(e) concluded

Figure 14- concluded

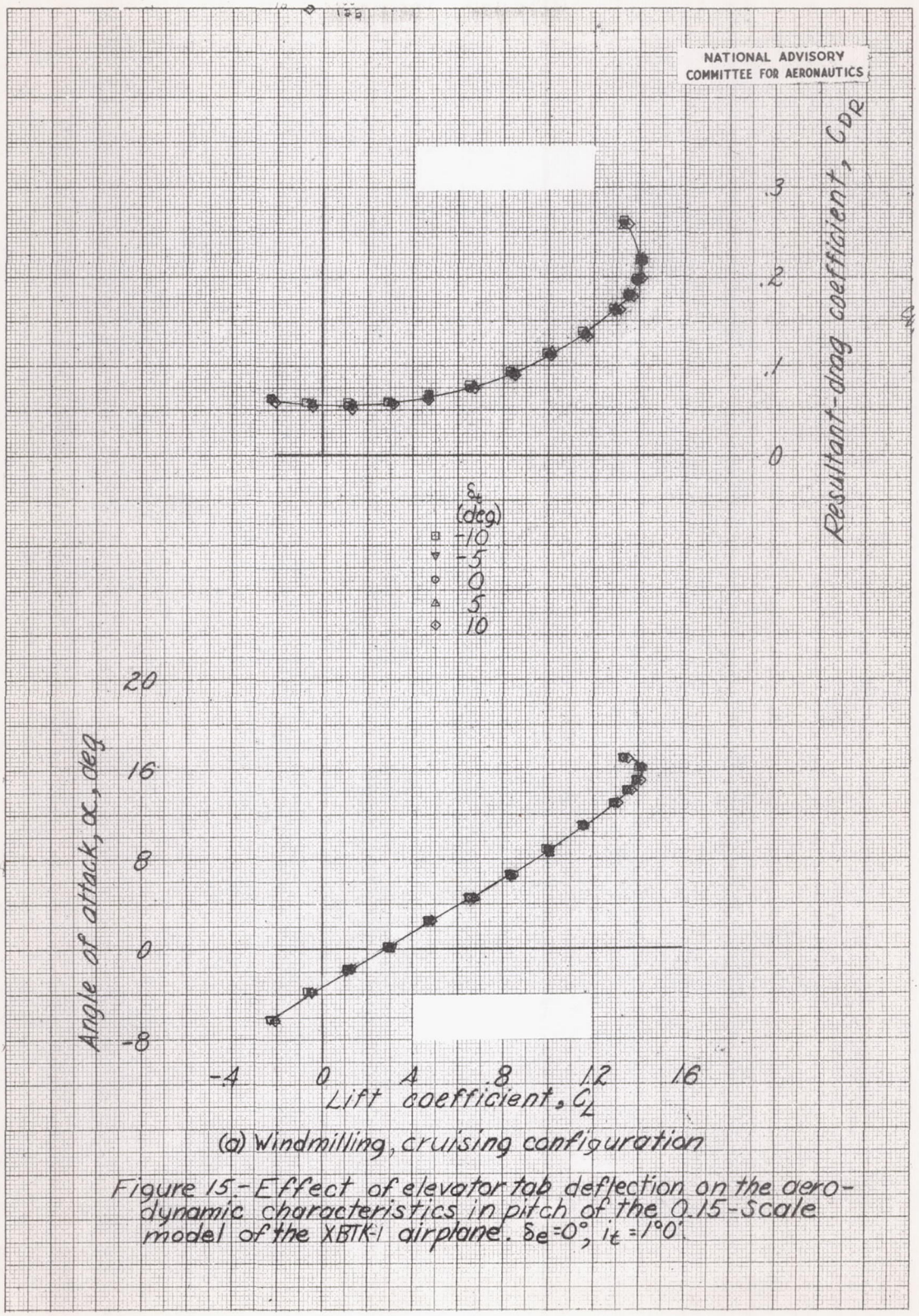

(a) Windmilling, cruising configuration

Figure 15.- Effect of elevator tab deflection on the aerodynamic characteristics in pitch of the 0.15-scale model of the XBTK-1 airplane. $\delta_e = 0°$, $i_t = 1°0'$.

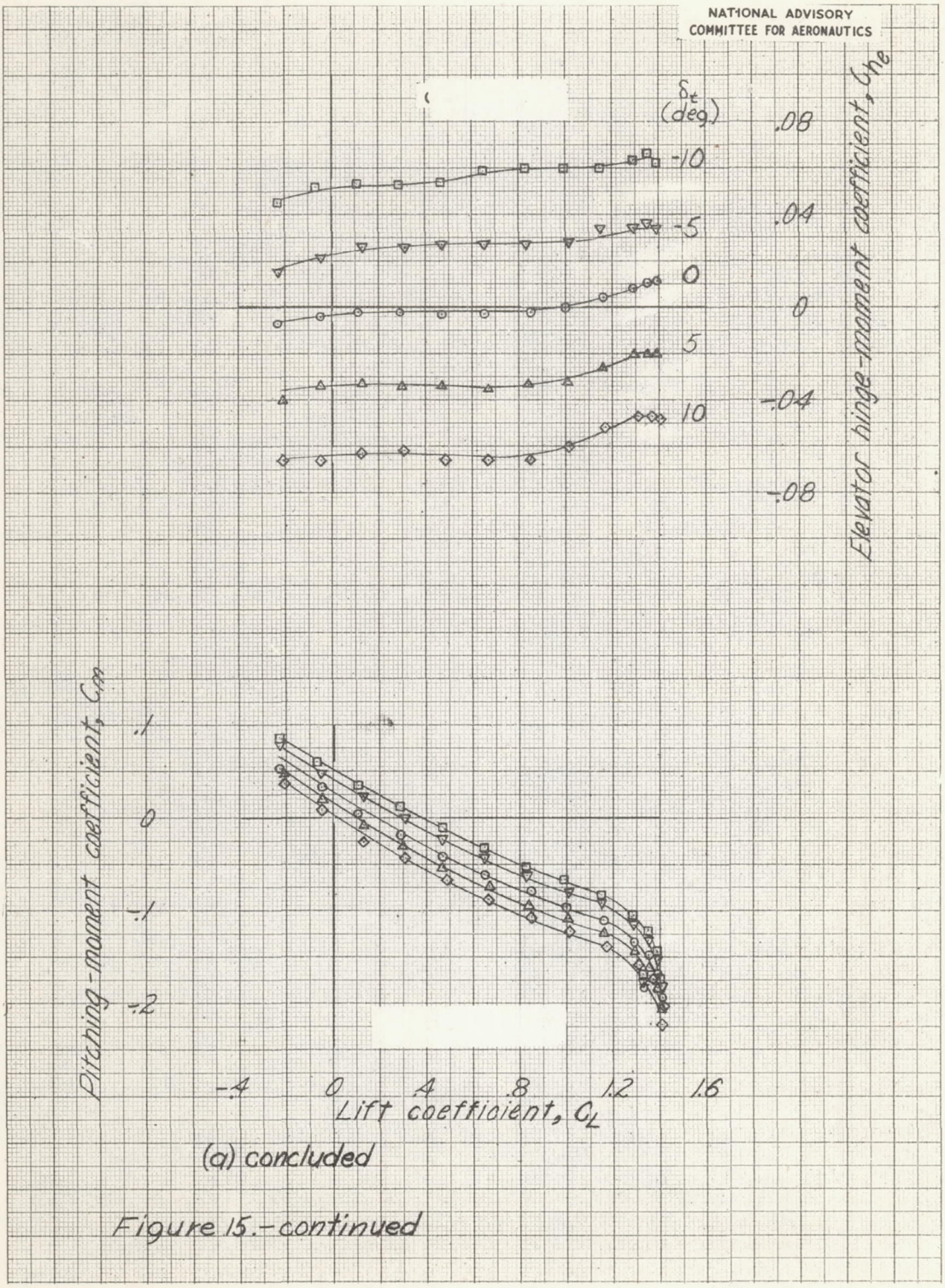

(a) concluded

Figure 15.- continued

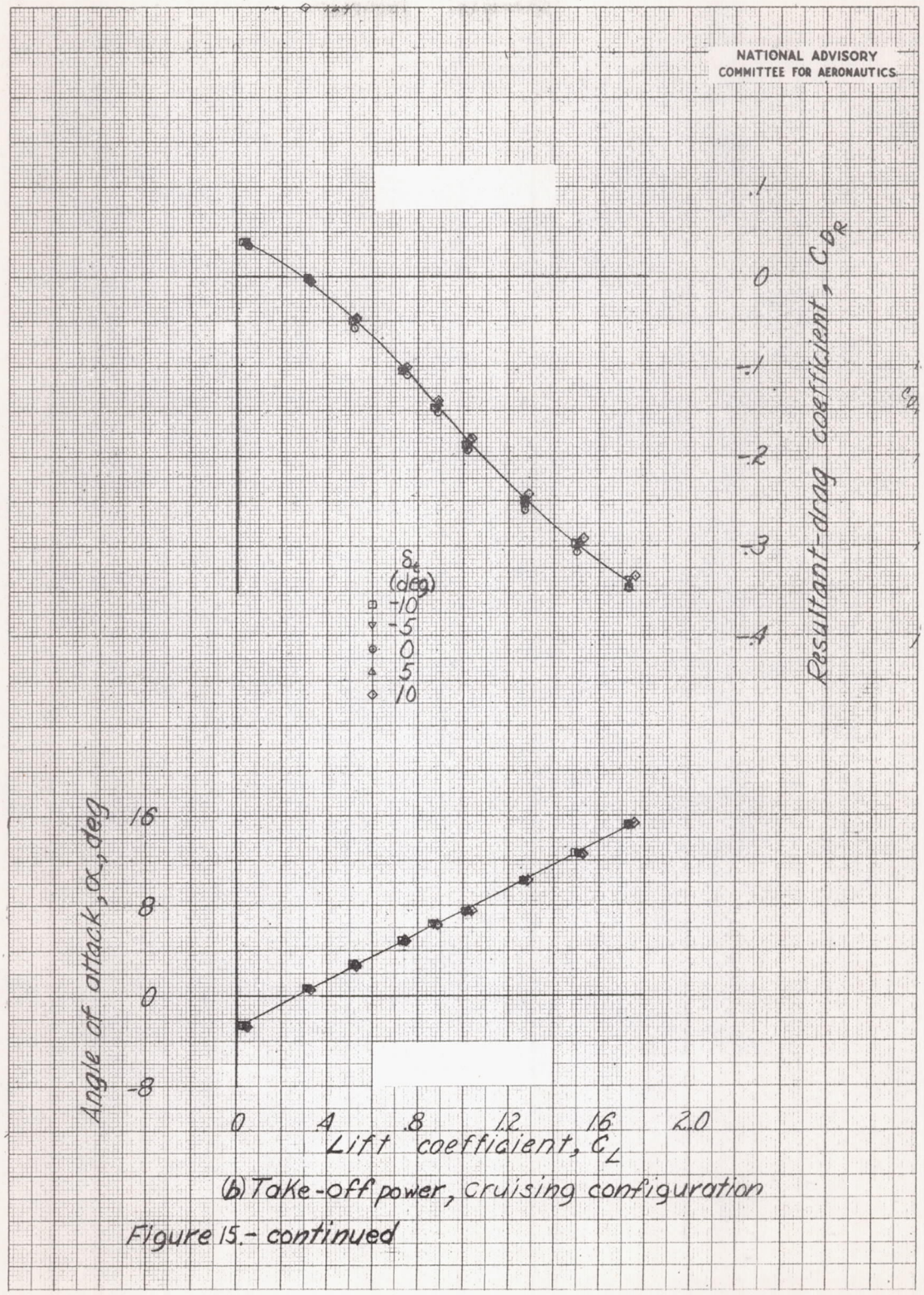

(b) Take-off power, cruising configuration

Figure 15.- continued

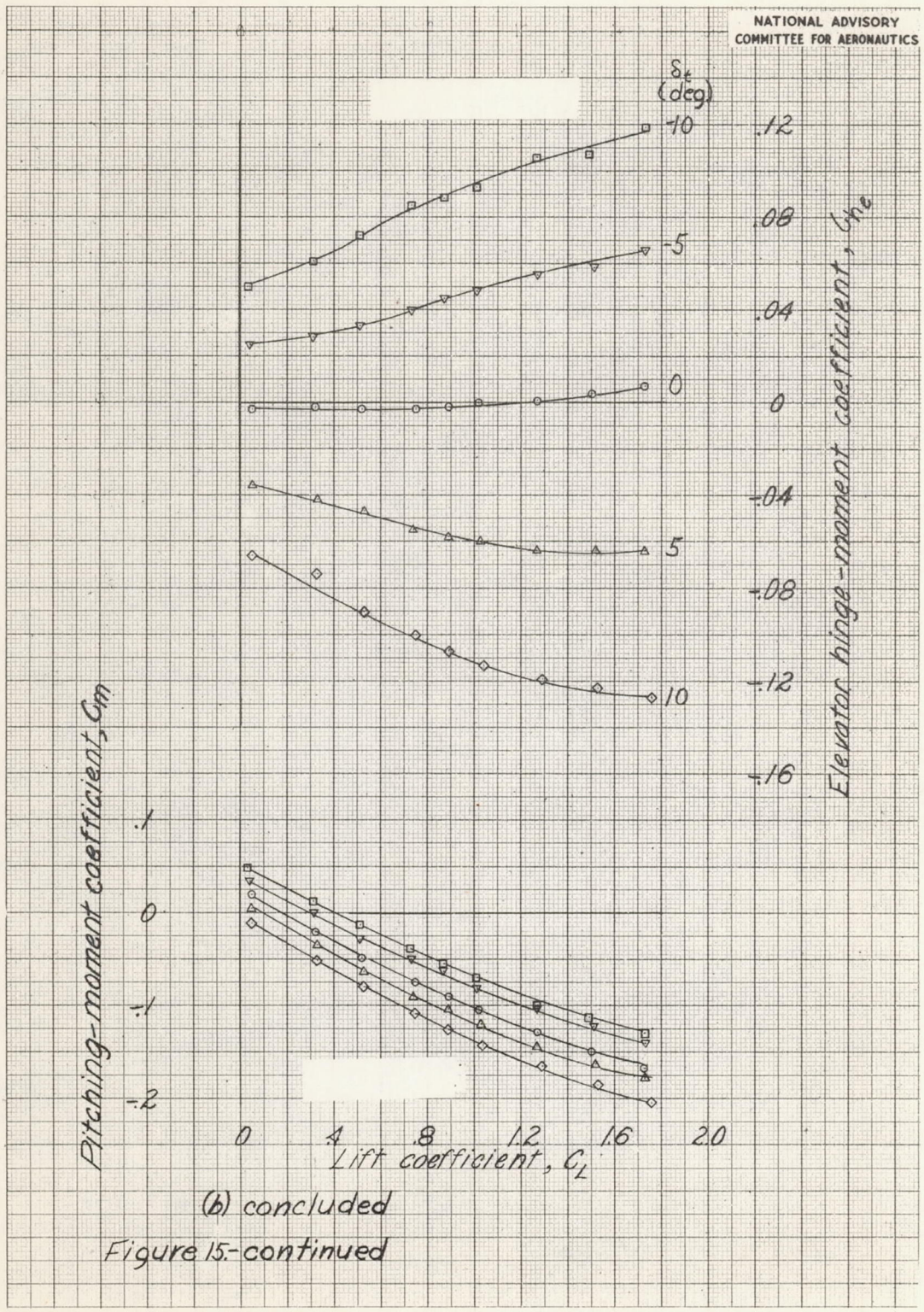

(b) concluded

Figure 15.-continued

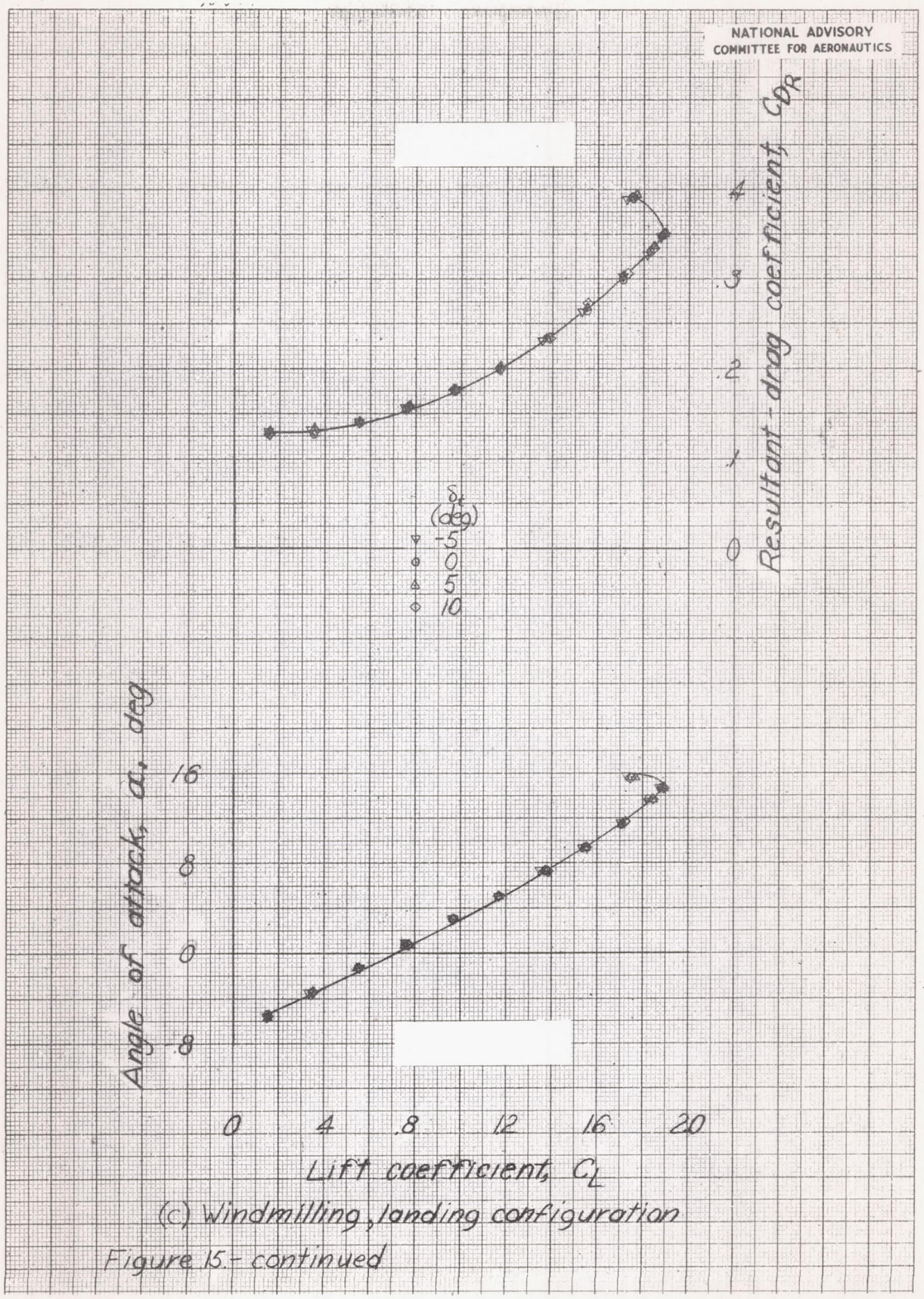

(c) Windmilling, landing configuration

Figure 15.- continued

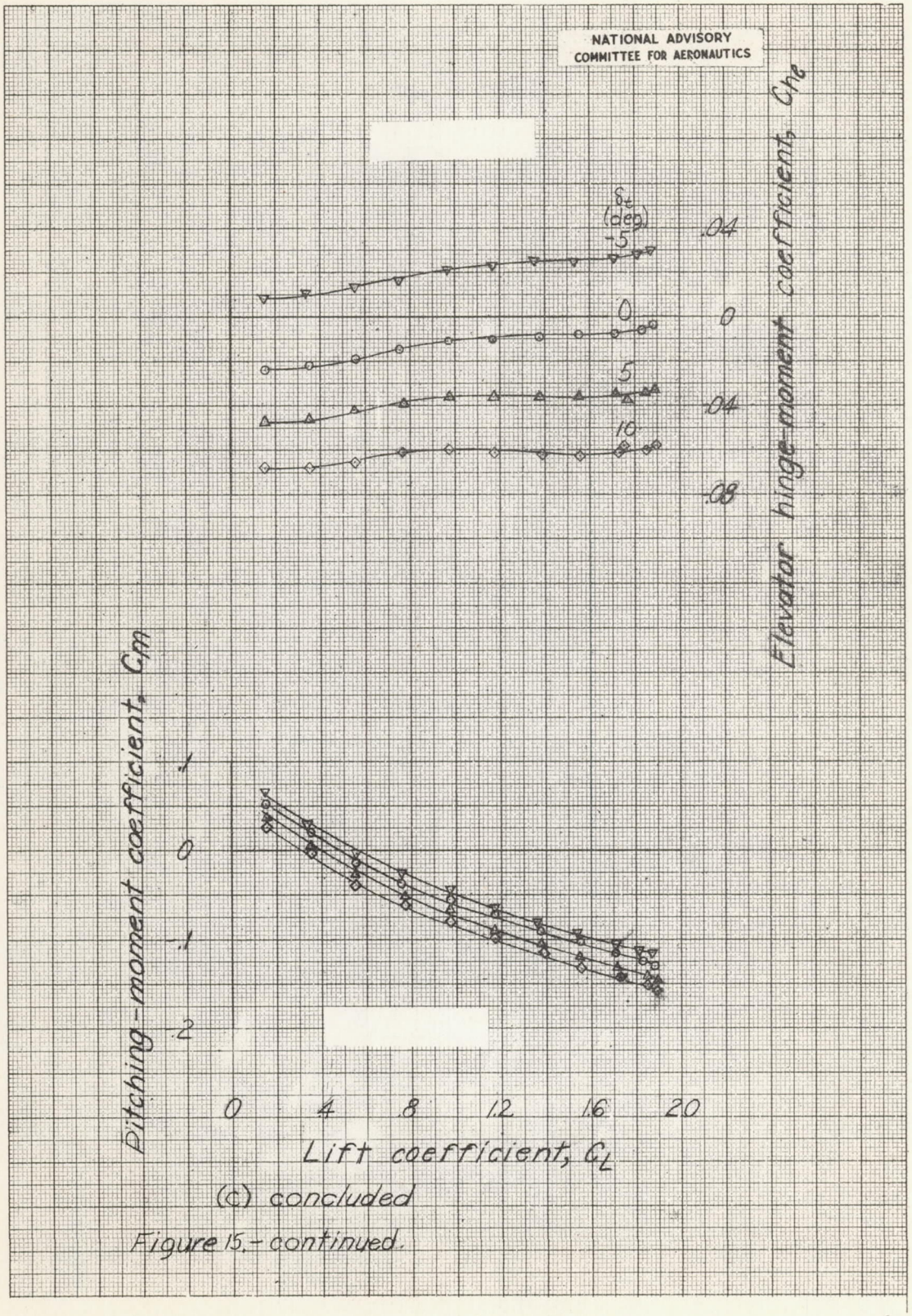

(c) concluded

Figure 15.- continued.

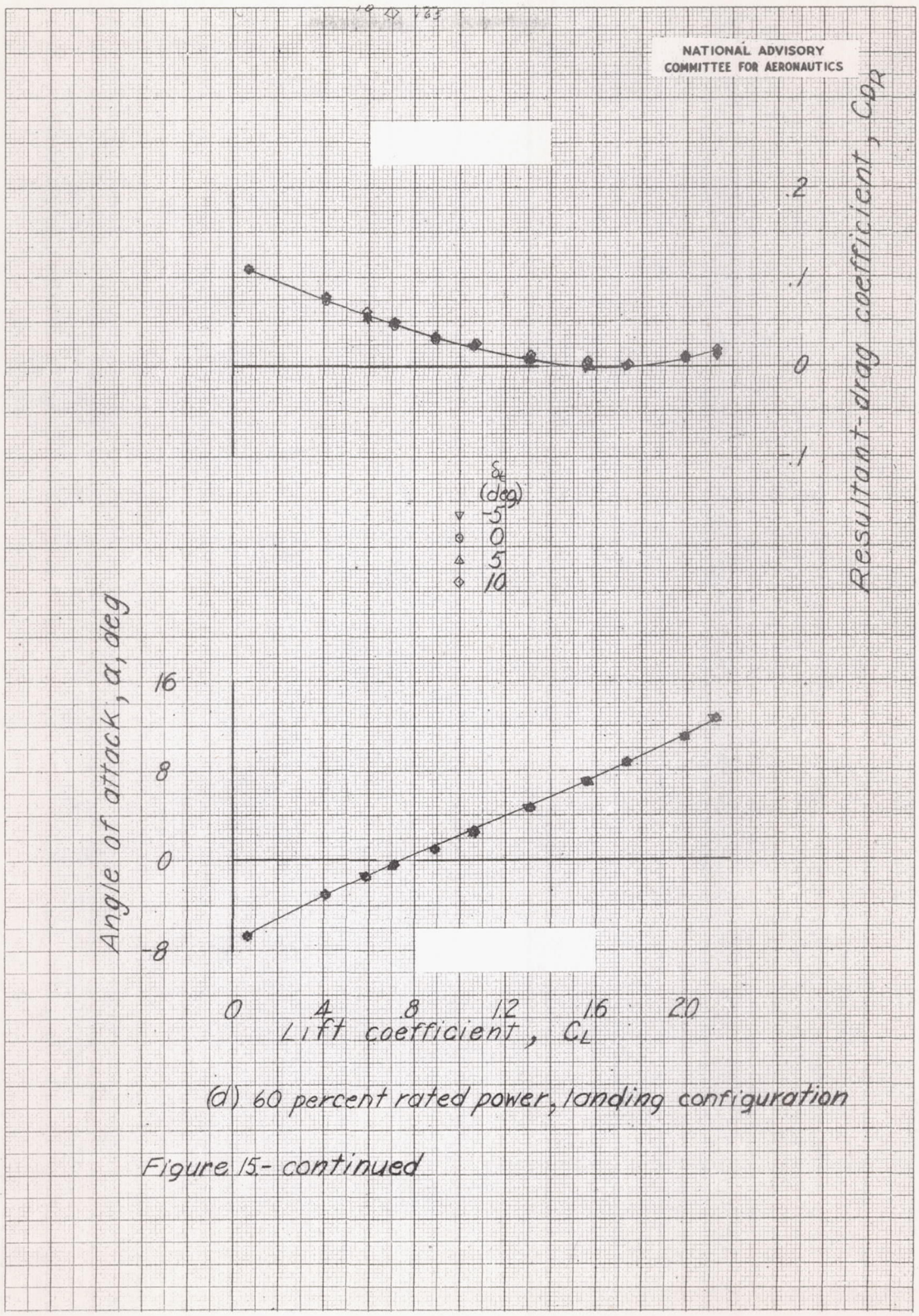

(d) 60 percent rated power, landing configuration

Figure 15.- continued

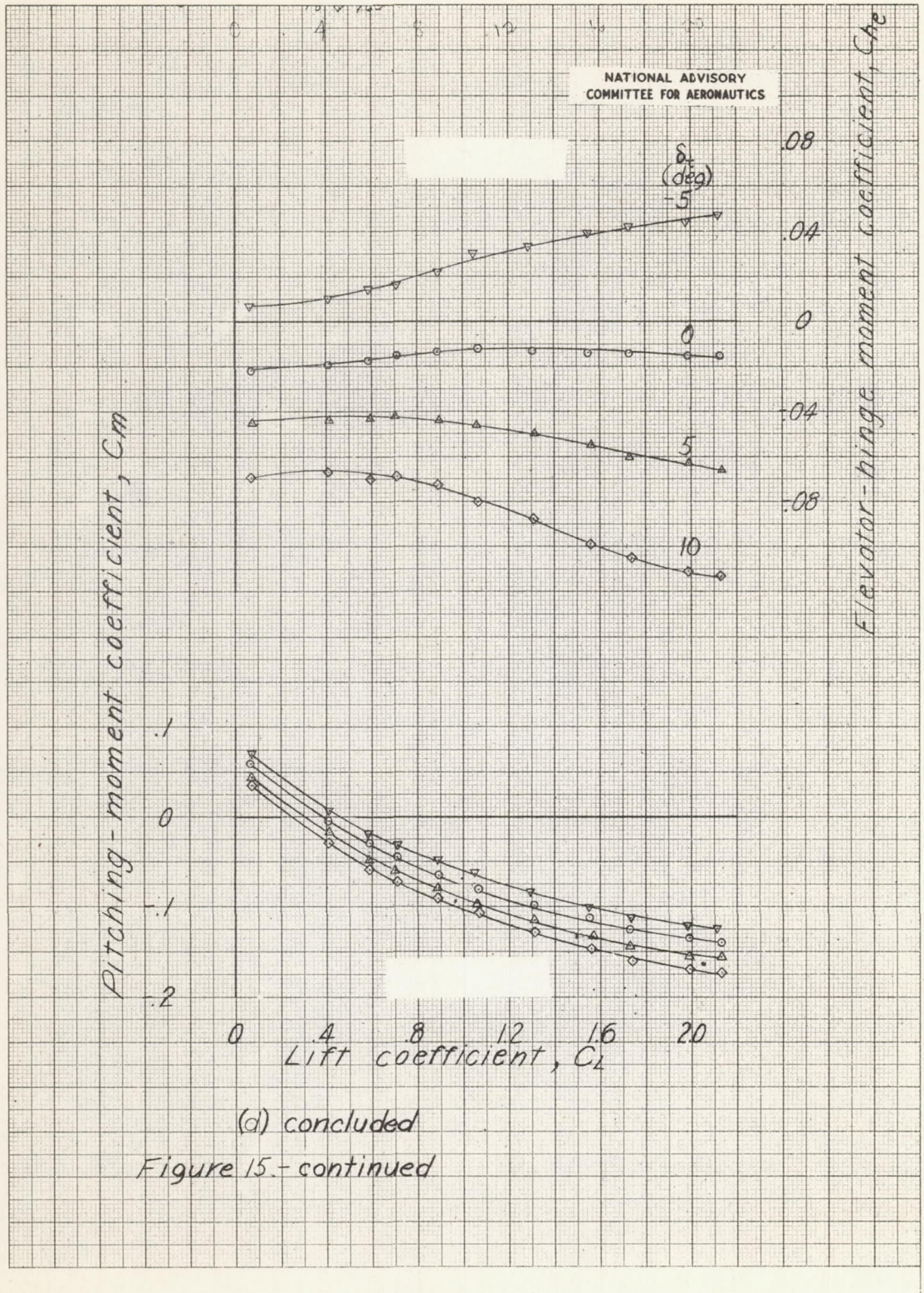

(d) concluded

Figure 15.- continued

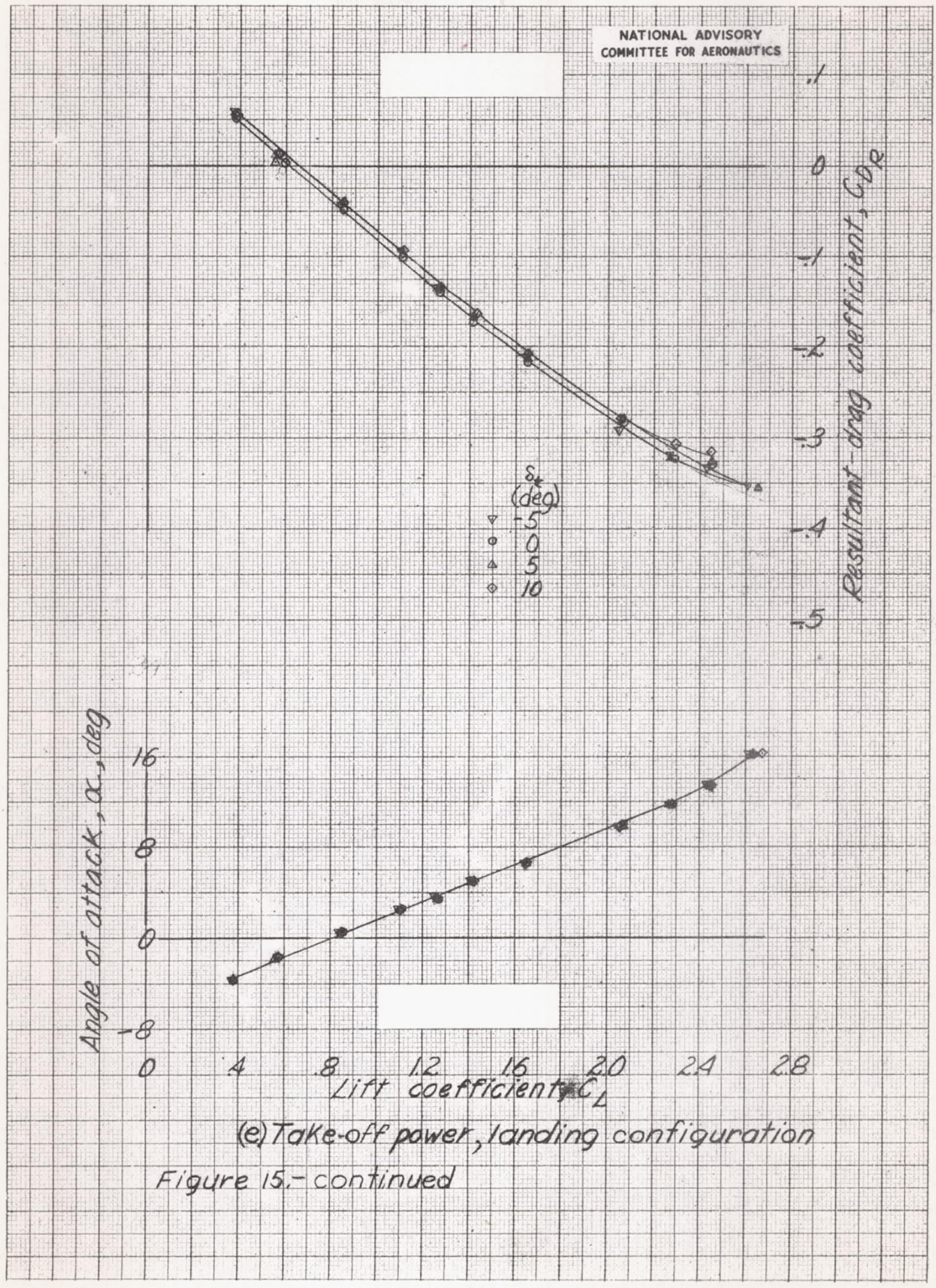

(e) Take-off power, landing configuration

Figure 15.- continued

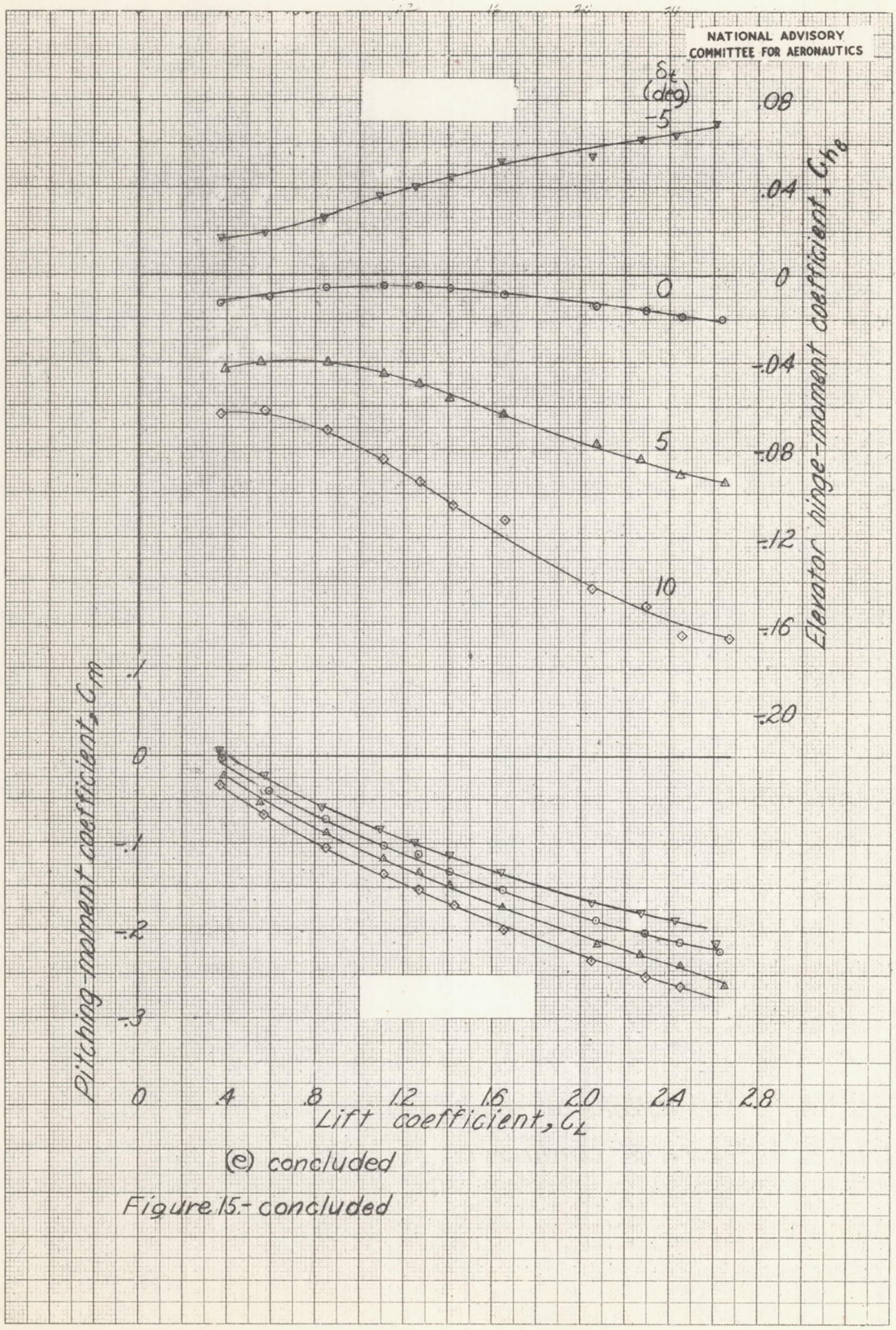

(c) concluded

Figure 15.- concluded

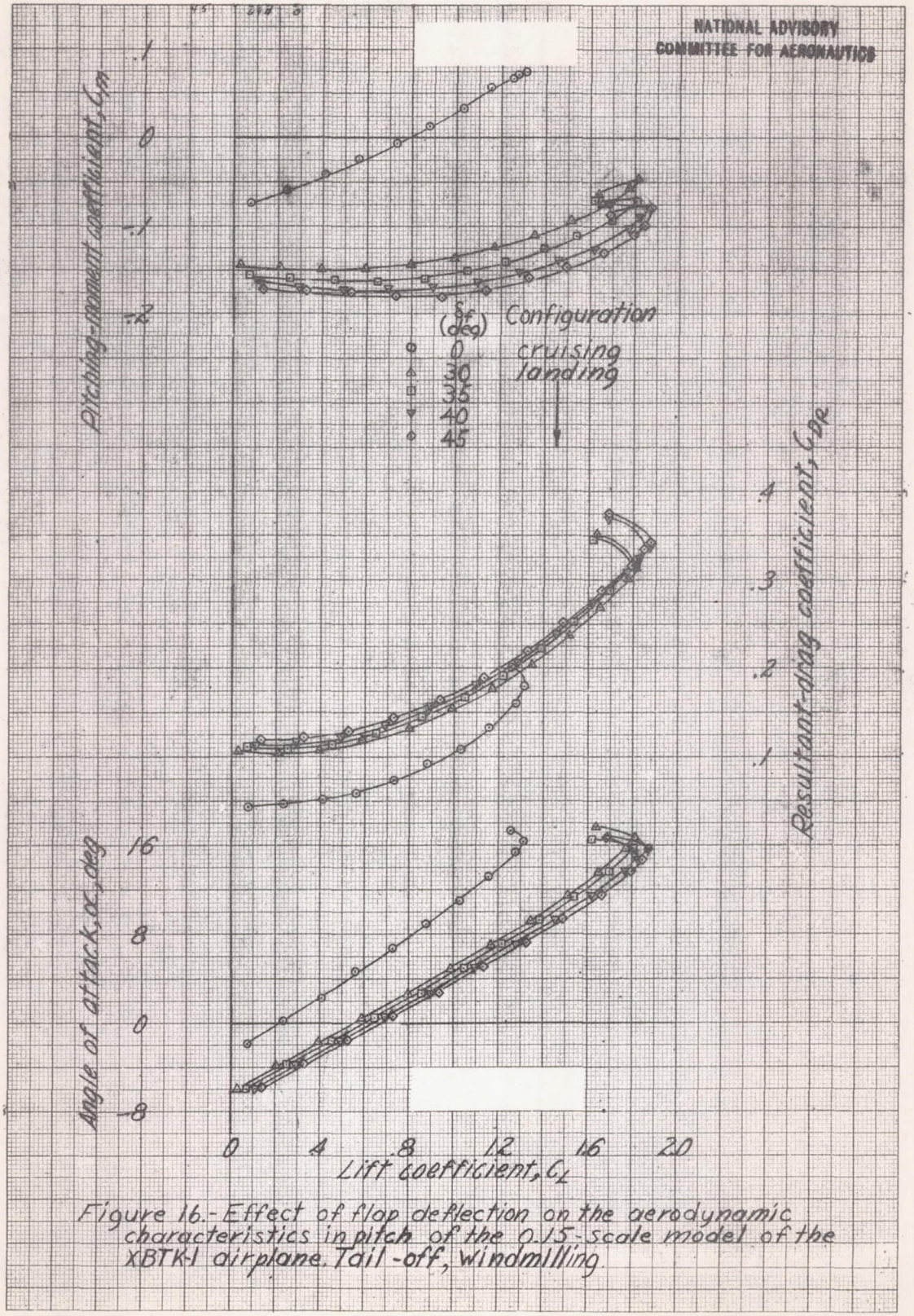

Figure 16.- Effect of flap deflection on the aerodynamic characteristics in pitch of the 0.15-scale model of the XBTK-1 airplane. Tail-off, windmilling.

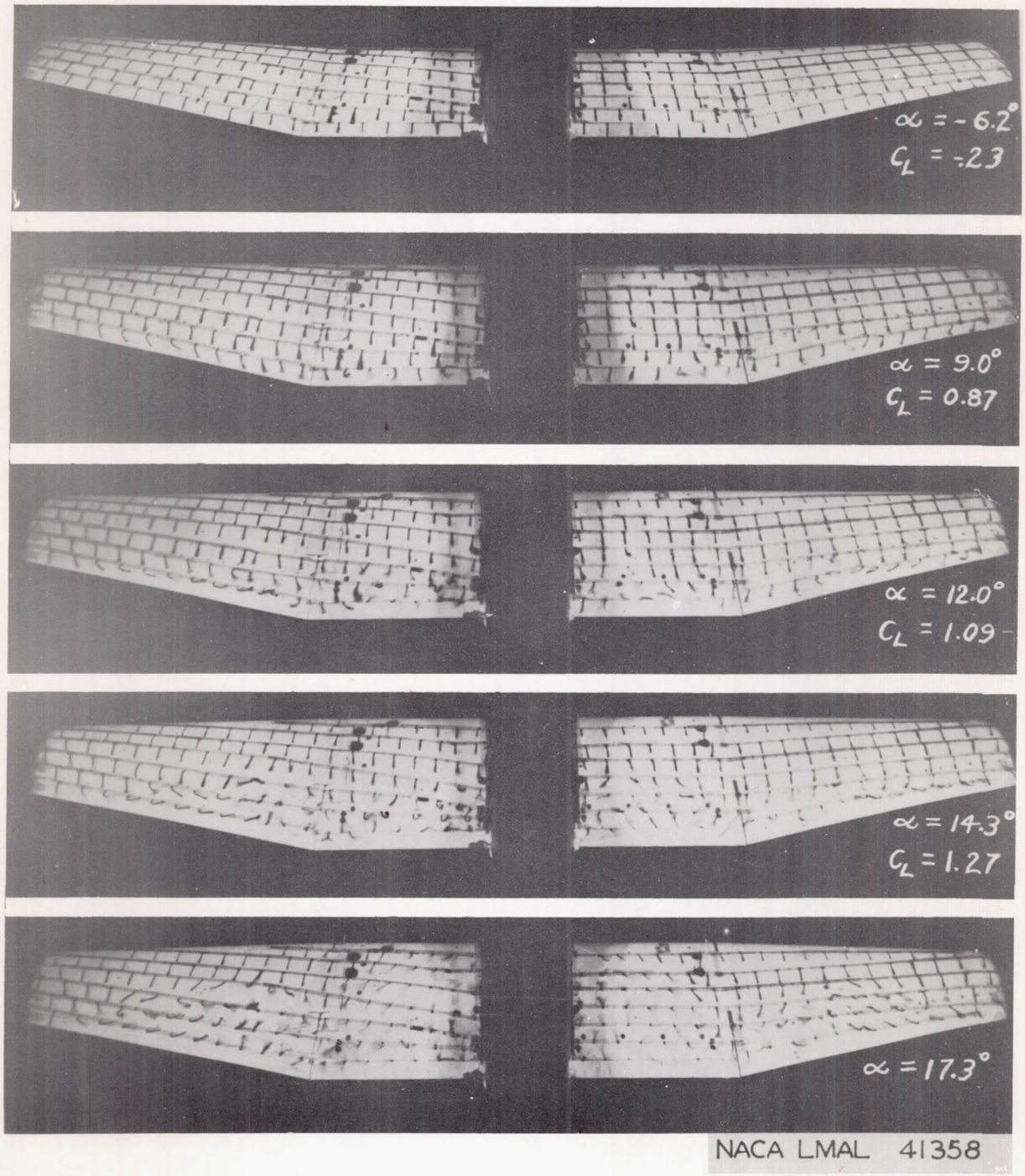

Figure 17.- Tuft study of 0.15-scale model of XBTK-1 airplane. Cruising configuration; windmilling; guns, fuel tank and radar on; tail-off.

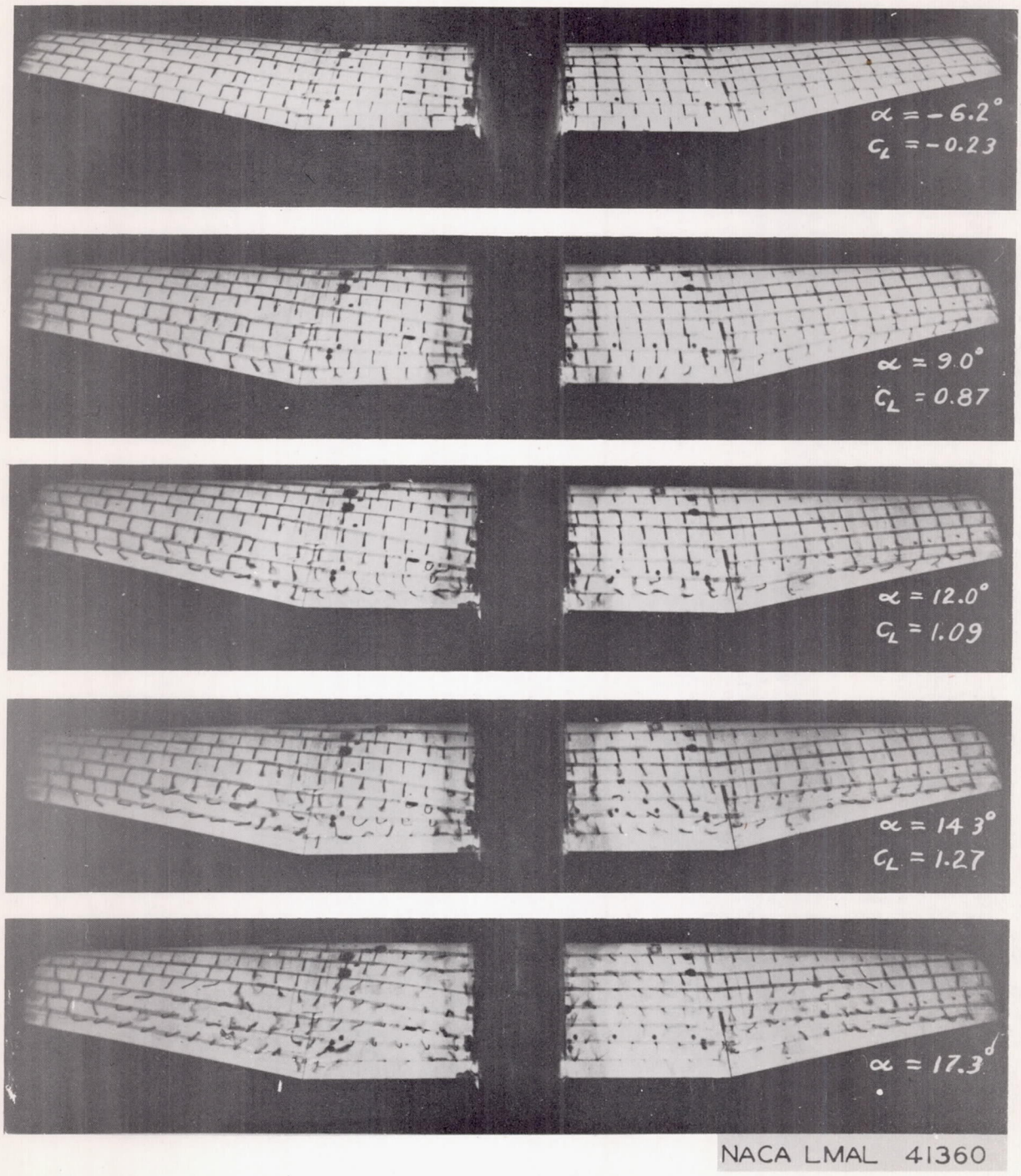

Figure 18.- Tuft study of 0.15-scale model of XBTK-1 airplane. Cruising configuration; windmilling; guns, fuel tank, and radar off; tail-off.

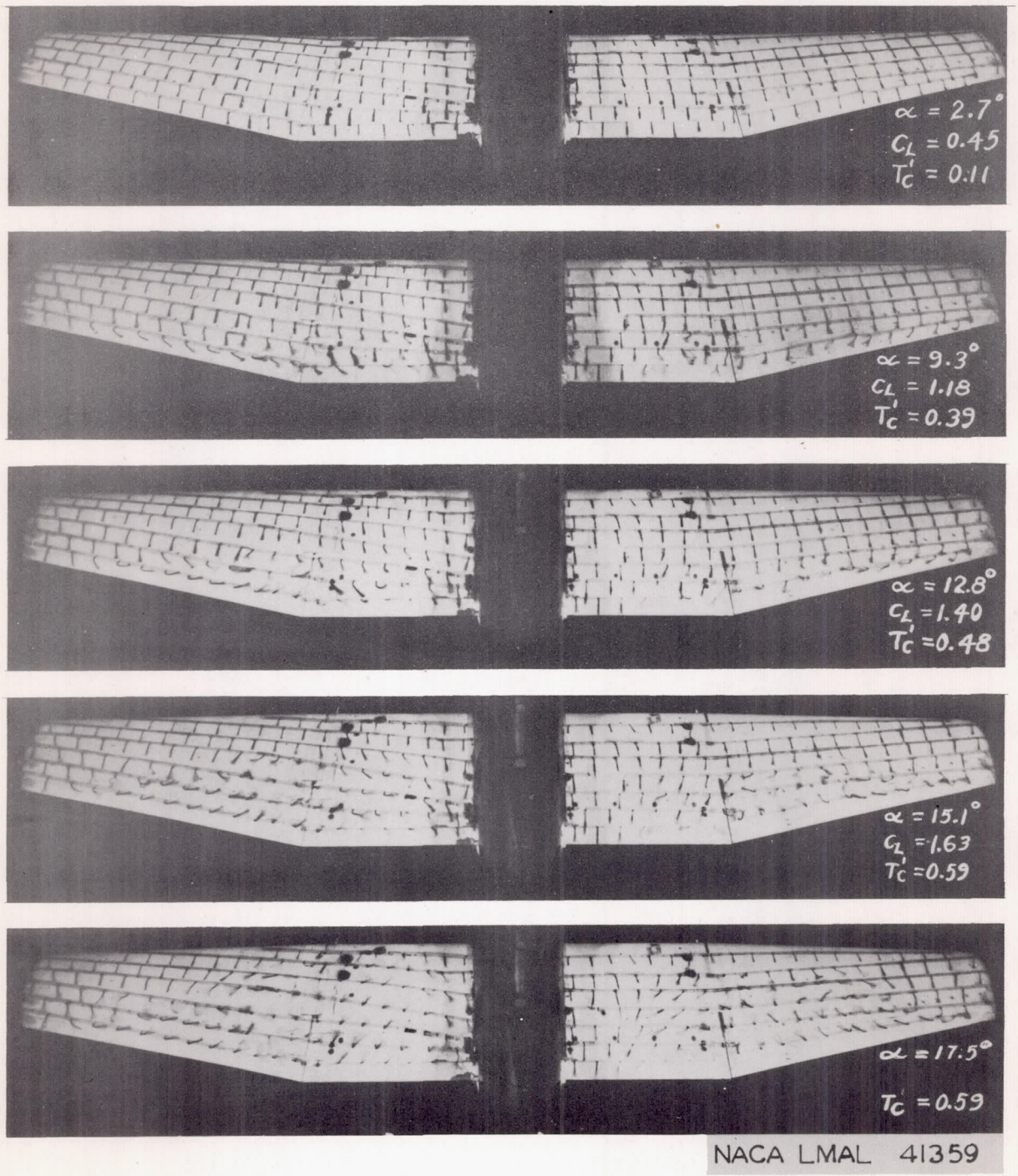

Figure 19.- Tuft study of 0.15-scale model of XBTK-1 airplane. Cruising configuration; take-off power; guns, fuel tank, and radar on; tail-off.

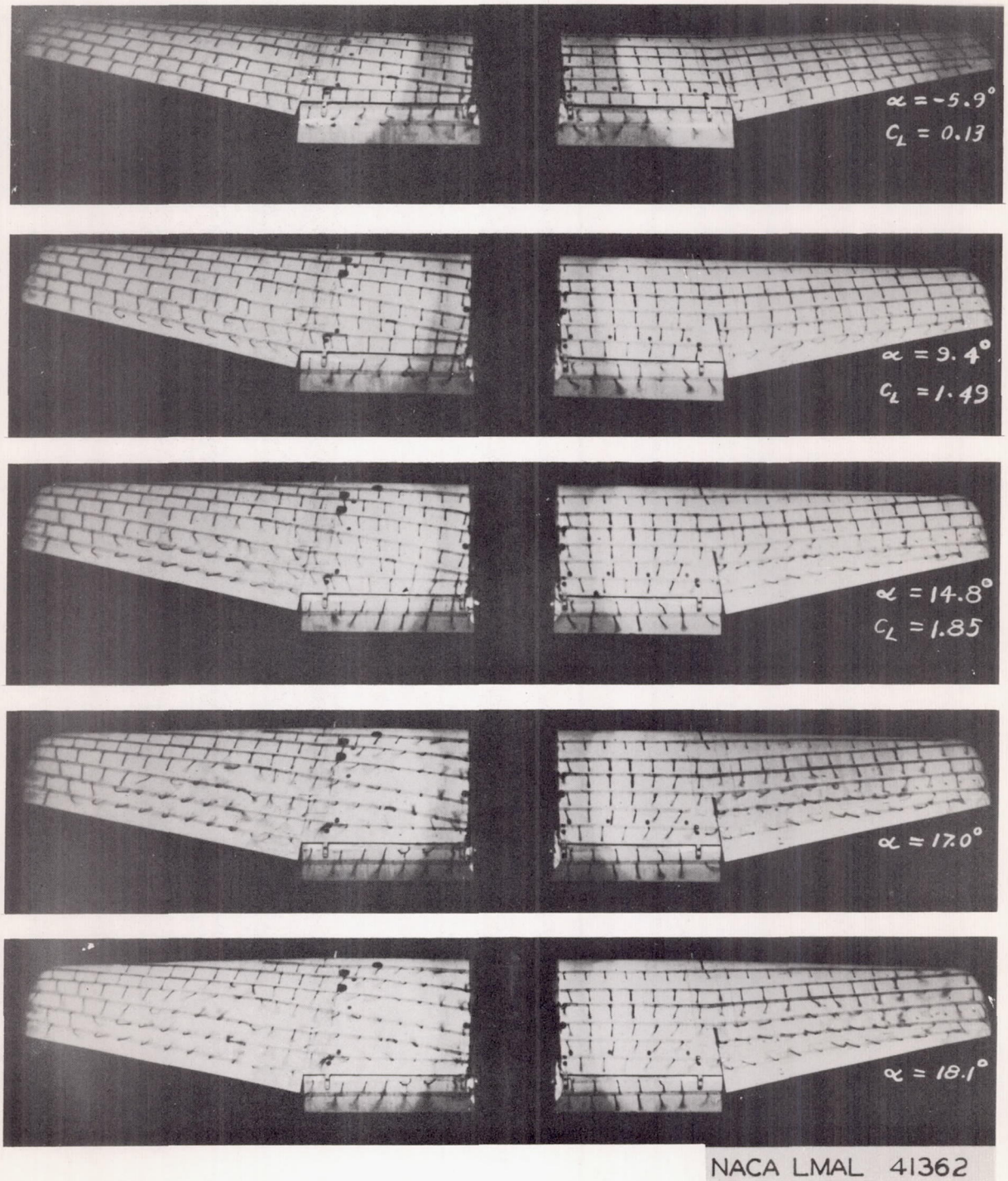

Figure 20.- Tuft study of 0.15-scale model of XBTK-1 airplane. Landing configuration; windmilling; guns, fuel tank, and radar on, tail-off.

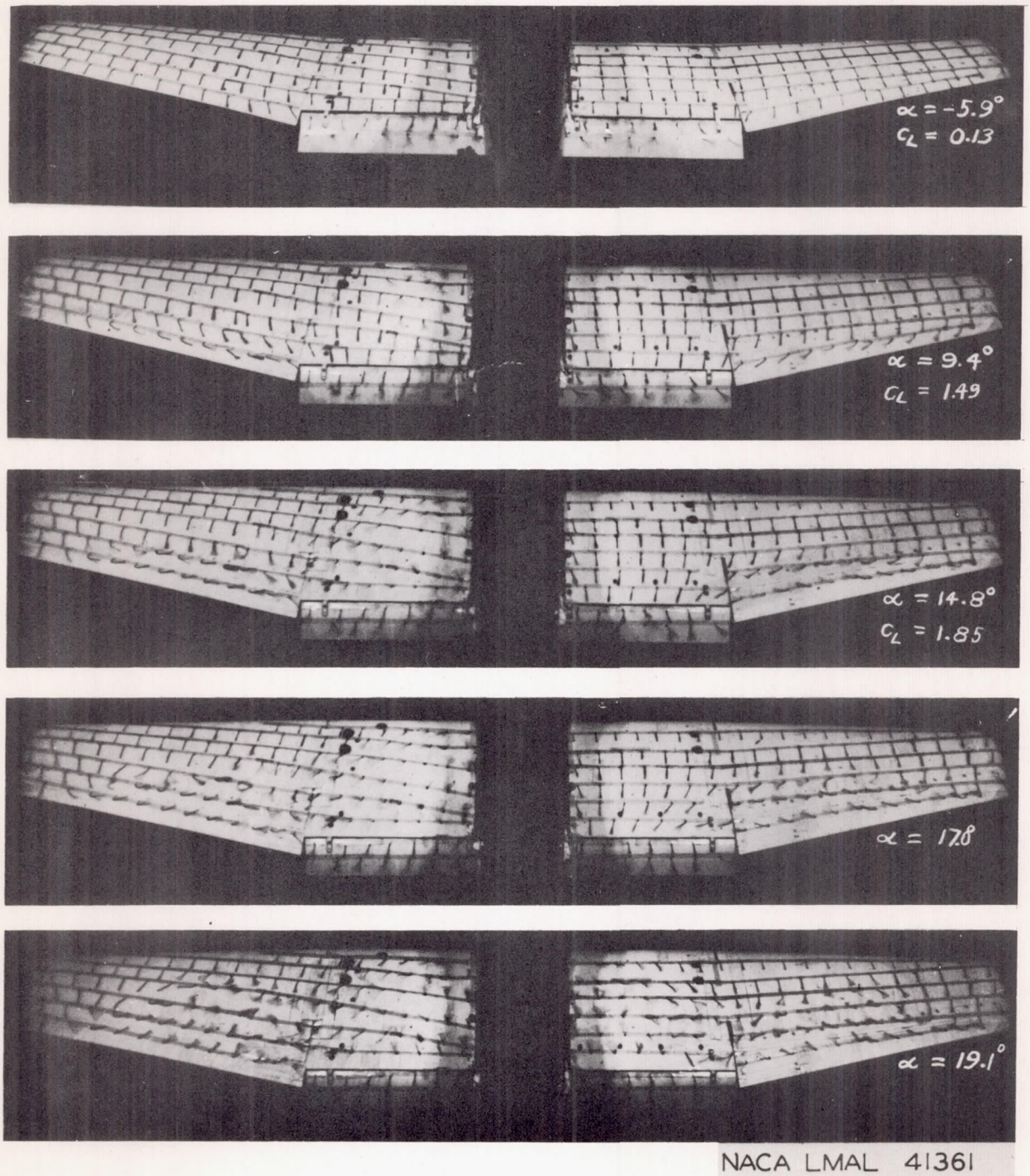

Figure 21.- Tuft study of 0.15-scale model of XBTK-1 airplane. Landing configuration; windmilling; guns, fuel tank, and radar off, tail-off.

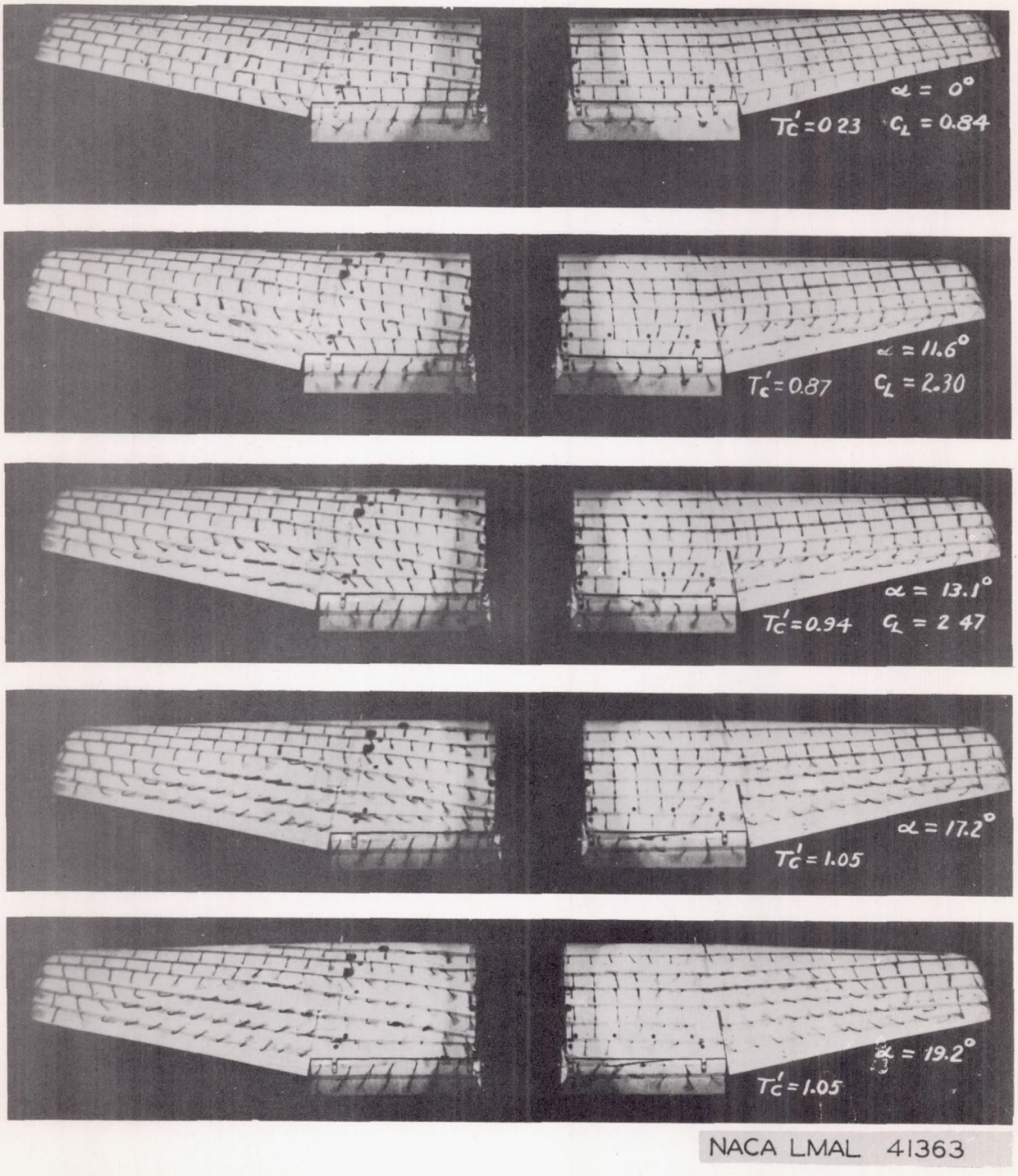

Figure 22.- Tuft study of 0.15-scale model of XBTK-1 airplane. Landing configuration; take-off power; guns, fuel tank, and radar on, tail-off.